UNIVERSITÀ
DEGLI STUDI
FIRENZE

DOTTORATO DI RICERCA IN
SCIENZE CHIMICHE

CICLO XXXIV

COORDINATORE Prof. PIERO BAGLIONI

Self-Assembled Microcapsules: understanding and controlling the release of payloads

Settore Scientifico Disciplinare CHIM/02

Dottorando
Dott. Xavier Castellví Corrons

Tutore
Prof. Debora Berti

Coordinatore
Prof. Piero Baglioni

Anni 2018/2022

THESIS OUTLINE

The goal of this thesis, funded by the European Union's Horizon 2020 research and innovation programme under the SAMCAPS project (grant agreement no. 814100), is to address the current need for bio-degradable materials and efficient encapsulating agents for home and beauty care products. To this aim, this work focuses on the liquid-liquid phase separation (LLPS) of an amphiphilic thermoresponsive copolymer that leads to the formation of micron-sized domains, known as simple coacervates, at room temperature and in surfactant-rich media, where control of liquid-liquid phase separation is particularly challenging. Additionally, these microstructures can entrap hydrophobic active principles from the medium and release them in a triggered way, rendering them as suitable encapsulating agents.

Chapter 1 briefly describes the benefits of fragrance microencapsulation and introduces the SAMCAPS project. Then, it explains the main features of amphiphilic and smart copolymers, including pH, ionic strength, light, and temperature-sensitive ones. Later, it defines liquid-liquid phase separation, differentiating between simple and complex coacervation, and concluding with the capacity of these polymeric microstructures to encapsulate and release hydrophobic active principles. Finally, it introduces the amphiphilic thermoresponsive graft copolymer (PEG-g-PVAc) employed for this work, consisting of a poly(ethylene glycol) backbone (6 kDa) with ~2-3 grafted poly(vinyl acetate) chains, and a PEG/PVAc weight ratio of 40/60.

Chapter 2 reports the materials used to perform all experiments as well as the methods and techniques employed throughout this work, including turbidimetry, UV-Vis spectrophotometry, microfluidics, optical and fluorescence confocal microscopy, and confocal Raman microscopy. The materials selected are commonly used in home and beauty care products, and the methodology is designed to provide relevant information to the consumer goods industry.

Chapter 3 includes the results and discussion of this work. First, it reports the effect of various water-soluble additives on the phase separation of PEG-g-PVAc, assessed through turbidimetry. Kosmotropes and non-ionic surfactants are found to decrease the phase separation temperature of the copolymer, while chaotropes and, above all, ionic surfactants increase it. Then, it focuses on the phase behaviour of PEG-g-PVAc in the presence of sodium citrate and a C14-15 E7 non-ionic surfactant (N45-7), defining the compositional range for the generation of coacervates at room

temperature and monitoring their formation with fluorescence confocal microscopy. After that, it explains how we determined for the first time the composition of the coacervates through confocal Raman microscopy, demonstrating the presence of PEG-g-PVAc, N45-7, and water. Interestingly, the concentration of N45-7 plays an important role in modulating the hydrophilicity of the coacervates and, thus, their affinity for actives with different hydrophobicity. Later, this chapter shows the capacity of PEG-g-PVAc coacervates to behave as encapsulating agents and confine hydrophobic actives in surfactant-rich media. Coumarin6, an hydrophobic dye, is used to demonstrate the spontaneous entrapping capacity of these coacervates through fluorescence confocal microscopy. Finally, taking advantage of the thermoresponsivity of PEG-g-PVAc, it proves the potential of these coacervates to release their contained actives in a triggered way. We use microfluidics and fluorescence confocal microscopy to visualize the destabilization of these coacervates, and UV-Vis spectrophotometry to measure in a more quantitative way the confinement and release of Coumarin6 from these coacervates. Both water dilution and urea addition are shown to be very effective release triggers.

Chapter 4 summarizes the main outcomes of this work and gives some suggestions for future work. Overall, the results gathered in this thesis expand the knowledge on self-coacervation of grafted copolymers and define the conditions in which PEG-g-PVAc coacervates can be obtained in a surfactant-rich medium at room temperature. The encapsulation and release properties of these coacervates demonstrate their feasibility as encapsulating agents for some consumer good products applications, such as shampoos and detergents. Remarkably, the destabilization of these coacervates leads to their complete dissociation into copolymer single chains and surfactant molecules, reducing their environmental impact to the copolymer and surfactant biodegradability profiles. Additionally, these findings sum up on the emerging interest to effectively control the formation of LLPS microdomains and be used as possible *in vitro* models to mimic membrane-less organelles of living cells.

“Aut viam inveniam aut faciam”

ACKNOWLEDGEMENTS

This thesis results from the combined efforts of a multitude of people, who I believe deserve to be acknowledged properly. These people have supported me both academically and emotionally throughout this journey, and to neglect to recognize their contributions would be a disservice.

First and most importantly, my deepest gratitude goes to Prof. Debora Berti, from the Chemistry Department of the University of Florence. As my academic supervisor, you provided me with thousands of interesting ideas, patiently taught me not only about research but also about life, and, most valuably, gave me so much of your time. Your vast knowledge and experience in polymer science clearly eased my progress and allowed me to complete this thesis. Among all your aptitudes, I must highlight your ability to quickly understand any new result and immediately suggest a possible meaning that had not previously crossed my mind. This thesis would have never been so fruitful without your constant support. I also want to express my most sincere gratitude to Dr. Jeremie Gummel, my industry supervisor from Procter&Gamble (Brussels Innovation Center). Your guidance during my stay at P&G made my learning and progress so much easier. I do want to thank you for the calmness and good mood you brought in me every time I came to you stressed or lost. I also want to thank Dr. Johan Smets for being an inspirational figure. Your career demonstrates what discipline, self-respect, and clear priorities can achieve. There is another person in P&G I would like to express my great appreciation to: Susana Fernandez Prieto. Even though you were not my direct supervisor, you behaved like one in case of need. You showed me the differences between research in academia and in a company, and made me see the acquired results from a different perspective. The collaboration of these mentors made it a very insightful project. An honourable mention to Prof. Piero Baglioni, Prof. Massimo Bonini, and Dr. Beth Schubert for your contributions to my project and interesting discussions during group meetings, as well as the other academic and technical staff at the University of Florence and the Procter&Gamble Company for your valued support.

Out of the long list of colleagues I shared this project with, I would like to express my greatest appreciation to Keo-Oudone Seymany. There is no doubt these three years would have been much harder without you by my side. Both inside and outside work, you have been a great companion, a wise advisor, and a source of joyful experiences. I also feel like thanking Constantina Sofroniou for your sweet behaviour and ever-present willingness to help and collaborate. You two, together with Aleksandra Zawadka, were great teammates, and together we grew so much during this project.

Mattia Collu, David Millan, Miguel Vega, and Andrea Grandy, I really feel grateful to have met you during this experience. I want to thank you for making my stay in P&G Brussels so engaging and creating such nice memories. Additionally, I wish to thank Jacopo Cardellini, Ciro Allarà, and Arianna Balestri for making me feel so warmly welcomed, teaching me the Italian lifestyle, and making my days in Florence so much better.

I have been fortunate to build my work from foundations laid by previous group members, mainly Dr. Arianna Bartolini and Dr. Paolo Tempesti. Thank you so much for the hard work you did performing the first tests and developing knowledge on the liquid-liquid phase separation of the copolymer I employed, allowing me to go one step further with this thesis. Thanks must also be given to the European Union's Horizon 2020 research and innovation programme and the Marie Skłodowska-Curie Actions for funding this project, to Procter&Gamble for opening its doors to Ph.D. students like me, and to the University of Florence and the CSGI for allowing me to complete my Ph.D. studies.

Impossible to forget the magnificent couple that raised me: Antoni and Cristina, you deserve the biggest of my acknowledgements. Your unselfish sacrifices, energetic encouragement, doubtless support, and unconditional love are the basis of all my achievements. Even in distance, you have been the main pillar of my emotional stability, and your lessons keep making me a better person every day. My little sister, Anna, thank you so much for being so sweet to me and being always by my side. The emotional strength your support provides me is priceless, and I believe we are a great team. My most heartfelt thanks go to you, Ramón, for having been such an extraordinary grandfather during all these years. You truly are a life reference for me, and your smile will always be an inexhaustible source of motivation. I feel so much appreciation for you too, Maria Àngels, for giving me the best of you under any circumstances and believing so much in me and my (hopefully) prosperous future. I cannot express how fortunate I feel to have such a caring and respectful family…I owe it all to you.

Last but not least, the person with who I have shared most of my time during these three years: Gabrielė. You have been my main source of happiness, growth, and motivation during this adventure. I will forever be grateful for your ability to paint my life in colour and add so much love to it, it would have not been the same without you.

CONTENTS

1. INTRODUCTION

1.1 SAMCAPS project

Microencapsulation refers to the retention of an active compound inside a micron-sized molecular structure which protects it against premature degradation and undesired diffusion, possibly until an external stimulus triggers its release [1]. This results in an enhanced stability of the final product, which extends its shelf-life. Currently, the microencapsulation of actives is widely used in the cosmetic, chemical, food, and pharmaceutical industries [2–5].

The inclusion of fragrances into complex formulations, such as the ones of beauty and home care products, is not easy, due to their usually poor water solubility, high volatility, and sensitivity to light and oxygen [6,7]. Therefore, normally fragrances are encapsulated in microstructures, mostly polymeric [8–12]. However, it is challenging to find a material capable of forming stable microcapsules in such harsh surfactant-rich formulations that keep intact throughout a whole wash cycle (**Figure 1-1**). Fortunately, microcapsules made of aminoplast resin, such as melamine formaldehyde, can be widely used in these formulations due to their superior performance, including acid/alkaline, heat and water resistance, low leakage, and mechanical robustness. In addition, these microcapsules are cheap and easy to synthesize [13–15]. Thanks to their efficient encapsulation, the total amount of fragrance used in consumer products can be notably reduced, which lowers the total cost of production. Additionally, the extended pleasant scent provided to the consumer is perceived as freshness, which decreases the frequency of washing cycles, reducing water and power usage [16].

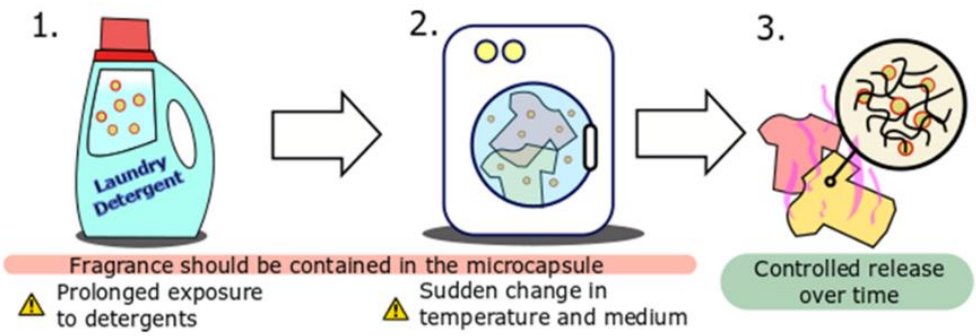

***Figure 1-1**: Main scenarios of microcapsule's life in the high-demanding laundry detergent application. The microcapsules must remain stable in a surfactant-rich medium for an extended period (1), survive the increased temperature, water dilution, and change of medium during the washing cycle (2), and finally deposit on fabrics to release their contained fragrance over time (3). Reprinted with permission from* [17]. *Copyright 2019 American Chemical Society.*

Even though melamine formaldehyde microcapsules show an excellent performance in these challenging formulations, their deposition, biodegradability, and release profiles can be improved. First, there is no active but passive interaction between the microcapsule and the substrate (fabrics for detergents or hair for shampoos). The use of a different material presenting favorable interactions with the fabrics or hair would enhance the deposition efficiency of these microcapsules. Second, the polymers forming the hard-wall of these microcapsules show an inefficient environmental and biodegradability profile [17]. Unavoidably, part of these microcapsules will end up forming part of wastewater after a washing cycle, reaching rivers, streams, and oceans. The encapsulation efficiencies of other materials with an improved biodegradability profile could be explored. Third, the fragrance release from these microcapsules can only be triggered by mechanical pressure, which causes the rupture of the shell and consequently the free diffusion of the fragrance [18,19]. However, there are other external stimuli such as temperature, water dilution, pH, light, and ionic strength that could be exploited to trigger the fragrance release as well [20].

The SAMCAPS project, which stands for Self-Assembled MicroCAPSules, was proposed to tackle these points and give rise to a microcapsule with improved

features. SAMCAPS is a Marie Skłodowska Curie European Industrial Doctorate project (grant agreement no. 814100) belonging to the Horizon 2020 framework which has financed the doctorate course of four early-stage researchers This project arises from the collaboration of two partners – CSGI (Center for Colloid and Surface Science) in Florence/Siena, Italy, and Procter&Gamble in Brussels, Belgium. The goal of the project is to develop biodegradable polymeric microcapsules for use in home and beauty care products with improved targeting, biodegradability, and fragrance release profiles. In this way, SAMCAPS addresses the challenge of the chemical industry as response to international agreements such as the Paris Climate Act and the Europe 2020 policies for smart, sustainable and effective chemical use. Since the number of industries using encapsulation technologies keeps growing, as demonstrated by the increasing number of companies filing patent applications on encapsulation, there is a need to lower the environmental impact of these systems while making them as efficient as possible for the social welfare. Considering these surfactant- and salt-rich media provide one of the biggest challenges in fragrance encapsulation, the successful results could be extended to pharmaceutical and food formulations.

The SAMCAPS project can be divided in the following main study points:

1. Synthesis of new polymers capable of forming microcapsules with an improved environmental footprint
2. Study of the formation and stability of these microcapsules in surfactant-rich media, as they are to be used in consumer good products
3. Research of novel mechanisms to trigger the fragrance release, such as a variation of temperature, ionic strength, or water content
4. Determination of the interactions between the microcapsules and the targeted surfaces

This thesis focuses on points two and three, concerning the formation and fragrance release of stimuli-responsive polymeric microcapsules, targeted for consumer good formulations. First, the formation of microcapsules with an amphiphilic thermoresponsive copolymer in surfactant- and salt-rich water solutions is assessed. The liquid-liquid phase separation of the copolymer in

these solutions is exploited to obtain microcapsules able to contain different fragrances. It is quite a special phenomenon to be able to form self-assembled microstructures in this environment without any cross-linking between polymer chains, since normally polymer assemblies, such as coacervates or vesicles, are destabilized by the presence of surfactants [21,22]. Second, the destabilization profile of these polymeric microcapsules is studied with the aim to trigger the release of the contained fragrance at a desired time. Considering this project works with thermoresponsive copolymers, both temperature variation and water dilution work as destabilization triggers. Remarkably, the destabilization of these microcapsules leads to their dissociation into copolymer single chains and surfactant molecules. Therefore, the environmental impact of these microcapsules is reduced to the copolymer and surfactant biodegradability profiles.

1.2 Polymer features

Polymers, from the Greek *poly-* (many) and *-mer* (part), are macromolecules consisting of many repeating subunits (monomers) covalently linked. A single polymer chain, or unimer, can be composed of the same (homopolymers) or different (heteropolymers or copolymers) type of monomers. Depending on the physical arrangement of monomers, polymers with different architectures – linear, comb, star, or branched – and compositions – homo-, block, gradient, alternating, random, or graft – can be obtained (**Figure 1-2**) [23]. At the same time, the functional groups of the monomers will determine the properties and interactions of the polymer with other molecules. Both the type of monomers and their arrangement can be modulated to design polymers with desired features. For instance, the combination of lipophilic and hydrophilic monomers in a specific order, such as block or graft structures, results in the synthesis of a copolymer that can interact with both oil and water [24]. This property is precisely beneficial for fragrance encapsulating systems in water solutions. As another example, the use of monomers containing functional groups sensitive to a variation of external stimuli provide the polymer with the same sensitivity [20]. This kind of sensitivity is requested to promote a triggered release of the contained fragrance from the polymeric microcapsule. Considering the aim of this project is to encapsulate fragrances in water solutions to then release them in a triggered manner, amphiphilic stimuli-responsive copolymers are of high interest.

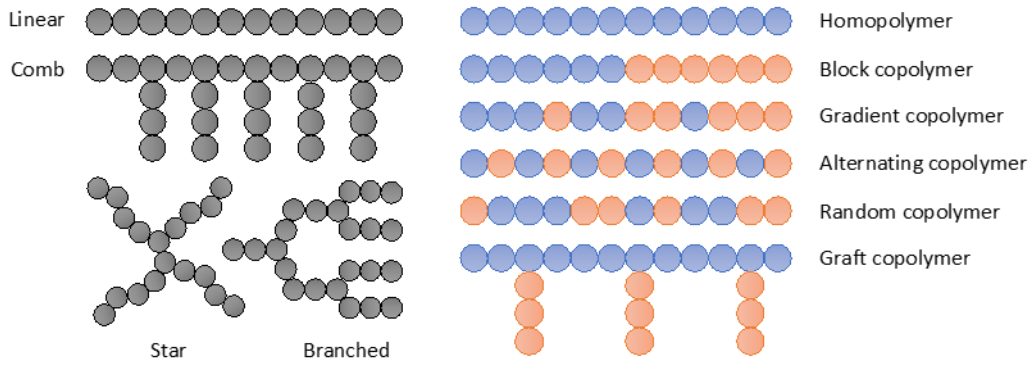

***Figure 1-2**: Different polymeric structures classified according to their architecture (left side) and composition (right side).*

1.2.1 Amphiphilicity

The word amphiphilic comes from the Greek and means "loving both". In chemistry, this term is used to define molecules with both a hydrophilic (water loving, polar) part and a lipophilic (oil loving, non-polar) one. Small amphiphilic molecules are generally named as surfactants, which stands for surface active agents. This name comes from their tendency to adsorb at surfaces and interfaces between two immiscible phases. Surfactants are normally classified by their polar group, differing between neutral (non-ionic) and charged (ionic) surfactants, the latter ones including anionic, cationic, and zwitterionic surfactants. Zwitterionic surfactants contain both an anionic and a cationic charge under normal conditions. The non-polar part is normally an alkyl chain that can be linear or branched. The degree of branching and the length of this chain, together with the choice of the polar group, determine the physicochemical properties of the surfactant [25]. Due to the amphiphilic nature of surfactants, the two parts of the same molecule interact in very different ways with either a polar or a non-polar solvent. Therefore, in the lack of a surface or interface to adsorb to, surfactants tend to aggregate, forming self-assembled structures in solution (**Figure 1-3**) [26]. In water, this structure formation is a consequence of both noncovalent interactions between surfactant molecules and energetically unfavorable interactions between their hydrophobic parts and

water [27]. This phenomenon leads to a variety of self-assembled structures [28], micelles being the structures obtained at a lowest concentration. The surfactant concentration at which micelles start forming is known as the critical micelle concentration (CMC) [25,29].

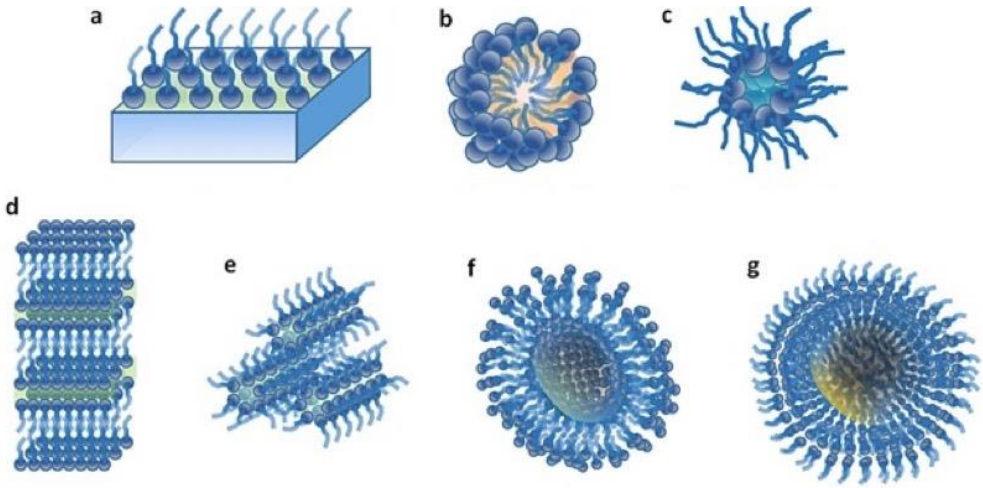

***Figure 1-3**: Schematic representation of some self-assembled structures formed by surfactants: monolayer (a), direct micelle (b), reverse micelle (c), lamellar liquid crystals (d), hexagonal bidimensional liquid crystals (e), direct vesicles (f) and reverse vesicles (g). The dark blue sphere represents the polar part of the surfactant while the light blue chain represents its non-polar part. Reprinted and modified with permission from* [30]*. Copyright 2015 John Wiley and Sons.*

Larger amphiphilic molecules, such as copolymers, can also be surface active agents with self-assembly properties that give rise to the same kind of structures described in **Figure 1-3** [31,32]. For that, the copolymer needs to be designed in a way that allows it to expose its hydrophilic parts in a polar environment and its hydrophobic parts in a lipophilic one [25]. This is the reason why the self-assembly of copolymers has been mainly studied with block copolymers, which structure resembles that of linear common surfactants [33]. However, graft copolymers, made of hydrophobic chains grafted to a hydrophilic backbone or hydrophilic chains grafted to a hydrophobic backbone, also present self-assembly properties [34,35]. In fact, surface active copolymers present a very strong driving force towards interfaces, with this tendency being less dependent on the physical variables than observed with low molecular weight surfactants[25], rendering them as interesting candidates for industrial applications. Specifically,

in the case of biphasic systems presenting an oil phase (such as a fragrance) and a water phase, these surface-active copolymers are able to stabilize the fragrance in the water solution at low concentrations and be less affected by physical conditions such as ionic strength or temperature changes. Although these amphiphilic copolymers have also been studied in organic solvents [36], their main use is in water solutions due to their widespread application possibilities in technical, biomedical, and industrial areas [37].

1.2.2 Smart polymers

As explained above, a copolymer with amphiphilic properties is useful to stabilize fragrances (oil phase) in water solutions. However, this project also aims to release the stabilized fragrance at a desired time/space. For that, a stimuli-responsive polymer, which reversibly adapts its properties in response to external stimuli, is required. A variation of pH, ionic strength, light, or temperature can be used as a trigger to induce a response in the molecular properties of these often-called smart polymers [38–42]. This remarkable behavior provides them with broad applications in fields such as drug delivery, sensors, and artificial actuators [43–46].

pH sensitive polymers

Polymers with pH sensitivity contain ionizable acidic or basic groups that either accept or release protons in response to a change in the environmental pH. Generally, polymers with basic or acid monomers behave as cationic or anionic polymers under acidic or basic conditions, respectively. Consequently, the polymer can change from non-ionic to ionic, and vice versa, by modulating the environmental pH, affecting its surface activity (amphiphilicity), solubility, and conformation. For instance, a pH change causing (de)protonation of the functional groups in the polymer can induce precipitation of homopolymers and micelle/vesicle formation of copolymers. Depending on the polymer's structure and composition, different self-assembly behaviors can be achieved (**Figure 1-4**). The self-assembly of these copolymers depends on their pH-sensitivity, which

can actually be tuned by using different monomers and polymer structures, allowing a precise control on the range of pH at which the polymer's behavior changes [41]. These unique properties make pH-responsive polymers very useful in applications where the targeted environment has a different pH. For instance, since the extracellular pH of most tumors is acidic (usually with a value between 5.8 and 7.2) [47], smart polymeric structures can be designed for anti-cancer drug delivery, where the release of drugs is triggered by pH decrease [48]. Moreover, synthetically, pH-responsive polymers can be produced using peptides, which are biocompatible and degradable. These natural polymers have great importance among pH-responsive polymers [49,50].

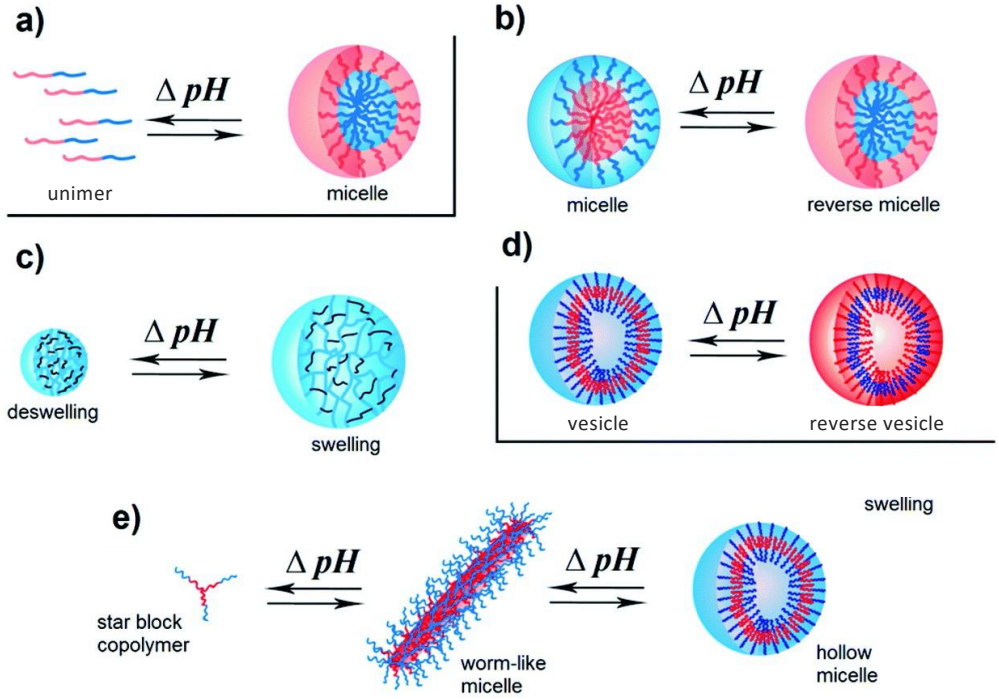

***Figure 1-4**: Different self-assembled structures of pH-responsive polymers: (a) unimer to micelle, (b) micelle to reverse micelle, (c) gel, (d) vesicle to reverse vesicle, and (e) unimer to worm-like micelle to hollow micelle. Reprinted and modified from* [41] *with permission from the Royal Society of Chemistry.*

Ionic strength sensitive polymers

Ionic strength sensitivity is also typical of polymers containing ionizable groups in their structure. Pretty much as it happens with pH-sensitive polymers, this class of smart polymers can change from ionic to non-ionic, and vice versa, by modulating the environmental ionic strength. Specifically, variations in the ionic strength can cause the screening of the charges present in the ionic monomers of the polymer [51]. This changes its charge density and, consequently, it also affects its surface activity, solubility, and conformation. The effect of ionic strength on polyelectrolyte complexes has been broadly reported [52–54], demonstrating that it affects their size and stability in different ways. First, the screening of the polyelectrolyte's charges can cause the shrinkage of the polymeric complex, due to a reduced repulsion between monomers [55,56]. Second, the charge screening can also reduce the hydrophilicity of the polymer, inducing its phase-separation [57,58]. Third, self-assembled systems stabilized by the attractive interaction between both polycations and polyanions (such as complex coacervates [59]) destabilize upon charge screening [60,61]. Taking advantage of these shrinkage and destabilization effects, ionic strength can be used as a release trigger of polyelectrolyte systems for biomedical applications [42,62]. Non-ionizable polymers will not be directly affected by ionic strength, but they can be indirectly affected by its effect on the medium they are found in – salting-in and salting-out processes [63].

Light sensitive polymers

Light sensitivity differs from pH and ionic strength sensitivities because the stimulus can be triggered from outside the system. Moreover, it can be localized in space and time, and the stimulus parameters, such as light intensity, wavelength, and irradiation time, can easily be modified to suit the requirements of the system [40]. Light sensitive polymers are synthesized with photosensitive moieties that can react either reversibly or irreversibly upon light irradiation through isomerization (*cis-trans*), bond forming, or bond breaking reactions. This allows to precisely form, degrade, functionalize, and crosslink this type of polymers [64]. The main application of this type of smart polymers is the light-

controlled polymeric self-assembly. In other words, the use of light to give or take the surface activity of the polymer, and thus monitor its self-assembly properties [65]. Normally, photo-responsive polymers contain light-sensitive moieties in the hydrophobic block or in the junction between this block and the hydrophilic one.

On the one hand, light irradiation can produce irreversible changes on the polymer structure. For instance, light can trigger the cleavage of photosensitive side groups and transform the hydrophobic domain into a hydrophilic one. As a result, the amphiphilicity is lost and the self-assembled structure destabilizes [66]. The same effect can be obtained in the reverse way: converting the hydrophilic domain into a hydrophobic one after photo-cleavage, inducing the formation of polymer self-assembled structures [67]. The photosensitive moieties can also be in the main chain of the hydrophobic block. In this case, light irradiation causes the degradation of the hydrophobic block and leads to disruption of the self-assembled structure [68].
On the other hand, light irradiation can induce reversible changes on the polymer structure, thus allowing to monitor both the formation and disruption of self-assembled structures with the same photosensitive moiety. Although this behavior seems more interesting for release applications, reversible light sensitive groups tend to display a weaker shift in the hydrophilic/hydrophobic balance and slower kinetics than irreversible sensitive ones [40]. Among light-sensitive molecules with reversible properties, azobenzenes are the most studied ones. Upon light irradiation, azobenzenes go through a reversible trans–cis isomerisation of their nitrogen double bond (**Figure 1-5**). The non-polar (*trans*) isomer is converted into the polar (*cis*) one by UV irradiation while the reversible process is triggered by visible light [69]. This change of polarity allows to control in a reversible way the self-assembly properties of polymers with azobenzenes in their structure [70,71].

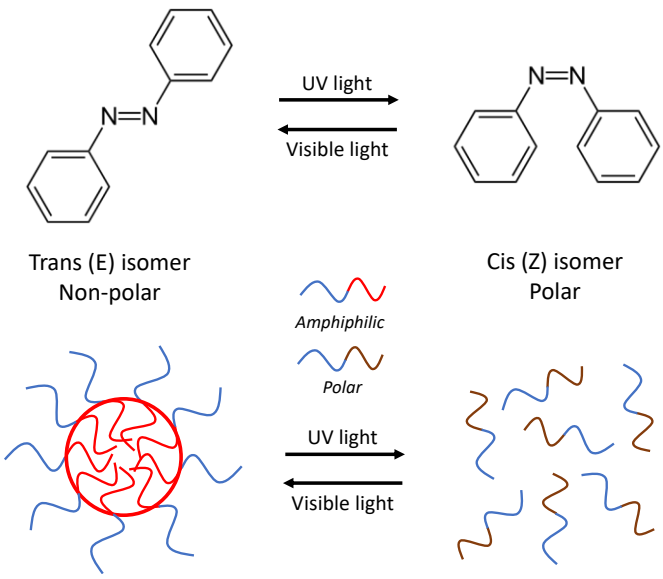

***Figure 1-5**: Chemical architecture change of azobenzene between its trans and cis isomers upon light irradiation (top), and schematic illustration of the disruption and formation of micelles from a copolymer containing azobenzenes (bottom).*

The ability to monitor the formation and destabilization of polymeric self-assemblies with light-sensitive moieties, either in a reversible or an irreversible way, can be applied for controlled encapsulation and delivery of an active (such as a drug or a fragrance) upon light irradiation [72,73].

Temperature sensitive polymers

Temperature sensitive polymers, also named as thermoresponsive polymers, are the most comprehensively studied smart polymers because of their reversible phase separation at a specific temperature [38,74]. Specifically, the polarity of this type of smart polymers is controlled by temperature, changing their solubility accordingly. Once a critical temperature is reached, often named as the cloud point temperature (CPT), the polymer-solvent interactions weaken and liquid-liquid phase separation (LLPS) takes place (*LLPS is further explained later in the introduction*). This critical temperature depends on the polymer structure as well as on the medium composition [75–77]. Therefore, both the polymer and the medium can be designed to tune the transition temperature [78].

Thermoresponsive polymers can be divided into two classes depending on their response to a temperature change: polymers that become insoluble above a critical temperature are called as LCST-type (Lower Critical Solution Temperature) [79,80], while polymers that lose their solubility below a critical temperature are named as UCST-type (Upper Critical Solution Temperature) [81,82]. LCST and UCST polymers are also known as "negative temperature-sensitive" and "positive temperature-sensitive", respectively [38].

The temperature and concentration dependence of these two classes of thermoresponsive polymers in solution can be represented in phase diagrams (**Figure 1-6**). In them, the phase boundary outlines the temperature and concentration where phase separation takes place. LCST polymers present a concave phase boundary while UCST polymers present a convex one. The critical temperature is defined as the extreme of the phase boundary – in other words, the minimum and the maximum temperatures of the phase separation boundary for LCST and UCST types, respectively [78].

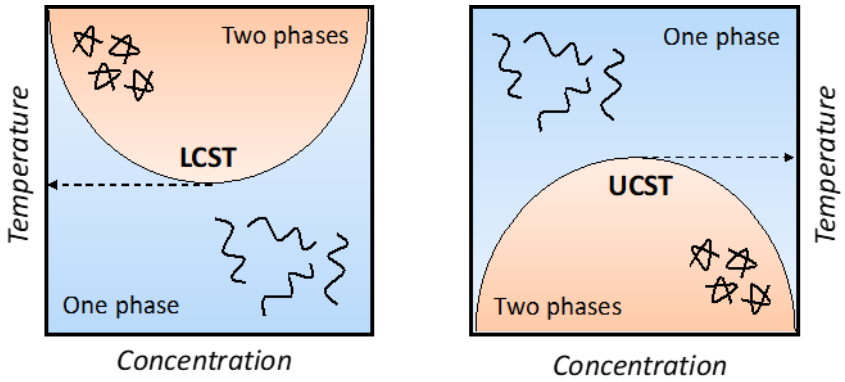

***Figure 1-6**: General phase diagrams of LCST (left) and UCST (right) thermoresponsive polymers in solution.*

Thermodynamics can be used to predict whether a polymer is soluble or not in a certain solvent at a specific temperature. The mixing enthalpy (ΔH_m) and the mixing entropy (ΔS_m) can be used to determine the Gibbs energy of mixing (ΔG_m) with the following equation: $\Delta G_m = \Delta H_m - T\Delta S_m$. A negative value of the Gibbs energy implies that the mixing of the polymer in that solvent is energetically favorable, while a positive value implies the opposite. To this regard, four different scenarios can be distinguished [78]:

1. Soluble polymer – the enthalpy is negative and the entropy is positive for all temperatures.
2. Insoluble polymer – the enthalpy is positive and the entropy is negative for all temperatures.
3. LCST polymer – both the enthalpy and the entropy are negative, so temperature determines the sign of the Gibbs free energy. If the temperature is above the critical value, the polymer is insoluble. Likewise, if the temperature is below this value, the polymer is soluble.
4. UCST polymer – both the enthalpy and the entropy are positive, so temperature determines the sign of the Gibbs free energy. Contrary to LCST polymers, if the temperature is below the critical value, the polymer is insoluble. Likewise, if the temperature is above this value, the polymer is soluble.

The critical temperature is so defined as the quotient of the enthalpy of mixing divided by the entropy of mixing.

The main application of thermoresponsive polymers is to combine them with another polymer and be able to control the amphiphilicity of the resulting copolymer with temperature. Depending on whether a LCST or a UCST type polymer is combined with a hydrophilic or a hydrophobic polymer, the copolymer amphiphilicity is gained below or above a critical temperature (**Table 1-1**). This critical temperature can be tuned by changing the polymer's architecture and composition [83,84], allowing to specify the temperature range at which the copolymer is amphiphilic. For instance, the critical temperature of a copolymer containing a LCST-type polymer can be decreased by combining it with a more hydrophobic polymer [85,86]. The temperature controlled amphiphilicity of these copolymers allows the reversible formation of self-assembled structures, offering the ability to encapsulate and release an active molecule (drug or fragrance) upon temperature variation. This phenomenon has been extensively used for biomedical applications [87], specially to design drug delivery systems with temperature responsiveness [88–90].

Thermosensitive copolymer	Below critical temperature	Above critical temperature
LCST + hydrophilic block	Soluble	Amphiphilic
LCST + hydrophobic block	Amphiphilic	Insoluble
UCST + hydrophilic block	Amphiphilic	Soluble
UCST + hydrophobic block	Insoluble	Amphiphilic

***Table 1-1**: Main combinations of a diblock copolymer with thermoresponsive behavior in water.*

Finally, multi-thermoresponsive polymers exhibiting two or more critical temperatures can be obtained by combining two or more LCST or UCST blocks in the same copolymer [78]. These copolymers show sequential transitions and stepwise turbidity changes according to their composition. On the one hand, a copolymer made of two LCST or two UCST blocks manifests amphiphilicity only in the temperature range between the two critical temperatures. Therefore, unimer-micelle-aggregate transitions are observed when increasing or decreasing the temperature of a copolymer with two LCST or two UCST blocks, respectively [91,92]. On the other hand, both LCST and UCST behaviors can be combined in the same copolymer, giving rise to the sometimes called "schizophrenic" copolymers [93,94]. Depending on whether the critical temperature of the LCST block is lower or higher than that of the UCST block , the copolymer undergoes either micelle-aggregate-micelle or micelle-unimer-micelle transitions, respectively [95,96].

1.3 Liquid-liquid phase separation

A homogenous system consists of a single phase, either gas, liquid, or solid. In homogenous solutions, one or more miscible components with favorable interactions between them coexist. However, de-mixing of these miscible components can become energetically favored at specific conditions due to a reduced interaction between solute and solvent molecules, despite the entropic loss ascribed to the formation of a two-phase system [97,98]. This is the case of a system made of vinegar and oil, in which the entropy is not enough to drive the system to a mixed state since the physical interactions between oil molecules and between vinegar ones are stronger. In the same way, once the interaction solute-solute is stronger than solute-solvent, phase separation takes place. It is important to remark that phase separation does not necessarily imply a phase transition (from liquid to solid, for instance). Among the different transformations of an homogeneous system, liquid-liquid phase separation (LLPS) is a reversible and thermodynamically driven process consisting in de-mixing a single phase into two distinct liquid phases with different solute concentrations [99,100]. The equilibrium between mixing and de-mixing depends not only on the components' concentrations but also on the environmental conditions, such as temperature, pH, pressure, etc. For instance, in the case of colloidal systems made of smart polymers in water, LLPS can take place by modifying the parameter to which the polymer is sensitive.

LLPS is a phenomenon commonly observed in nature, specifically in cells, which organize molecules in membrane-free organelles [98,101,102]. This sequestration provides temporal control over the recruitment or release of signaling molecules [103]. Moreover, the lack of membrane allows the molecular exchange with the environment, while their liquid-like nature allows molecular diffusion in its interior. The assembly and disruption of these micron-sized organelles is regulated by environmental conditions, adapting to the needs of the cell. The regulation of these LLPS domains is so important that its malfunctioning has been related to possible diseases [104]. At the same time, these membrane-less organelles formed through LLPS have been employed to assemble

synthetic/artificial cells. Since these droplets permit generating chemically enriched domains, they can be used to reproduce the interior of cells, selectively sequestrating biomolecules in liquid domains to favor biochemical reactions while ensuring facile matter exchange with the surrounding medium [105,106].

1.3.1 Simple and complex coacervation

The term coacervation was originally introduced back in 1911 [107], and later systematically studied from 1929 [108] to describe the associative phase separation for the system of gum arabic-gelatin. Later, coacervates were named in one of the first hypotheses on the origin of life on Earth, as Aleksandr Oparin explains in his famous book entitled *The Origin of Life* (1936). The main argument of the book is that life could possibly have been originated inside coacervates containing high concentrations of different organic molecules, since these liquid droplets form autonomously even in dilute conditions [109]. The compartmentalization ability of coacervates is still being discussed and studied as models of membranelles cell organelles [106,110–112].

Coacervation is a liquid-liquid phase separation (LLPS) that gives rise to the formation of a dense colloid-rich liquid phase, generally called coacervate, and a very diluted colloid-poor phase [113]. The formation of the coacervate phase is the result of a subtle balance between electrostatic and hydrophobic interactions, as well as hydrogen bonds, van der Waals forces and other weak interactions. If these interactions are feeble, coacervation is suppressed, and if they are strong, precipitation may occur [114]. The coacervate phase has certain properties that distinguish it from the original solution. For instance, the coacervate can remain as a turbid suspension of micro- or nano-droplets with stirring, or it can coalesce and form a liquid layer at the top or bottom of the solution, depending on its density (**Figure 1-7**). Additionally, the coacervate is usually more viscous, denser, and often has the property of adsorbing onto a surface, as well as absorbing other molecules with a lower solubility present in the system [115]. This latter feature has been leveraged to extract, concentrate,

and purify molecules from a solvent in a process known as coacervate-based extraction [116,117].

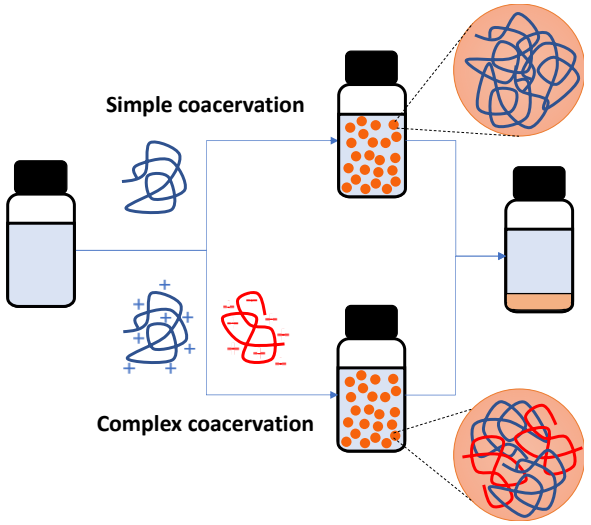

***Figure 1-7**: Schematic representation of simple and complex coacervation of macromolecules, such as polymers. Eventually, coalescence and liquid-layer formation take place.*

Coacervation has been broadly studied and divided into two different types: simple and complex coacervation [114,118–121] (**Figure 1-7**). Simple coacervation takes place in systems containing only one macromolecule (generally a polymer or a surfactant) that phase separates due to a decreased solvation, induced by the addition of some dehydrating agent, such as salts or alcohols, or a variation of environmental conditions, such as temperature or pH. The temperature from which coacervation takes place is generally known as the cloud point temperature (CPT), owing to the cloudy appearance that the sample acquires once the coacervate droplets are formed [122,123]. At one point, self-assembly occurs due to a combination of forces promoting inter-colloid interactions over colloid-solvent ones, including hydrophobic (mainly), electrostatic, and van der Waals. Simple coacervation also applies to single ionic macromolecules that self-assemble in solution due to the neutralization of its charges upon salt or alcohol addition [124]. On the other side, complex coacervation concerns the liquid-liquid phase separation of at least two ionic macromolecules with opposite charge, mainly driven by attractive electrostatic interactions. It typically takes place under conditions of electroneutrality, when

the two macromolecules neutralize each other, and their solubility is lost. Other weaker interactions such as van der Waals, hydrophobic, and hydrogen bonding, and parameters such as the molecular structure, concentration, mixing ratio, ionic strength, pH, and temperature also play an important role in the formation of complex coacervates [59,112].

Coacervates for active encapsulation and release

The ability of coacervates to absorb and contain molecules from the medium renders them as potential encapsulating agents. In fact, coacervation is often considered as the original method of encapsulation due to the use of this technique in 1955 by Green & Scheicher. Currently, coacervation is extensively used for the encapsulation and release of different compounds mainly in the food, pharmaceutical, and textile industries [125–130].

To form polymeric microcapsules either through simple or complex coacervation, a process is applied to a dilute polymer solution to reduce the solubility of the system and induce liquid-liquid phase separation. This process can be performed in an aqueous phase for the encapsulation of hydrophobic compounds or in the organic phase for the encapsulation of hydrophilic compounds. The consequent polymer-rich phase, or coacervate, is used to contain the compounds with poor solubility and protect them against environmental degradation. The general procedure to generate polymeric coacervates to be used as capsules can be summarized with the following steps [115]:

1. Select the polymer that presents the features needed for the desired application. This includes molecular weight, chemical structure, charge distribution, and degradability. To add the possibility of triggering the release of the compounds contained in the coacervates, smart polymers with sensitivity to a variation of temperature, pH, ionic strength, or light should be employed.
2. Select the solvent so that it dissolves the polymer but preferably not the compound to encapsulate. The insoluble or poorly soluble compound can

be either previously mixed with the polymer or added later while mixing the polymer solution.

3. Mix both the polymer and the solvent and induce the liquid-liquid phase separation of the polymer by either adding a non-solvent, a kosmotrope, another polymer with an opposite charge, or varying environmental conditions such as temperature, pressure, light, or pH. With stirring, the new conditions promote the formation of coacervate droplets, which are more viscous, but still fluid, and can be used as microcapsules. On the one hand, the phase-separated polymer can be deposited around the insoluble compound, leading to the formation of a shell and encapsulating it. On the other hand, if the coacervate nucleates and grows on its own, the insoluble compound is spontaneously concentrated in the coacervates due to preferred interactions with the polymer-rich phase than with the solvent.
4. If the stability of the coacervate droplets does not depend on the presence and composition of the polymer-poor phase, the solvent can be removed by evaporation and the microcapsules collected and rinsed to remove any unwanted solvents or excipients. Thermal desolvation and crosslinking can be used to "harden" these microcapsules, making them more stable and eliminating their dependence on the solvent.

Although simple coacervation can be used to generate microcapsules [131], complex coacervation has been more broadly studied and employed. This is mainly because encapsulation is easy to achieve through complex coacervation by controlling the pH and following a thermal, cross-linking, or desolvation technique to form a stable and resistant polymeric shell around the active molecule (**Figure 1-8**) [125,130]. This approach generates capsules with several advantages, including high payload efficiency, simplicity of preparation at room temperature, low cost, scalability, and reproducibility. However, since complex coacervation depends on electrostatic attraction, sensitivity to pH and ionic strength is a major limiting factor to its commercial application. Complex coacervation takes place within a narrow pH window, and so only compounds that are not sensitive to the coacervation pH can be encapsulated. Additionally,

the presence of salt can hamper the formation of complex coacervates due to charge screening, and so salt-free conditions are required [59].

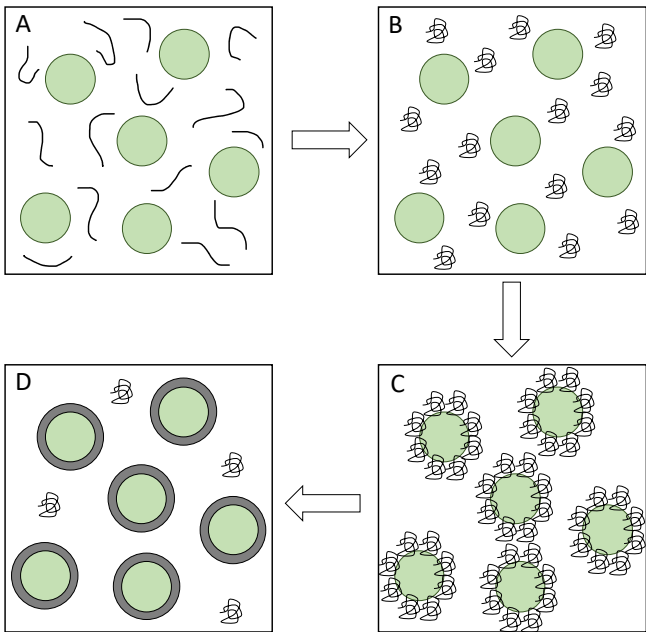

***Figure 1-8**: Schematic representation of coacervation and wall hardening to from core-shell capsules. The process involves four steps, including (A) the emulsification of the compound to encapsulate in a solution containing the shell forming polymer/s, (B) the coacervation of the polymer/s, (C) accumulation of the coacervates on the surface of the compound, and (D) addition of a cross-linking agent to generate a hard shell.*

Among the many applications of coacervates as encapsulating agents, textiles represent one of the most investigated ones [8,128]. Fragrances are commonly added to textile-related products to provide freshness and odor control [132]. However, they are generally volatile compounds that have a scarce affinity to fabric fibres, hence they do not remain for long deposited on textiles. Through encapsulation, fragrances can be protected from early degradation or evaporation and released on a later stage, thus prolonging the aroma sensation and improving consumer satisfaction [133]. Fragrance release can be triggered by a pressure, pH, or temperature difference, as well as by capsule degradation. Even though the encapsulation of fragrances is standardly obtained via polycondensation of melamine and formaldehyde [15], it can also be achieved through simple or complex coacervation [8].

1.4 PEG-g-PVAc – Poly(ethylene glycol) and poly(vinyl acetate) copolymer

Poly(ethylene glycol) (PEG), also known as poly(ethylene oxide) (PEO), is one of the most popular thermoresponsive homopolymers presenting a LCST-type profile. PEG is also broadly employed for biomedical and drug delivery applications due to its biocompatibility, stealth effect, and stearic stabilization properties [134,135]. This non-ionic polymer is based on oxyethylene groups, and so its water solubility at low temperatures comes from the hydration of the ether oxygens. However, the polymer-solvent hydrophilic interaction gradually weakens as temperature increases. Consequently, PEG becomes insoluble in water above a certain temperature and liquid-liquid phase separates (LLPS) from the medium. This phenomenon has previously been ascribed to a change in the conformation of the oxyethylene groups – at higher temperatures the polymer switches to a conformation that disfavors solubility and induces phase separation [123].

The temperature at which this LLPS takes place is generally known as the cloud point temperature (CPT) [122,123], and it depends both on polymer concentration and molecular weight [136,137]. Generally, the CPT of PEG is above the boiling point of water due to its high hydrophilicity, which hinders the study of its phase separation properties. Fortunately, since this phase separation has to do with the polymer-medium interaction, any additive which interacts with either the polymer or the water affects the CPT. In regard, several studies have taken place measuring the effect of different additives on the CPT of PEG in water solution [138–140].

Poly(vinyl acetate) (PVAc) is a thermoplastic polymer that presents a poor water solubility. PVAc is mainly used in the construction and adhesive industries [141–143]. Since PVAc has been approved by the FDA and added to the inactive ingredient database [144], this polymer has potential applications in the fields of food, biomedicine, cosmetics, and detergency. Currently, it has several applications in the food industry, being a major component of chewing gums. Even though its poor water solubility is an obstacle to its biodegradation, PVAc

swells when exposed to water, facilitating the degradation by biologically active substances and microbes [145].

Over the years, PEG has been extensively conjugated with hydrophobic polymers to obtain amphiphilic copolymers with self-assembly properties. For instance, PEG has been conjugated with poly(propyleneoxide) (PPO) to generate the pluronic or poloxamer family [146–148], but also with poly(N-isopropylacrylamide) (PNIPAM) [149–151], polycaprolactone (PCL) [152–154], poly(N-vinylcaprolactam) (PVCL) [155,156], and poly(lactic-co-glycolic acid) (PLGA) [157,158], to name a few. As explained below, PEG has also been conjugated with PVAc to give raise to a very interesting set of amphiphilic thermoresponsive copolymers.

1.4.1 PEG-g-PVAc

This thesis leverages the properties of the amphiphilic thermoresponsive graft copolymer resulting from the conjugation of PEG with PVAc. Specifically, a poly(ethylene glycol)-g-poly(vinyl acetate) copolymer (PEG-g-PVAc, Mw = 18.100 Da) consisting of a comb-like macromolecular structure with a 6000 Da PEG backbone and a grafting point every ~50 units of ethylene glycol (~1-3 grafted PVAc chains per backbone) (**Figure 1-9**).

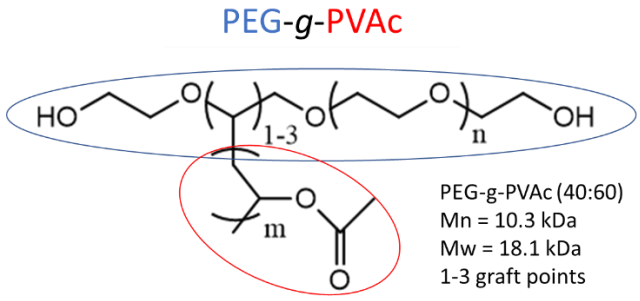

***Figure 1-9**: Chemical structure of the PEG-g-PVAc copolymer used throughout this thesis.*

Graft copolymers, consisting of a backbone and side chains, present interesting properties in solution that can differ from linear diblock copolymers with the same composition [159,160]. They have been found to form a variety of self-assembled aggregates in water and organic solvents, which depend on the hydrophilic/hydrophobic features of the backbone and side chains [34,35,161–163]. Specifically, PEG-g-PVAc's self-assembly properties depend on the balance between the hydrophobic PVAc grafts and the hydrophilic PEG backbone, as well as on the number and length of the PVAc grafts.

The self-assembly properties of a similar PEG-g-PVAc (Mw = 13.100 Da, 1-2 grafting points every ~100 units of ethylene glycol) in water have been reported in the recent past, showing the formation of single-chain nanoparticles (SCNPs) at concentrations below 10% w/w [164], and a progressive structuration of the SCNPs into hierarchically complex systems when increasing the concentration up to 90% w/w [165]. The thermoresponsivity and LCST profile of this PEG-g-PVAc was also demonstrated, reporting a critical temperature of 58 °C for a concentration of 1% w/w [164].

PEG-g-PVAc's self-assembly was further investigated in formulations containing surfactant mixtures [166], identifying a region with LLPS at room temperature. Interestingly, this LLPS gave rise to micron-sized coacervates, whose size and stability against coalescence depend on the composition of the aqueous medium. Moreover, these coacervates were able to confine different active principles to a larger extent than simple micelles could, including the hydrophobic poly(dimethylsiloxane) bis(3-aminopropyl) and the hydrophilic (Z,Z)-disodium distyryl-biphenyl disulfonate. This work did not only open the door to the application of PEG-g-PVAc coacervates as encapsulating agents, but also built the bases to perform all the research described in this thesis.

Industrial relevance

On the industrial side, PEG-g-PVAc has attracted interest as detergent additive for the formulation of home and beauty care products. The benefit it provides is double: first, due to its adsorption properties, it promotes a reduction of soil redeposition on garments, especially in hard water conditions [167–169]; second, its capacity to encapsulate compounds with different hydrophilicities in a surfactant-rich medium is a very interesting property which can be exploited to extend the life-time of fragrances and boost product performance. The application of PEG-g-PVAc self-assemblies for the encapsulation of fragrances has recently been studied in the absence of surfactant [170,171], showing that the individual properties of each fragrance molecule are very important, since they affect the structure of the copolymer assemblies and their phase behavior in ternary (i.e. PEG-g-PVAc/fragrance/water) systems.

Home and beauty care formulations are rich in surfactants and salts, among other additives, which can destabilize conventional self-assembled structures [21,22]. Therefore, in this thesis, PEG-g-PVAc coacervation has been studied in model aqueous formulations containing surfactants and salts, developing a thorough understanding and control of the formation, composition, and destabilization of these polymeric microdomains in such complex formulations.

1.5 Kosmotropes, chaotropes, and ion-specific effects

More than a century ago the Czech scientist Franz Hofmeister reported that ions affect in different ways the solubility of egg white protein in water [172]. He proposed the famous Hofmeister series ranking the ability of cations and anions to stabilize (salting-in effect) or precipitate (salting-out effect) that protein. On the one hand, salting-in is caused by the interaction of weakly hydrated ions with the solute, which increases its solubility. On the other hand, salting-out results from the effect of strongly hydrated ions on the solute solubility, removing water molecules from the solute surrounding and dehydrating it [173]. The greatest effect is ascribed to the most strongly hydrated anions for salting-out and to the most weakly hydrated ones for salting-in. Anions reportedly render a more pronounced effect than that exhibited by cations, although the specific salt effects on the solute solubility are a cumulative result of both the anion and cation [174]. It was soon realized that the effects described in this series, or more correctly "specific ion effects", do not only apply to aqueous protein solutions.

Salts dissolved in water dissociate into hydrated ions which electric field causes the dipolar water molecules to rearrange themselves and form a hydration shell around them. Consequently, the water structure of the hydration shell differs from that of bulk water, providing it with a different density [175]. From here, the terms "water structure making" and "water structure breaking" have been applied to various ions [176], depending on their interaction with water and the consequent formation of the hydration shell. The terms "kosmotrope" (from Greek κοσμος, order) and "chaotrope" (from Greek χαος, disorder) have been used as the equivalent of structure makers and breakers, respectively, generally accepted and applied by the scientific community. Kosmotropes are normally related to a salting-out effect in aqueous environments, while chaotropes are related to a salting-in effect. However, some publications have challenged the generalized use of these terms and emphasize the ion-specific effect [177–180].

During the last decades, the ion specificity effects have been extensively studied due to their high impact in biological and physicochemical science [181,182],

leading to the belief that specific ion effects are ubiquitous in both aqueous and non-aqueous media [183]. Although the validity of the terms kosmotrope and chaotrope has been reaffirmed for dilute solutions [184–186], the effect of these ions over the solubility of a complex system with one or more solutes cannot be solely described by the hydration capacity of these in the bulk solution. Instead, the cross-effects and interplay between all existing components (ion-water, ion-solute, solute-water, ion-ion, solute-solute, and water-water) must be considered [174,187]. Each of these specific interactions can contribute directly or indirectly to the solute stability in solution.

Considering this, the terms “kosmotrope” and “chaotrope” are merely used as jargon throughout this thesis to easily categorize different additives. These terms do not entirely describe their interaction with the chosen copolymer nor the effect they have on its solubility. The mechanism of action of each additive is described in the results section (*3.2 Effect of additives on the LLPS of PEG-g-PVAc*), where ion-specific effects are considered.

2. MATERIALS AND METHODS

In this chapter, I mention the materials and instrumentation used for the experimental research and report the methodology followed to obtain the results of this work. The outcomes are extensively described and discussed in the next chapter of this thesis.

2.1 Materials

The materials selected for this project are commonly found in beauty and home care products, and can be divided into seven categories:

1. Polymer (see chemical structure in **Figure 2-1**):
    - Poly(ethylene glycol)-graft-poly(vinyl acetate) (PEG-g-PVAc) is a non-ionic amphiphilic grafted copolymer from BASF. It has been provided by Procter & Gamble throughout the whole project. The PEG/VAc weight ratio is 40/60, with a M_n = 10.3 kDa and a M_w = 18.1 kDa (thus, with a polydispersity index (PDI) of 1.8). This copolymer has approximately one grafting point every 50 units of ethylene glycol, meaning that there are ~1-3 grafted PVAc chains per PEG backbone (which is of 6 kDa). PEG-g-PVAc was covalently labelled with rhodamine B isothiocyanate, according to a previously described procedure [166], so that it could be observed under the fluorescence confocal microscope.

Surfactant synthesis generally produces surfactants with different chain lengths. This implies that in the same batch there could be surfactants with varying hydrophilicities that will interact differently with the copolymer. The details of the suppliers regarding the chain length distribution have been mentioned below. We must also consider there could be isomers in the product that interact differently with the copolymer too. This latter case is likely the one of HLAS, which benzene sulfonate group can be linked to different carbons of the alkyl chain. Since we have used the products as received, without any further purification, the results come from the combination of the effects of all the surfactants present in the same batch, including different chain lengths and the possibly present isomers.

2. Non-ionic surfactants (see chemical structure in **Figure 2-1**):
    - Neodol 45-7 (N45-7) is a primary alcohol ethoxylate, with the non-polar part consisting of an alkyl chain of 14-15 carbon atoms and the polar part consisting of 7 ethoxylate groups (C14-15 EO7). It has a molecular weight of 519-573 g/mol, and it is from Shell Chemical.
    - Surfonic L24-9 (L24-9) is also a primary alcohol ethoxylate, with an alkyl chain length of 12-14 carbon atoms attached to 9 ethoxylate groups (C12-14 EO9). It has a molecular weight of 582-610 g/mol, and it is from Huntsman.

3. Ionic surfactants (see chemical structure in **Figure 2-1**):
    - SOLFODAC AC-3-H (HLAS) is a linear alkylbenzene sulfonate anionic surfactant with an alkyl chain length of 10-13 carbon atoms. It was acquired from Tellerini s.p.a with a molecular weight of 312-360 g/mol.
    - Tensagex EOC970B (AE3S) is a sodium lauryl ether sulphate anionic surfactant with an alkyl chain length of 12 carbon atoms and 3 ethoxylate groups. An aqueous solution of this surfactant (70%) was acquired from KLK Tensachem S.A with a molecular weight of 420 g/mol.
    - Cetyltrimethylammonium bromide (CTAB) is a cationic alkyltrimethylammonium bromide surfactant with an alkyl chain length of 16 carbon atoms. It was acquired from Sigma-Aldrich with a molecular weight of 364.5 g/mol and purity above 99%.
    - Cetyltrimethylammonium chloride (CTAC) is a cationic alkyltrimethylammonium chloride surfactant with an alkyl chain length of 16 carbon atoms. It was acquired from Alfa Aesar with a molecular weight of 320 g/mol and purity of 96%.
    - Dodecyltrimethylammonium bromide (DTAB) is a cationic alkyltrimethylammonium bromide surfactant with an alkyl chain length of 12 carbon atoms. It was acquired from Sigma-Aldrich with a molecular weight of 308.3 g/mol and purity above 98%.
    - Dodecyltrimethylammonium chloride (DTAC) is a cationic alkyltrimethylammonium chloride surfactant with an alkyl chain length of 12 carbon atoms. It was acquired from Sigma-Aldrich with a molecular weight of 263.9 g/mol and purity above 98%.

4. Kosmotropes (see chemical structure in **Figure 2-1**):
    - Trisodium citrate dihydrate (NaCit) is a sodium salt of citric acid. It was acquired from Jungbunzlauer with a molecular weight of 294.1 g/mol and purity above 98%.
    - Sodium chloride (NaCl) was acquired from Sigma-Aldrich with a molecular weight of 58.4 g/mol and purity above 99%.
    - Sodium bromide (NaBr) was acquired from Sigma-Aldrich with a molecular weight of 102.9 g/mol and purity above 99%.

5. Chaotropes (see chemical structure in **Figure 2-1**):
    - Monopropylene glycol (MPG) is a water miscible diol. It was acquired from INEOS Oxide with a molecular weight of 76.1 g/mol.
    - Urea is a carbonyl group with two carbon-bound amine groups. It was acquired from VWR International with a molecular weight of 60.1 g/mol.
    - Sodium cumene sulfonate (NaCS) is an anionic hydrotrope. An aqueous solution (40%) was acquired from Sasol, with a molecular weight of 222.2 g/mol.

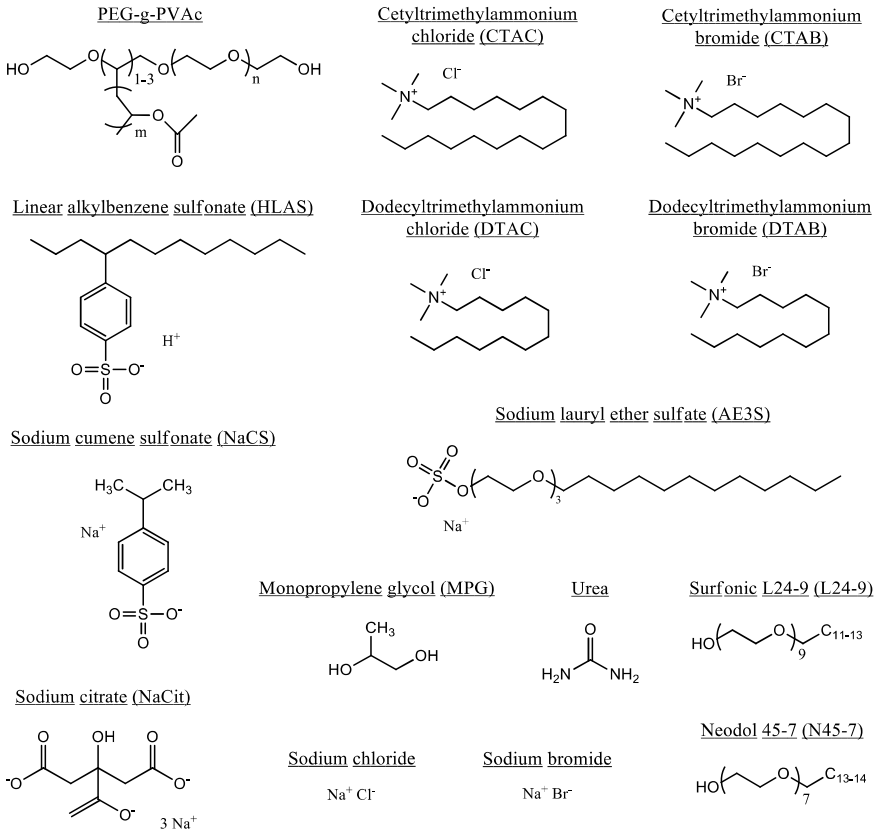

***Figure 2-1**: Chemical structure of the copolymer, surfactant, kosmotropes and chaotropes used throughout this work.*

6. Fragrances (see chemical structure in **Figure 2-2**):
    - Phenyl ethanol, with a molecular weight of 122.16 g/mol, has an octanol/water partition coefficient of 1.36.
    - Carvone, with a molecular weight of 150.22 g/mol, has an octanol/water partition coefficient of 2.74.
    - Linalool, with a molecular weight of 154.25 g/mol, has an octanol/water partition coefficient of 2.97.
    - Florhydral, with a molecular weight of 190.29 g/mol, has an octanol/water partition coefficient of 3.02.
    - Citronellol, with a molecular weight of 156.27 g/mol, has an octanol/water partition coefficient of 3.3.

- Pinene, with a molecular weight of 136.24 g/mol, has an octanol/water partition coefficient of 4.44.
- Limonene, with a molecular weight of 136.24 g/mol too, has an octanol/water partition coefficient of 4.57.

All fragrances were provided by Procter&Gamble):

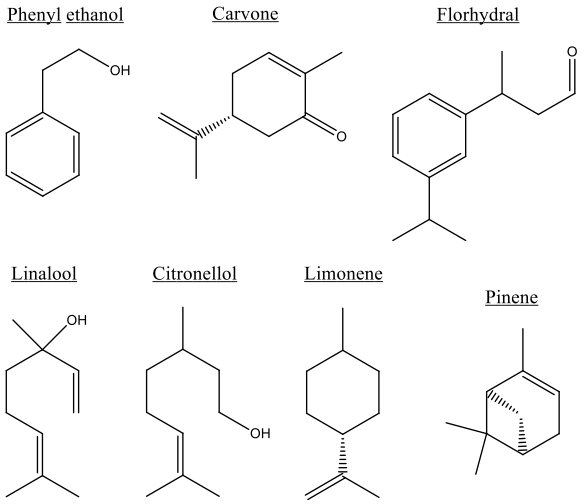

***Figure 2-2**: Chemical structure of the fragrances used throughout this work.*

7. Others
    - Rhodamine B isothiocyanate (RBITC) is a red fluorescent hydrophobic dye. It was acquired from Sigma-Aldrich, with a molecular weight of 536.08g/mol.
    - Rhodamine 110 chloride (R110C) is a green fluorescent hydrophilic dye. It was acquired from Sigma-Aldrich, with a molecular weight of 366.80 g/mol.
    - Coumarin6 is a green fluorescent hydrophobic dye. It was acquired from Sigma-Aldrich, with a molecular weight of 350.43 g/mol.
    - Water of MilliQ grade (18.2 MΩ.cm at 25 °C).

All materials were used as received without any further purification.

2.2 Methods

The methodology of this work was designed to provide relevant information to the consumer good industry. We focused on understanding and controlling the conditions inducing the coacervation of PEG-g-PVAc, assessing the potential of the generated microdomains as encapsulating agents of active principles, and studying the ways to trigger their destabilization and consequent release of the contained actives.

2.2.1 Sample preparation

For all samples, the copolymer PEG-g-PVAc, a wax-like solid with a melting point above room temperature, was firstly warmed at 70 °C for better manipulation. Then, appropriate amounts of molten PEG-g-PVAc, water, and the selected components for the study were weighted in a glass vial with an analytical balance (Mettler Toledo XSR603S, accuracy of ±1 mg). The samples were then mixed with a magnetic stirrer until a homogeneous dispersion was obtained.
PEG-g-PVAc concentration was kept at 1% w/w unless otherwise stated.

To map the phase behavior of PEG-g-PVAc with NaCit and N45-7 (**Figure 3-8**), five samples were prepared in glass vials containing a fixed amount of PEG-g-PVAc (1% w/w) and varying amounts of non-ionic surfactant N45-7 (1, 5, 10, 15 and 20% w/w) in water. After dissolving the copolymer and the non-ionic surfactant, the samples were titrated with sodium citrate while mixing at room temperature. All samples got cloudy after enough NaCit was added to induce LLPS (**Table 2-1**), and optical microscopy was then used to check the presence of coacervates (**Figure 6-4**). Then, more NaCit was added to achieve a liquid-liquid bulk phase separation (**Table 2-1**).

Initial concentrations (% w/w)		NaCit for LLPS	NaCit for bulk phase
PEG-g-PVAc	*N45-7*	(% w/w)	separation (% w/w)
1.0	1.0	4.8 ± 0.2	10.7 ± 0.5
1.0	5.0	3.8 ± 0.2	9.9 ± 0.5
1.0	10	2.4 ± 0.1	9.1 ± 0.5
1.0	15	1.0 ± 0.1	8.3 ± 0.4
1.0	20	/	7.4 ± 0.4

Table 2-1: *Initial concentrations of the five samples used to study the phase behavior of PEG-g-PVAc (**Figure 3-8**), and corresponding concentrations of NaCit necessary to achieve LLPS and liquid-liquid bulk phase separation.*

2.2.2 Turbidimetry

The Cloud Point Temperature (CPT) was determined by turbidimetry using a Crystalline Particle Viewer, from Technobis. However, its four real time particle viewers were not operative; thus, we could only use the instrument for turbidity measurements with temperature control. The samples were analyzed in standardized glass vials of 8 mL, measuring transmittance at 623 nm between 20 °C and 90 °C, with a heating rate of 0.5 °C/min and a cooling rate of 5 °C/min, while mixed with a magnetic stirrer at 800 rpm. The CPT was considered as the temperature corresponding to 50% transmittance with respect to the initial and final values. Each measurement was repeated at least three times.

The CPTs of aqueous solutions of PEG-g-PVAc at different concentrations (0.25, 0.5, 1, 2, 3, 4, 6, 10% w/w, see **Figure 3-3**) were first measured to reveal the LCST-type profile of the copolymer and determine its critical temperature of 51 °C, found for 1% w/w (approximately $5.5x10^{-4}$ mol/L).

Since the effect of ionic surfactants on the CPT is so strong, samples were prepared in a different way. In this case, a 0.1% w/w solution of the specific ionic surfactant was dropwise added to a sample of 1% w/w PEG-g-PVAc and then mixed until homogenous. The CPT was measured after every addition. At higher concentrations, samples containing HLAS, AE3S, CTAB, or CTAC showed a marked Tyndall effect that prevented measuring properly the CPT at temperatures higher than 66 °C.

2.2.3 Optical microscopy

The optical pictures were acquired using an optical microscope from ZEISS, model AXIO Imager A1, with an Axiocam 305 color camera from ZEISS as well, while using dry objectives of 10x/0.30 and 40x/0.75. Samples were placed between glass slides to delay water evaporation.

2.2.4 Fluorescence Confocal Microscopy

Fluorescence confocal microscopy imaging was carried out using a Leica TCS SP8 DMi8 confocal microscope. Rhodamine B isothiocyanate (RBITC) and rhodamine 110 chloride (R110C) were excited with an OPSL laser at 552 nm and 488 nm,

respectively, while Coumarin6 was excited with an Argon laser at 458 nm. The fluorescence emission was acquired using a hybrid SMD detector for a spectral window of 40 nm, starting from a wavelength 20 nm higher than the excitation wavelength. Dry objectives of 20x/0.75 and 40x/0.60 were used to image all samples, which were placed in an 8-well device (Lab-Tek Chambered 1.0 Borosilicate Coverglass System, Nalge Nunc International). The concentrations of fluorophore used for the samples assessed under the fluorescence confocal microscope were ≈0.01% w/w of rhodamine B isothiocyanate-labelled PEG-g-PVAc, ≈0.01% w/w of rhodamine 110 chloride, and ≈0.005% w/w of Coumarin6. All samples were observed under the microscope one day after preparation.

2.2.5 Confocal Raman Microscopy

Raman spectra were acquired with a Renishaw inVia Qontor Confocal Raman Microscope (Renishaw software WiRE v.5.2), using a 532 nm excitation laser (Nd:YAG solid state type, 50 mW, 1800 l/mm grating, working at 50% intensity), and a Renishaw Centrus 1UTR57 detector. A dry objective 50Lx/0.5 was employed for all samples, which were previously deposited on a silicon substrate to avoid detecting Raman scattering from the background and covered with a glass slide to delay water evaporation. Samples were observed with the front-illuminated CCD camera (256 × 1024 px). The exposure time was set to be 10 s for individual spectra acquisitions and 1 s for the two-dimensional intensity maps, which we rebuilt from spectra acquired every 0.5 µm along both x and y directions. The confocal microscope (Leica DM 2700) was crucial to peak the regions of interest for acquiring the Raman spectra of the medium, the LLPS microdomains, and the precipitated copolymer. High-confocality mode was used for all measurements.

According to Renishaw, the laser spot size is <1 µm. Then, according to the Mark Wainwright Analytical Centre [188], the Renishaw inVia Qontor Confocal Raman Microscope laser spot size is around 1.5 µm at 50x magnification for standard mode. However, a smaller spot size of 0.5 µm is possible when using confocal mode, the one used during our studies.

Since N45-7 and PEG-g-PVAc share some functional groups, their Raman profiles are similar (**Figure 6-6**), with main peaks in the region between 2800 and 3100 cm^{-1} (corresponding to C-H bonds' stretching). Therefore, the identification of N45-7 is challenging in an environment rich in PEG-g-PVAc. The largest difference

between the two profiles is found on the shoulder of N45-7 at 2852 cm^{-1}. On the other side, the relatively intense peak at 1730 cm^{-1} arises from the C=O vibration of the ester group of PVAc, clearly not present for N45-7. Based on these differences, we were able to distinguish the presence of PEG-g-PVAc from N45-7.

A set of reference samples for PEG-g-PVAc in water (5, 10, 15, 20, 25% w/w) and N45-7 in water (3, 6, 9, 12, 15% w/w) were measured through confocal Raman microscopy to get the calibration curves and assess the PEG-g-PVAc/water and N45-7/water mass ratios, respectively. At least five spectra were acquired for each sample, focusing the beam on different spatial spots. To build the calibration curves, three peaks from the Raman profiles of the PEG-g-PVAc solutions (1730, 2893, and 2940 cm^{-1}) and three peaks from the N45-7 solutions (2852, 2887, and 2922 cm^{-1}) were considered. After normalizing all Raman spectra to the peak of water (at 3420 cm^{-1}), the intensities of each of the three peaks selected for PEG-g-PVAc and each of the three peaks selected for N45-7 were determined. The average intensity value of each sample, together with its standard deviation, was used to plot the calibration curves, reported in **Figure 6-7A** (for PEG-g-PVAc) and **Figure 6-7B** (for N45-7). These curves were then used to infer the PEG-g-PVAc/water and N45-7/water mass ratios of other samples. It is important to notice that the values obtained are not absolute but relative – ratios of PEG-g-PVAc/water and N45-7/water.

2.2.6 Microfluidics

Samples with RBITC-labelled PEG-g-PVAc coacervates (red) and aqueous solutions containing R110C (green) were poured in two different glass syringes (Hamilton gas tight #1001, 1 mL). These were placed on a Nemesys Syringe Flow Pump to push the sample through PTFE-based tubes (outer diameter of 1/16" and inner diameter of ≈300 µm) and finally reach the microfluidics chip.

The microfluidics chips were made of polydimethylsiloxane (PDMS), a hydrophobic polymer commonly used to fabricate this kind of chips due to its excellent mechanical and optical properties, with minimal background and autofluorescence [189]. Moreover, it is inert, non-toxic, and non-flammable. The procedure to fabricate the meander-type chips was the following:

1. Design the architecture of the microfluidics chips using a software to later stamp it through photolithography on a silicon wafer, which will be used as a mold (*this part was done by another research group*).
2. Mix 55 g of PDMS with 5 g of curing agent (Sylgard 184) for at least 30 seconds. Later, degas it under soft vacuum for at least 30 minutes.
3. Prepare a recipient with aluminum foil to hold the PDMS mixture on top of the non-adherent silicon wafer. Be careful to do not let any hole in the recipient or the PDMS mixture will flow out.
4. Gently cast the PDMS mixture on the silicon wafer surrounded by the aluminum foil and cure it at 80 °C for 2 hours.
5. Let it cool down at room temperature for 30 minutes before uncasting the solid PDMS from the silicon wafer.
6. Cut the chips with a bistoury and punch holes with biopsy punchers of 1 mm diameter on a clean, flat and soft plastic surface. Residues of PDMS can be later removed with tape. Additionally, the chips can be rinsed with isopropanol in ultrasound to clean them further. In the latter case, the solvent must be carefully evaporated after the ultrasounds.
7. Add clean glass coverslips (50x24 mm, 170 µm thick) and the chips in a plasma cleaner. Carefully connect the vacuum pump and switch on plasma for 30 seconds. Then, put in contact the top parts of the cover glasses and the chips to seal them.
8. Cure the sealed chips at 60 °C for 30 minutes to finish sealing.

The MAESFLO 3.3.1 software was used to control the flow rate, which values were changed between 0.01 and 0.1 µL/s depending on the viscosity of the sample. The meander-type chips employed to assess PEG-g-PVAc coacervates had only one entrance and one exit, and their dimensions can be found in the annex (**Figure 6-10**).

The procedure consisted of first flowing the sample with PEG-g-PVAc coacervates to hold some of them in the traps of the meander chip. Then, the flow of the sample with coacervates was stopped to allow the entrance of water. Fluorescence confocal microscopy was used to observe the microfluidics chip and distinguish the destabilization of the coacervates (in red) after the arrival of the water solution (in green).

2.2.7 UV-Vis spectrophotometry

An Agilent Cary 3500 UV-Vis spectrophotometer with a multicell (8x samples) holder was employed to measure the absorbance of samples containing Coumarin6 (≈10 mg/mL) between 350 and 650 nm at room temperature. The supernatants of the previously centrifuged samples were poured in PMMA semi-micro cuvettes of 1.5 mL with a path length of 1 cm.

A Neya 16R with a Neya Rotor A24-2 was used to centrifuge Eppendorfs containing no more than 2 mL sample in order to separate all the LLPS PEG-g-PVAc (including the coacervates) from the solution. To determine the optimal centrifuging speed, different Eppendorfs containing the same reference sample (1% w/w PEG-g-PVAc, 5% w/w N45-7, 5% w/w NaCit, and ≈10 mg/mL Coumarin6) were centrifuged for 10 minutes at different speeds (500, 1000, 1500, 2500, 5000, 10000, and 15000 rpm). The absorptions of the supernatants were then evaluated with the UV-Vis spectrophotometer (**Figure 6-12**) and it was decided to perform the release experiments centrifuging at 10000 rpm for 10 minutes.

3. RESULTS AND DISCUSSION

3.1 Liquid-liquid phase separation of PEG-g-PVAc

The results presented in this thesis follow and extend the experimental work performed by Arianna Bartolini and Paolo Tempesti in our laboratory to understand the liquid-liquid phase separation (LLPS) of the copolymer PEG-g-PVAc (**Figure 1-9**). According to their published work [166], the LLPS of PEG-g-PVAc can give rise to four different scenarios, depending on the concentration of salts and surfactants. These four scenarios can be identified as:

1. No LLPS, the copolymer is dispersed in the continuous phase
2. LLPS of PEG-g-PVAc takes place, producing micron-sized coacervates rich in copolymer, while the continuous phase is depleted of it
3. LLPS of PEG-g-PVAc takes place, producing micron-sized coacervates like in scenario 2 but with inner polymer-depleted sub-domains
4. LLPS of polymer-depleted micron-sized coacervates in a polymer-rich continuous phase

Following the instructions of this publication, these four different scenarios were reproduced in water by mixing PEG-g-PVAc with different concentrations of sodium citrate (NaCit), non-ionic surfactant (N45-7), and anionic surfactant (HLAS). The specific concentrations are shown in **Table 3-1**.

	Formulation 1	**Formulation 2**	**Formulation 3**	**Formulation 4**
H_20	99	79	79	79
NaCit	-	5	5	5
N45-7	-	15	9	4
HLAS	-	-	6	11

***Table 3-1**: Concentrations in w/w % of the different samples prepared to reproduce the four phases of PEG-g-PVAc, as described in Bartolini's paper* [166].

The concentration of PEG-g-PVAc used in their work was 5% w/w. However, we noticed that at this concentration much PEG-g-PVAc was remaining dispersed in the continuous phase even after inducing LLPS; this was due to the different

molecular weight of the copolymer, coming from a distinct batch despite nominally being the same copolymer. Instead, when reducing the concentration to 1% w/w, the amount of PEG-g-PVAc in the medium became negligible. This can be clearly observed in the fluorescence confocal microscope pictures shown in **Figure 3-1**, where PEG-g-PVAc appears in red due to its covalently labelled rhodamine B isothiocyanate (RBITC) (see section 2.1 Materials for further details).

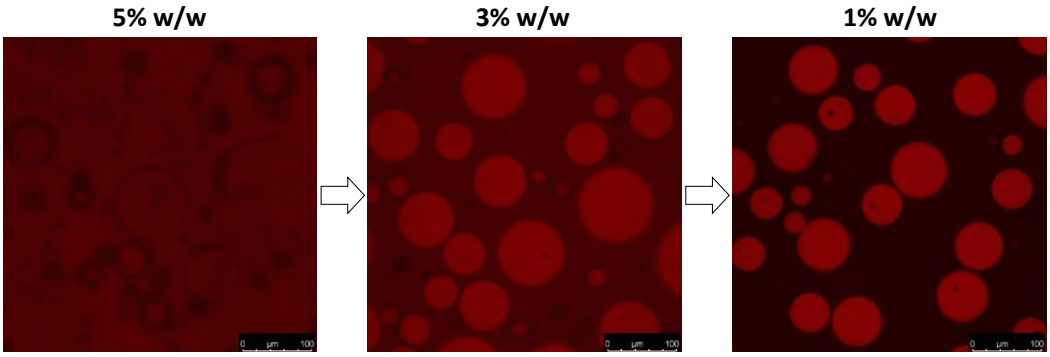

***Figure 3-1**: Fluorescence confocal microscopy pictures showing the effect of reducing the RBITC-labelled PEG-g-PVAc concentration in a sample presenting coacervation.*

Therefore, we decided to work with a PEG-g-PVAc concentration of 1% w/w and reproduce the four different scenarios described in their paper, as shown in **Figure 3-2**.

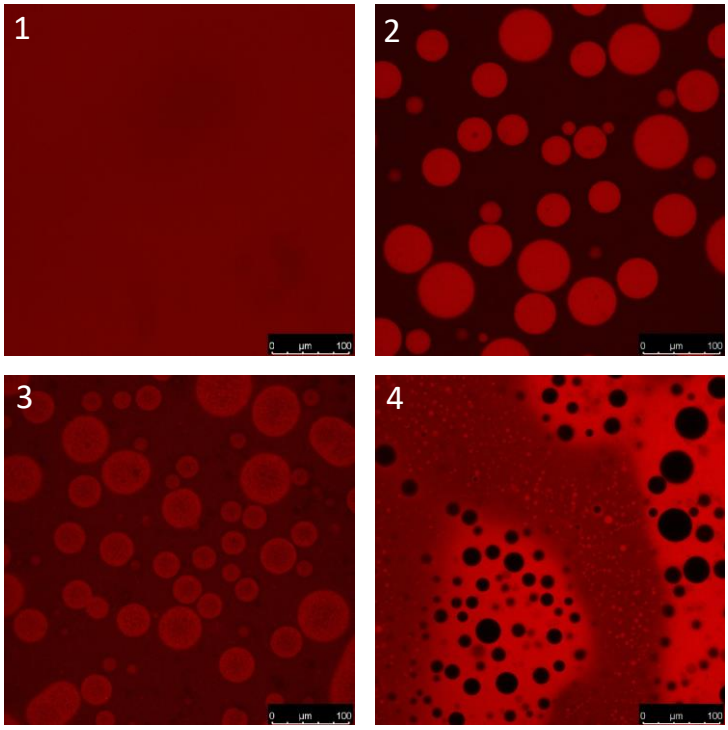

***Figure 3-2**: Fluorescence confocal microscopy pictures of all four different scenarios of RBITC-labelled PEG-g-PVAc's LLPS.*

These first experiments were instrumental to better understand the LLPS of PEG-g-PVAc by use of salts and surfactants. Among all four different scenarios, the SAMCAPS project was focused on the PEG-g-PVAc micron-sized coacervates that appear in the presence of sodium citrate, N45-7, and the absence of HLAS, due to their capacity to encapsulate active principles. Therefore, this thesis focused on understanding and controlling the formation and stability of the coacervates that appear in scenario 2.

3.2 Effect of additives on the LLPS of PEG-g-PVAc

PEG-g-PVAc is a thermoresponsive polymer that liquid-liquid phase separates (LLPS) from the medium once a critical temperature is reached. Previous studies demonstrated that the critical temperature of thermoresponsive copolymers is affected by the presence of other compounds such as kosmotropes, chaotropes, non-ionic and ionic surfactants [138–140,190]. To this regard, the first step was to determine which compounds increase and which decrease the critical temperature of PEG-g-PVAc.

First, the Cloud Point Temperature (CPT) of water solutions of PEG-g-PVAc at different concentrations (0.25, 0.5, 1, 2, 3, 4, 6, 10% w/w, **Figure 3-3**) were measured, revealing the LCST-profile of this copolymer, with a critical temperature of 51 °C at 1% w/w. This concentration, corresponding to approximately $5.5x10^{-4}$ mol/L, was chosen to investigate the effect of selected additives. Non-ionic surfactants based on ethylene oxide groups also show LLPS above a critical temperature [114,121]. Therefore, the CPT of water solutions of the two non-ionic surfactants used throughout this study at different concentrations (0.5, 1, 5, 10, 15, 20% w/w, **Figure 3-3**) were also measured.

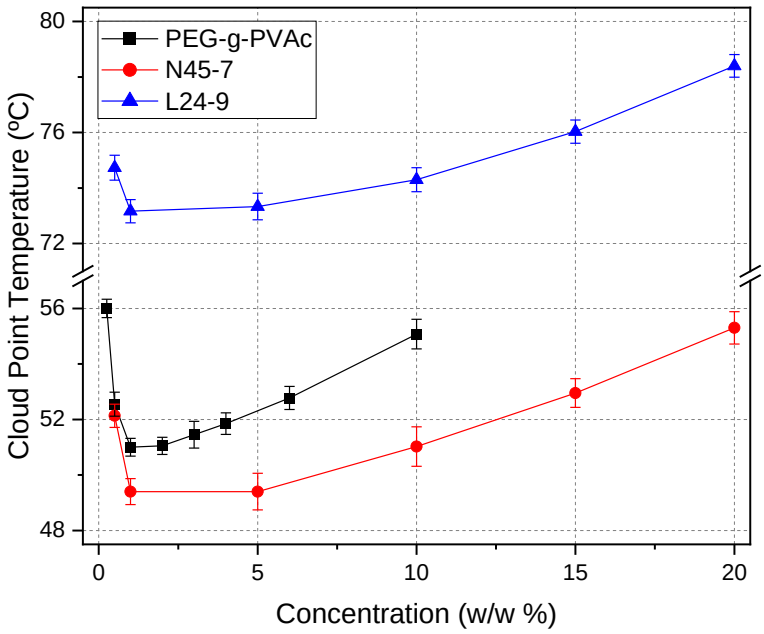

***Figure 3-3**: Evolution of the cloud point temperature of the copolymer PEG-g-PVAc and the non-ionic surfactants Neodol 45-7 and Surfonic L24-9 according to their concentrations in water. All three components show a Lower Critical Solution Temperature (LCST) profile. There is a cut in the scale of the Y axis for ease of comparison.*

The selected additives include kosmotropes (1), chaotropes (2), non-ionic surfactants (3), and ionic surfactants (4) that are commonly used in beauty and home care formulations. Since the concentrations used for industrial formulations are normally reported in w/w %, the results are hereby reported in the same units. The first group includes sodium citrate (NaCit), sodium chloride (NaCl), and sodium bromide (NaBr). The second group covers sodium cumene sulfonate (NaCS), monopropylene glycol (MPG), and urea. Then, the third group includes Neodol 45-7 (N45-7) and Surfonic L24-9 (L24-9). Finally, the fourth group includes both cationic (CTAB, CTAC, DTAB, and DTAC), and anionic (HLAS, and AE3S) surfactants (see **Figure 2-1** for chemical structures). The evolution of the CPT of a 1% w/w PEG-g-PVAc aqueous solution as a function of the w/w % concentration of these additives is plotted in **Figure 3-4**, **Figure 3-6**, and **Figure 3-7**.

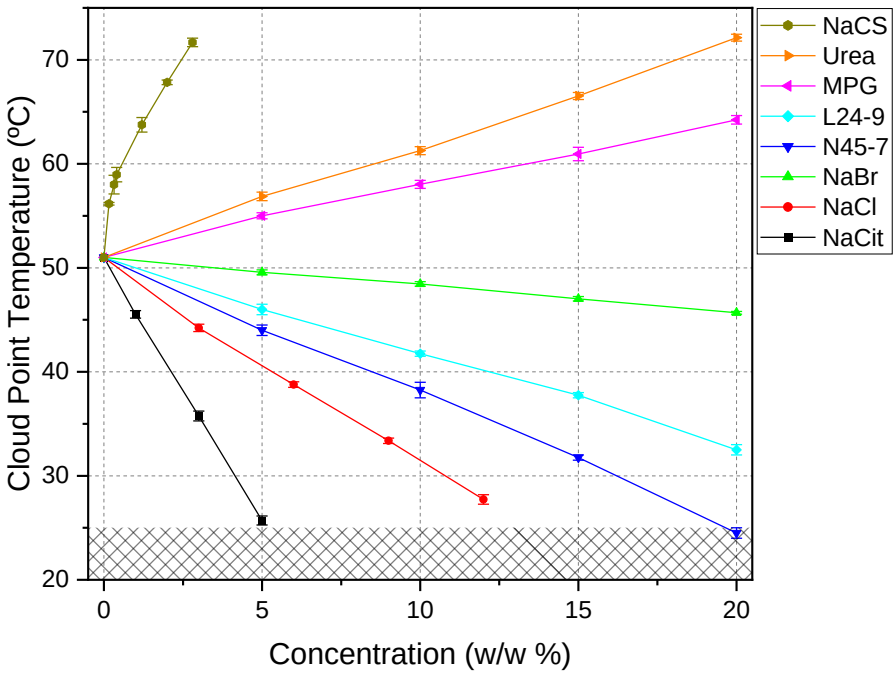

***Figure 3-4**: Effect of kosmotropes, chaotropes, and non-ionic surfactants on the CPT of 1% w/w PEG-g-PVAc in water measured through turbidimetry. A patterned region has been added to indicate where LLPS at room temperature would be expected. Each point corresponds to the average of at least three measurements. Some of the error bars are not visible because they fall within the data points drawn.*

The kosmotropic additives of group 1 decrease the CPT of PEG-g-PVAc as their concentration raises, with their effectivity following the order NaCit > NaCl > NaBr. The same order is followed when their concentration is reported in mol/L (**Figure 6-1**). It is known that both anions and cations are responsible for shifts in the CPT [190], but since the cation is shared among the three selected salts, the different effect over the CPT must be ascribed to the anions. According to the Hofmeister series and the salting-out effect [172], their different activity is related to their hydration. It is generally accepted to say that highly hydrated kosmotropes are "water structure-makers", which increase water surface tension and decrease the solubility of other solutes [140]. Indeed, it has been observed that kosmotropes affect the solvency of the ethylene oxide groups of Pluronics [191]. This is in line with the results reported in **Figure 3-4**, with NaCit being the most effective additive to reduce the CPT. Some studies have justified the decreased solvency by a direct interaction of the anions with the solute and its hydration shell [190,192]. Other recent studies suggest that the effect of these

anions should not be defined only by their influence on the structure of water, since the same effects have been observed in non-aqueous solvents [193,194]. Therefore, a more complex interplay between water, PEG-g-PVAc, and kosmotropic agent should be considered to understand our observations on the evolution of the CPT.

Assuming the salt effects over the CPT follow a linear trend, a concentration of 5.1% w/w (0.17 mol/L) of NaCit or 13.3% w/w (2.28 mol/L) of NaCl would be needed to phase separate 1% w/w of PEG-g-PVAc in water at room temperature. Remarkably, the extrapolated concentration for NaCit agrees with the experimental results summarized later in **Figure 3-8**.

On the other side, all the compounds from group 2 increase the CPT of PEG-g-PVAc as their concentration is raised, with their effectivity following the order of NaCS > urea > MPG. The same order is obeyed when measured in mol/L (**Figure 6-1**). The different effect of these chaotropes on the CPT is due to a combination of both direct and indirect interactions with PEG-g-PVAc, as seen with the kosmotropic salts. Interestingly, the variation of the CPT follows a non-linear trend upon addition of NaCS for concentrations below 1% w/w (**Figure 3-4**). This non-linear behavior, previously reported for other chaotropes on PNIPAM [192], can be related to a direct binding of the anion to the copolymer, which results in a solubility increase of the latter (ion-specific effect). After saturation of the available binding sites, the effect on the CPT would solely arise from anion-water interaction, in agreement with a linear dependence. For concentrations above 1% w/w, the chaotropic effect of NaCS can be explained by its low charge density, which translates into a reduced interaction with water and thus in a salting-in effect. Studies on the effect of NaCS over the CPT of non-ionic molecules are rather scarce, but some years ago a similar effect was observed on the CPT of an ethoxylated non-ionic surfactant (Neodol 25-9) [195].

The effect of urea over water solubility of other compounds has been extensively described and discussed in the literature. It is accepted that its effect arises from two main mechanisms: (i) a direct one, in which the formation of hydrogen bonds between urea and water around the hydrophobic portions of the solute causes the displacement of some water molecules from the hydration shell, resulting in a solubility increase; and (ii) an indirect one, whereby urea acts as a water structure breaker, facilitating the hydration of the solute [140,196,197]. Although

the latter has been widely employed in literature, several studies have proved the direct interaction of urea with the solute to be the major contribution to its increased solubility. Some have suggested that urea binds to the hydrophobic regions of the copolymer, weakening the hydrophobic interaction [198], while others have proved that urea preferentially interacts with the PEG blocks of Pluronics, enhancing its solubility [199–201]. Regarding the effect of urea over PEG-g-PVAc, the increase of its CPT is likely due to a combination of both a direct interaction of urea with the copolymer and an indirect one coming from the effect of urea over water solubility.

MPG is a short chain alcohol, whose effect on the CPT also arises from a combination of an indirect mechanism, making the medium less polar and decreasing the amphiphilicity of the copolymer, and a direct one, due to MPG's interactions with the hydrophobic blocks of the copolymer, which loosens the hydrophobic interaction between grafted chains [140,202,203].

Surfactant	Alkyl chain length	Ethoxy groups	Charge	CMC (10^{-3} mol/L)	CMC (10^{-3} w/w %)
N45-7	14-15	7	/	0.01 [204]	0.546
L24-9	12-14	9	/	0.034 [205]	2.03
AE3S	≈12	3	-	0.7 [206]	29.4
HLAS	≈12	/	-	1.2 [207]	40.3
DTAB	≈12	/	+	15 [208]	462
DTAC	≈12	/	+	23 [209]	607
CTAB	≈16	/	+	1 [208]	36.5
CTAC	≈16	/	+	1.3 [208]	41.6

***Table 3-2**: Basic characteristics of the eight surfactants used throughout this study. Their CMCs are expressed both in mol/L and w/w % for ease of comprehension.*

The other components that decrease the CPT are the non-ionic surfactants N45-7 and L24-9 of group 3. Their basic features are summarized in **Table 3-2**. In line with the kosmotropes, the addition of either N45-7 or L24-9 causes a depression of the CPT (**Figure 3-4**) since both promote copolymer-copolymer over copolymer-medium interactions. This can be attributed both to the effect of these surfactants in dropping water solvency and to the formation of copolymer-surfactant complexes due to hydrophobic interactions [210,211]. Indeed, previous works have justified this CPT depression with the presence of copolymer-surfactant mixed micelles interconnected through polymer chain

bridging [212–214], also known as the “necklace and bead” model (**Figure 3-5**). In regard, the depression of the CPT of PEG-g-PVAc should be mainly coming from hydrophobic interactions between the non-ionic surfactant and the PVAc grafts of the copolymer. There is, however, some interaction between the non-ionic surfactant and the PEG backbone that is likely collaborating on the depression of the CPT too, as previously demonstrated [215].

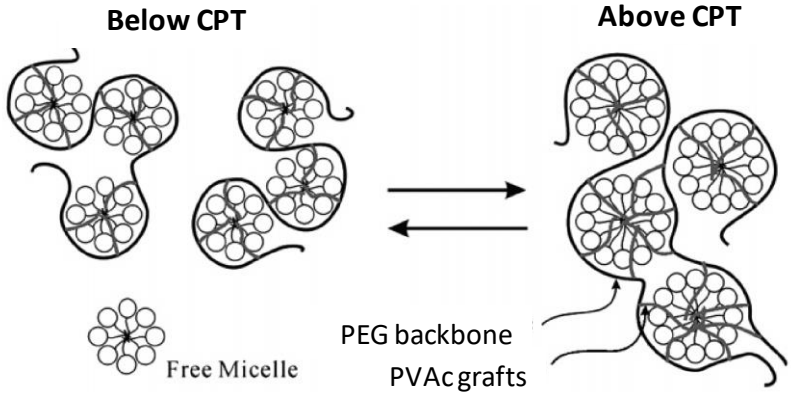

Figure 3-5: Schematic representation of the necklace and bead model for PEG-g-PVAc in the presence of surfactant. Adapted from [214].

The higher effectivity of N45-7 over L24-9 in decreasing the CPT of PEG-g-PVAc can be explained by its shorter ethoxy chain, resulting in a weaker interaction with water, thus a higher association with the copolymer and an enhanced stability of the copolymer-surfactant complex [216]. This lower hydrophilicity is consistent with the lower CMC and LCST of N45-7 (**Table 3-2**), the latter being approximately 24 °C lower than that of L24-9 (**Figure 3-3**). Additionally, the fact that the mixture of PEG-g-PVAc and either of these non-ionic surfactants presents CPT values below those of the two individual components (**Figure 3-3**) proves the associative polymer-surfactant interaction.

In some copolymer-surfactant systems, a low concentration of surfactant leads to the formation of mixed micelles, causing a decrease of the CPT, while a higher concentration of surfactant promotes the formation of surfactant micelles around single hydrophobic chains of the copolymer, enhancing the water affinity of the copolymer and increasing back the CPT [216–218]. This effect causes a

minimum in the trend of the CPT as the concentration of surfactant increases. However, in the concentration range selected for this work, the CPT decreases linearly with the addition of the two non-ionic surfactants (**Figure 3-4**). This behavior could be ascribed to a higher affinity between PVAc blocks than between PVAc and non-ionic surfactant. The extrapolation of their linear trend allows predicting that a concentration of 19.8% w/w (0.363 mol/L) of N45-7 or 28.9% w/w (0.485 mol/L) of L24-9 is needed to phase separate 1% w/w of PEG-g-PVAc in water at room temperature (see **Figure 6-1** for concentrations in mol/L). Remarkably, the extrapolated concentration for N45-7 agrees with the experimental results summarized later in **Figure 3-8**.

The last group of additives includes six ionic surfactants, consisting of four cationics (CTAB, CTAC, DTAB, and DTAC), and two anionics (HLAS and AE3S). Among them, DTAB, DTAC, HLAS, and AE3S share the same alkyl chain length (12 carbon atoms) while CTAB and CTAC have a longer alkyl chain (16 carbon atoms). Their CMCs are reported in **Table 3-2**. **Figure 3-6** and **Figure 3-7** show that all six ionic surfactants increase the CPT of PEG-g-PVAc, and the effect is much stronger than that observed for the chaotropic additives. The same increased solubility was previously reported for a PEG-g-PVAc with a Mw = 13100 Da [166]. This suggests a direct interaction between PEG-g-PVAc and these ionic surfactants. Indeed, a synergistic interaction has been recently observed at the air-water interface between an anionic surfactant (sodium dodecyl sulfate) and PEG-g-PVAc [219].

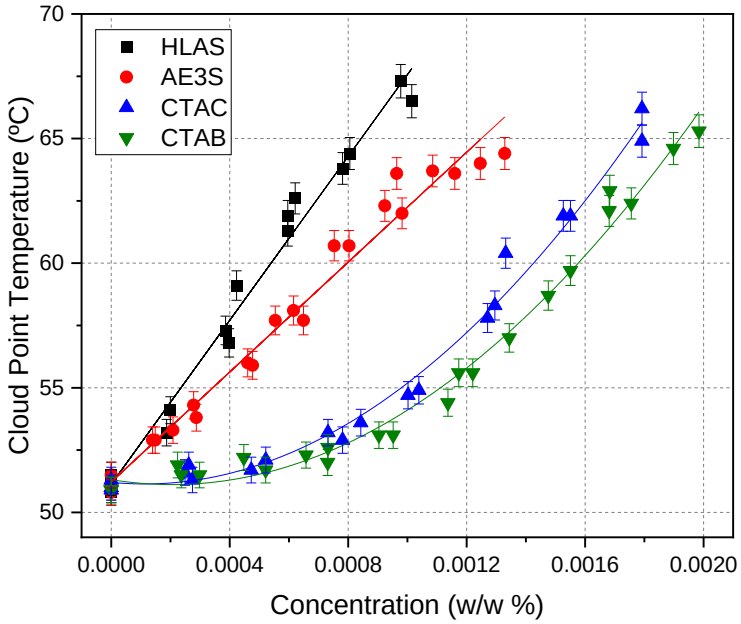

***Figure 3-6**: Effect of the two anionic surfactants (HLAS and AE3S) and the two cationic surfactants with a longer alkyl chain (CTAC and CTAB) on the CPT of 1% w/w PEG-g-PVAc in water, measured through turbidimetry. Each point corresponds to a single measurement due to the difficulty in obtaining the same low concentrations.*

Figure 3-6 includes the four ionic surfactants that induced the highest increase on the CPT of PEG-g-PVAc. The same graph with concentrations in mol/L can be found in the annex (**Figure 6-2**). Their effect over the CPT is remarkable: in order to detect the CPT increase in a measurable temperature range, concentrations below their CMCs (**Table 3-2**) had to be used. The two anionic surfactants (HLAS and AE3S) were slightly more effective in increasing the CPT than the two cationic surfactants (CTAB and CTAC), even though these latter two have a longer alkyl chain. The increase of the CPT follows a linear trendline for anionic surfactants, while a lag phase followed by a rather linear trendline was observed for both CTAB and CTAC. This trendline evolution has been previously reported for other polymer-surfactant systems [220,221]. Unfortunately, a Tyndall effect was noticed once the CPT reached levels above 66°C, which prevented to properly study the effect of higher concentrations of these ionic surfactants over the CPT.

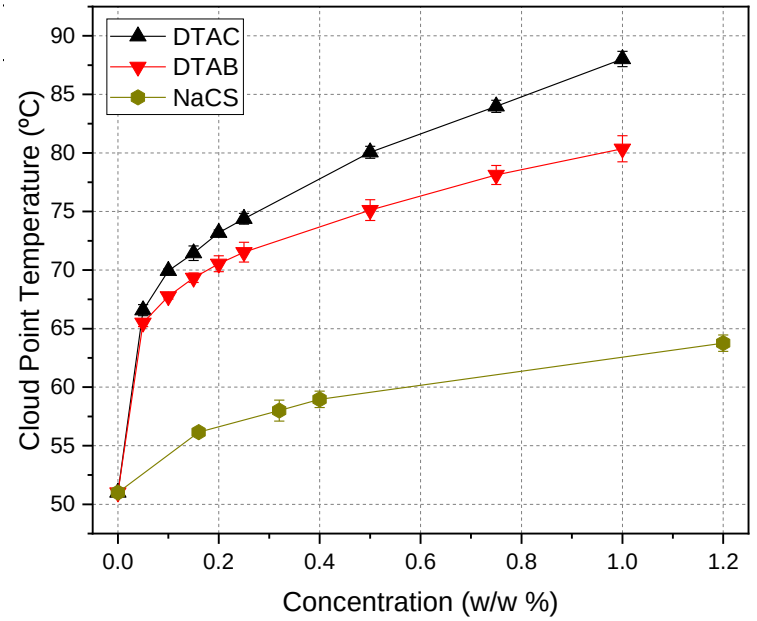

***Figure 3-7**: Effect of the two cationic surfactants with a shorter alkyl chain (DTAC and DTAB) plus NaCS on the CPT of 1% w/w PEG-g-PVAc in water, measured through turbidimetry. Each point corresponds to the average of three measurements. Some of the error bars are not visible because they fall within the data points drawn.*

Figure 3-7 shows the effect of the other two cationic surfactants (DTAB and DTAC) over the CPT. These two ionic surfactants increased the CPT of PEG-g-PVAc to a minor degree, which allowed the comparison of their effect over the CPT with NaCS (see **Figure 6-3** for concentrations in mol/L). Even though the alkyl chain length of these two cationic surfactants is as long as that of HLAS and AE3S, there is a noticeable difference in their effect over the CPT – while around 0.0012% w/w ($3x10^{-5}$ mol/L) of anionic surfactant is enough to increase the CPT of PEG-g-PVAc to 65 degrees, close to 0.05% w/w ($2x10^{-3}$ mol/L) of DTAB or DTAC is needed to obtain the same increase. It can be observed that the evolutions of the CPT of PEG-g-PVAc as a function of the concentrations of DTAB, DTAC, or NaCS follow a similar trend: parabolic at low concentrations and rather linear at higher ones. No Tyndall effect was observed when using these two cationic surfactants, which permitted assessing the effect of higher concentrations.

These results agree with the literature on the effect of ionic surfactants on the CPT of copolymers from the ethylene oxide family [146,203,222–224]. Generally, a significant increase on the CPT of water-soluble copolymers is observed after addition of either anionic or cationic surfactants. This phenomenon was justified with the formation of a copolymer-surfactant complex, which can be originated from hydrophobic interactions, following the previously mentioned "necklace and bead" model (**Figure 3-5**) [225,226], but also from electrostatic ones, considering the charged nature of the ionic surfactants' headgroups [219,227,228]. This "charged" copolymer-surfactant complex, which could be considered as a polyelectrolyte [229], leads to both a better solvation of the copolymer and a higher electrostatic repulsion between complexes, thus hampering aggregation and consequently raising the CPT.

Following this explanation, the fact that the two anionic surfactants increase more effectively the CPT than any of the other four cationic surfactants suggests that the copolymer-surfactant complex of PEG-g-PVAc with anionic surfactants forms at lower concentrations and possesses a higher solubilizing effect than the complex formed with cationic surfactants, presumably due to a stronger interaction of the sulfate group than the trimethylammonium group with PEG-g-PVAc. Anionic surfactants have proved to be more effective than cationic surfactants in increasing the CPT of other systems as well [191,230,231]. Additionally, assuming again the formation of a copolymer-surfactant complex, a longer alkyl chain provides a higher hydrophobicity to the surfactant and reduces the repulsion factor between close polar head groups of the micelle, thus strengthening the interaction between the surfactant and the copolymer [232]. This explains why a longer alkyl chain brings a more noticeable increase on the CPT among the four cationic surfactants studied in this work. The same trend has been previously reported in other polymer-surfactant systems [146,224,230].

Regarding the effect of counterions, the difference between bromide and chloride shows a minimum influence on the effect of CTAB and CTAC over the CPT for the concentration range studied (clearly visible in **Figure 6-2**), in agreement with the literature [230,233]. However, a more noticeable difference is discernible between DTAB and DTAC, which is accentuated at higher

concentrations (**Figure 3-7**). Their different effectivity in increasing the CPT of PEG-g-PVAc can be explained by the different polarizability of bromide and chloride. It is known that chaotropic counterions bind more strongly to the micellar surface than kosmotropic counterions do, thus promoting micellar growth more effectively and reducing the CMC [234–236]. Indeed, the CMC of DTAB is lower than the one of DTAC (**Table 3-2**) because bromide interacts more favorably with the positively charged cationic surfactant than chloride does. A stronger binding of the counter-ion means a higher screening of the charged surfactant and thus a lower ionization degree, leading to a smaller solubilizing effect over the copolymer, hence a smaller increase on the CPT.

Other publications have proved that the addition of salts can counteract the strong effect of ionic surfactants over the CPT of copolymers, up to a point in which the polar head is completely screened and they behave like a non-ionic surfactant, decreasing rather than increasing the CPT [237,238].

3.3 Compositional range for PEG-g-PVAc coacervates

As observed while reproducing the work of Bartolini [166], the LLPS of PEG-g-PVAc can give rise to micron-sized domains, or coacervates, rich in copolymer (scenario 2 of **Figure 3-2**). These coacervates were obtained by mixing specific concentrations of PEG-g-PVAc, Neodol 45-7 (N45-7) and sodium citrate (NaCit). This makes sense since, as explained in the previous section of this thesis, kosmotropic salts and non-ionic surfactants decrease the CPT of PEG-g-PVAc. The most effective kosmotrope was NaCit and the most effective non-ionic surfactant was N45-7. Aiming to identify not a specific concentration of these two compounds but the range of concentrations at which PEG-g-PVAc coacervates can be obtained, the phase behavior of PEG-g-PVAc was studied for a range of NaCit and N45-7 concentrations.

Figure 3-8 presents a mapping of the compositional space of an aqueous solution of 1% w/w PEG-g-PVAc in presence of NaCit and N45-7. Depending on the medium composition, four main scenarios occur: homogeneous (monophasic) dispersion (1); formation of PEG-g-PVAc coacervates with the absence (2) or presence (3) of precipitated copolymer; and liquid-liquid bulk phase separation (4). The experimental procedure used to assess the boundaries between regions of **Figure 3-8** is explained in section 2.2.1 Sample preparation. In short, NaCit was stepwise added to five samples, each containing 1% w/w PEG-g-PVAc and varying concentrations of N45-7. The blue line separating region 1 from 2 and 3 marks the appearance of a cloudy suspension, while the upper red line identifies the boundary from cloudy to biphasic.

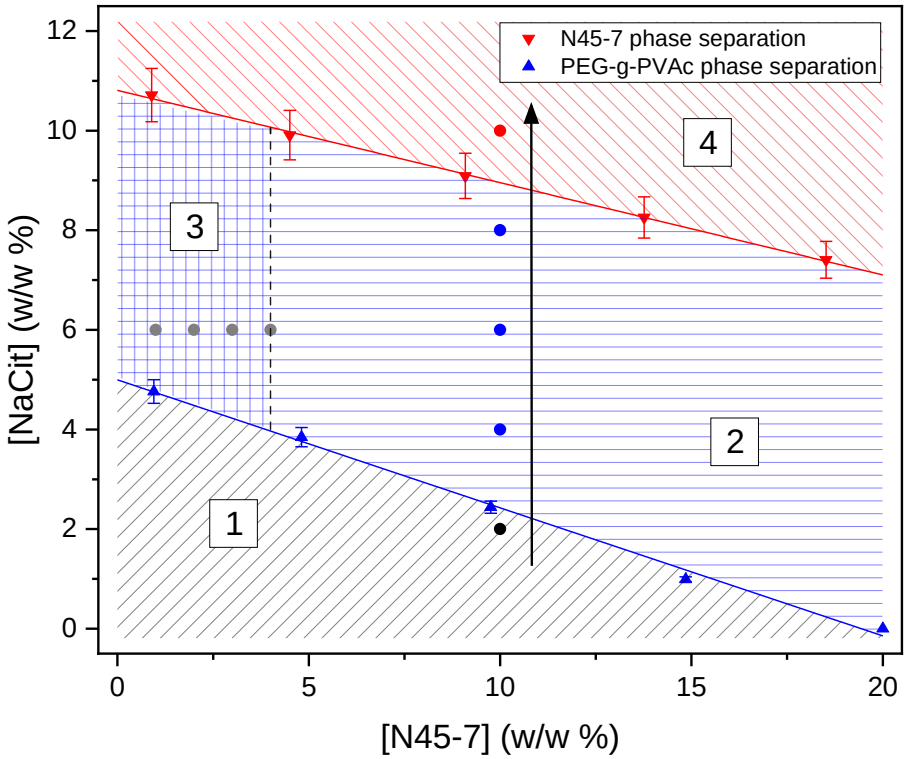

***Figure 3-8**: An aqueous solution of 1% w/w PEG-g-PVAc shows four different behaviors depending on the concentrations of both NaCit and N45-7 (A): in region 1, the copolymer is dissolved along the medium, showing a monophasic system; in region 2, LLPS of the copolymer takes place giving rise to kinetically stable coacervates; in region 3, coacervates are distinguished together with polymer precipitates; finally, in region 4, liquid-liquid bulk phase separation takes place with the copolymer being found in the top phase.*

Since PEG-g-PVAc is an LCST-type copolymer, a monophasic system was expected for low concentrations of NaCit and N45-7, where its CPT is still above room temperature, rendering the copolymer soluble in water. However, after adding enough of these two components, liquid-liquid phase separation takes place, caused by the depression of the copolymer's CPT. In these conditions, the optical microscope showed the presence of coacervates (**Figure 6-4**). The difference between regions 2 and 3, both containing PEG-g-PVAc coacervates, stems from the absence or presence of copolymer precipitation, respectively. The simultaneous presence of liquid-liquid and liquid-solid phase separation has also been detected and investigated for complex coacervates [239–241].

Interestingly, both additives lower the CPT in ternary systems (**Figure 3-4**), but while the addition of only N45-7 gives raise to the liquid-liquid phase separation of PEG-g-PVAc or coacervation (region 2), the addition of only NaCit induces its liquid-solid phase separation or precipitation (region 3). We ascribe the different effect of these two additives to a higher degree of copolymer desolvation in the presence of NaCit, as later indicated in **Figure 3-13**. This also indicates that non-ionic surfactant is necessary to form PEG-g-PVAc coacervates. Moreover, if the concentrations of both PEG-g-PVAc (1% w/w) and NaCit (6% w/w) are kept constant and the dispersion is titrated with N45-7, a visible decrease of the amount of precipitated PEG-g-PVAc is observed (**Table 3-3**, plotted as grey dots on region 3 of **Figure 3-8**). The absence of PEG-g-PVAc precipitation is found for a concentration of 4% w/w N45-7, marking the boundary between regions 2 and 3.

[N45-7] (% w/w)	[NaCit] (% w/w)	Sample state
1	6	Extended precipitation + coacervation
2	6	Precipitation + coacervation
3	6	Scarce precipitation + coacervation
4	6	Coacervation
10	2	Monophasic
10	4	Coacervation
10	6	Coacervation
10	8	Coacervation
10	10	Liquid-liquid bulk phase separation

***Table 3-3**: Composition of the two sets of samples used to determine the limit between regions 2 and 3 (minimum of N45-7, **Figure 3-8**), as well as to show the visual differences between regions 1, 2 and 4 (see **Figure 3-9**).*

According to the linear boundary separating region 1 from regions 2 and 3, 5% w/w of NaCit or 19.6 % w/w of N45-7 is needed to phase separate PEG-g-PVAc. These two approximated concentrations are very close to the values obtained from the results of **Figure 3-4** (these being 5.1% w/w and 19.8% w/w, respectively). The fact that this transition boundary follows a linear regression suggests that the combined effect of NaCit and N45-7 over the CPT of PEG-g-PVAc is not synergistic but rather the sum of their individual effects.

To understand the role of NaCit to obtain the different regions of **Figure 3-8**, the phase behavior of five samples with constant concentrations of PEG-g-PVAc (1% w/w) and N45-7 (10% w/w), but different concentrations of NaCit (**Table 3-3**), was assessed. A day after sample preparation, three different scenarios could be distinguished in this set of samples (**Figure 3-9**). The sample with 2% w/w of NaCit was transparent (region 1), the samples with 4, 6, and 8% w/w of NaCit were cloudy (region 2), while the sample with 10% w/w of NaCit was showing a liquid-liquid bulk separation (region 4). RBITC-labelled PEG-g-PVAc was used in the sample presenting bulk phase separation with the aim to find out its distribution. As observable, PEG-g-PVAc could only be distinguished in the top phase. This phenomenon is attributed to the kosmotropic-induced phase separation of the non-ionic surfactant, since a sample of 1% w/w PEG-g-PVAc without N45-7 did not present this liquid-liquid bulk phase separation at high NaCit concentrations (12% w/w), while a sample of N45-7 (10% w/w) and NaCit (10% w/w) without PEG-g-PVAc did present this liquid-liquid bulk phase separation. Interestingly, the optical microscope showed that both phases of region 4 present micron-size coacervates. However, no further research was performed on this region.

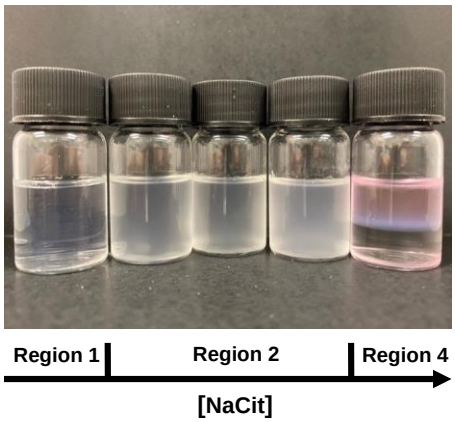

***Figure 3-9**: Five samples with constant concentrations of PEG-g-PVAc (1% w/w) and N45-7 (10% w/w), but different concentrations of NaCit, are shown to illustrate the optical difference between regions 1, 2, and 4. From left to right, the first sample shows a monophasic system, the next three show a cloudy system, while the last one shows a biphasic system. In the latter sample, RBITC-labelled PEG-g-PVAc is used to prove its exclusive presence in the top phase.*

To further study the role of the kosmotropic effect on the formation of coacervates, another set of five samples with a fixed concentration of PEG-g-PVAc (1% w/w) and different concentrations of sodium chloride (NaCl) was studied (graph of **Figure 3-10**). After adding enough N45-7 to induce LLPS, PEG-g-PVAc coacervates were successfully obtained in all five samples, which presented the same morphological features as the ones obtained with NaCit

(images of **Figure 3-10**). These results demonstrate that NaCit is not specifically needed to obtain coacervates, but just a kosmotrope (such as NaCl) to decrease the CPT of PEG-g-PVAc and allow their formation at lower temperatures.

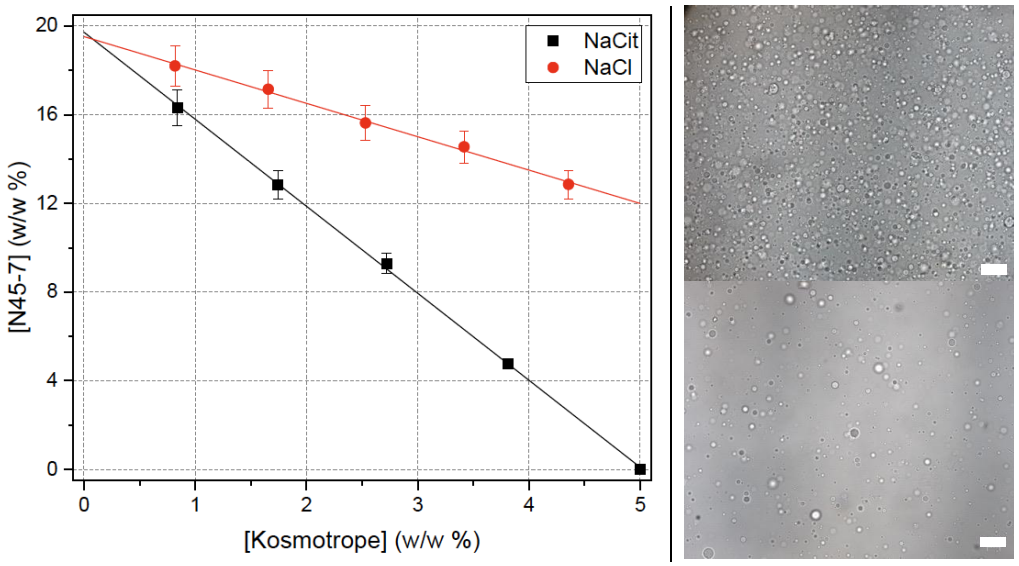

***Figure 3-10**: The graph compares the amount of non-ionic surfactant (N45-7) required to obtain LLPS at room temperature in a 1% w/w PEG-g-PVAc solution when using NaCit (black) or NaCl (red). Below the trendline the sample is monophasic, while above it is cloudy. On the right, optical microscopy pictures of coacervates from samples containing PEG-g-PVAc (1% w/w), N45-7, and NaCl. The white bars are equivalent to 100 µm.*

The presence of PEG-g-PVAc in these coacervates can be demonstrated through fluorescence confocal microscopy, as previously shown in **Figure 3-1** and **Figure 3-2**. In this case, three different samples with 1% w/w PEG-g-PVAc (RBITC labelled), 5% w/w NaCit, and 5, 10, or 15% w/w N45-7, were observed under the fluorescence confocal microscope (**Figure 3-11**). This instrument showed the presence of coacervates rich in PEG-g-PVAc in all three samples, with a typical diameter around 50 µm. The copolymer appears to be homogeneously distributed within these coacervates, not following a core-shell structure. Due to the resolution of this technique, particles with a size below ~500 nm cannot be distinguished. However, considering previous studies [164], the presence of sub-micron structures made of PEG-g-PVAc and/or N45-7 is likely. It is relevant to add that these coacervates are kinetically stable, and thus sedimentation and coalescence takes place over time (**Figure 6-5**). The microphase separation was stable for at least three, five, or seven days at room temperature for the samples

with 5, 10, or 15% w/w N45-7, respectively. The kinetic stability of this system is extended by increasing the concentration of surfactant due to the incremented sample's viscosity, which slows down the diffusion of these microstructures. The same effect can be achieved by addition of a structuring agent, as commonly used in industrial formulations.

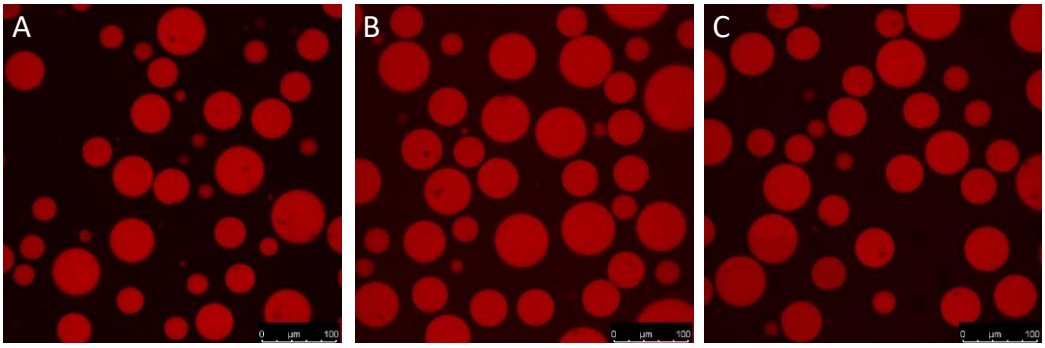

***Figure 3-11**: Fluorescence confocal microscopy pictures of the coacervates from samples containing 1% w/w RBITC-labelled PEG-g-PVAc, 5% w/w NaCit, and 5 (A), 10 (B), or 15% (C) w/w N45-7.*

3.4 Composition of PEG-g-PVAc coacervates

Fluorescence confocal microscopy (**Figure 3-11**) suggests that the coacervates contain PEG-g-PVAc. However, this technique cannot determine the distribution of N45-7 nor assess the presence of water in the microstructure. Therefore, we selected a representable sample with coacervates (1% w/w PEG-g-PVAc, 5% w/w NaCit, and 10% w/w N45-7) for further investigation through confocal Raman microscopy. The reference Raman spectra of pure PEG-g-PVAc and N45-7 can be found in the annex (**Figure 6-6**). As expected, the Raman spectrum obtained from the coacervates differs with respect to the one from the suspending medium (**Figure 3-12**). The presence of PEG-g-PVAc (main peak at 2940 cm^{-1}, C-H stretching), water (broad peak around 3420 cm^{-1}, O-H stretching), and N45-7 (little shoulder around 2852 cm^{-1}, C-H stretching) can be appreciated in the coacervate's spectrum, while the medium shows mainly the presence of N45-7 (with its three diagnostic peaks at 2852, 2887, and 2922 cm^{-1}, originating from different C-H stretching modes), and water. We cannot rule out the presence of PEG-g-PVAc dissolved in the medium, but its occurrence does not emerge in this Raman analysis. From these results, we can qualitatively conclude that the coacervates show an enrichment of PEG-g-PVAc, in line with the images from the fluorescence confocal microscope, while N45-7 is slightly more concentrated in the medium, as the comparison of the peaks' intensities at 2852 cm^{-1} indicates (inset of **Figure 3-12**).

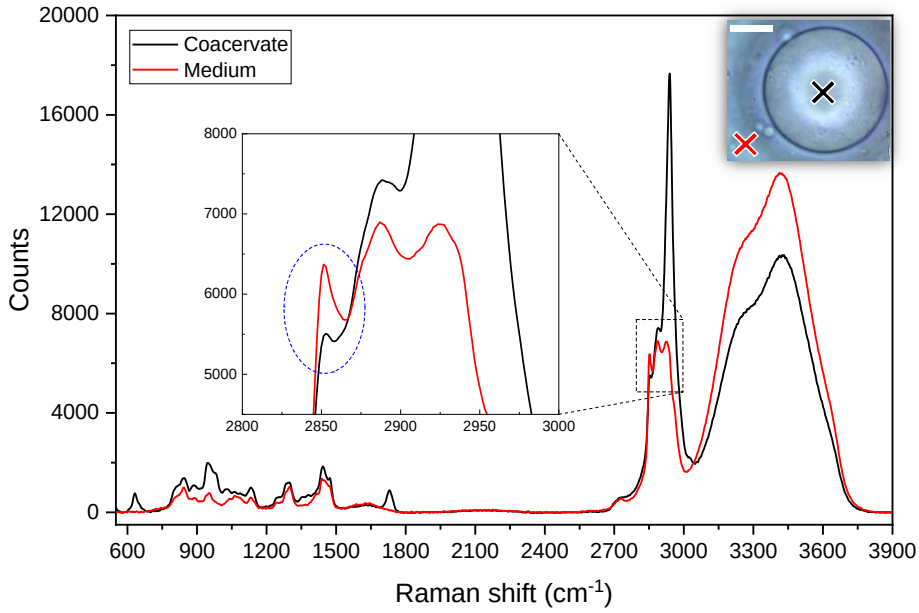

***Figure 3-12**: Raman profiles of a PEG-g-PVAc coacervate (black) and the medium (red) from a sample made of 1% w/w PEG-g-PVAc, 5% w/w NaCit, and 10% w/w N45-7. The inset shows the three N45-7 diagnostic peaks, highlighting the different intensity of the one at 2852 cm^{-1} between the two Raman profiles. An optical microscope picture of a coacervate is enclosed at the top right corner of this figure, where the scale bar is equivalent to 20 µm, marking the spots from where the two Raman spectra were acquired.*

Since all the diagnostic peaks from N45-7 are in a spectral range where also PEG-g-PVAc presents Raman scattering (**Figure 6-6**), the accurate detection of the non-ionic surfactant in the coacervates is challenging to achieve. To address this issue, at least fifty Raman spectra from the coacervates, each normalized with respect to the main peak of PEG-g-PVAc (2940 cm^{-1}), were averaged and compared to those of two reference samples: (i) 25% w/w PEG-g-PVAc in water, and (ii) precipitated copolymer from 1% w/w PEG-g-PVAc and 6% w/w NaCit (**Figure 3-13**). The spectrum of pure PEG-g-PVAc can be found in **Figure 6-6** for comparison. The Raman profiles of these three samples presented some obvious differences in the region of the O-H stretching of water (between 3000 and 3700 cm^{-1}) and C-H stretching of alkanes (between 2800 and 3100 cm^{-1}). Regarding the water region of the spectra, the coacervates still have a high content of water, as highlighted by a comparison with the reference samples (PEG-g-PVAc dissolved in water and precipitated). This result is expected and in line with other reports pointing that coacervates, even though they result from a liquid-liquid phase

separation, have a high content of water [242,243]. Moreover, the decreased water content of the precipitated copolymer sample suggests that this liquid-solid phase separation is ascribed to a higher desolvating effect of NaCit than N45-7, as previously commented for the results of **Figure 3-8**. For the alkane region, the spectra from 25% w/w PEG-g-PVAc in water and that from precipitated PEG-g-PVAc are very similar. However, when comparing the averaged spectrum obtained from the coacervates to these two other profiles, we can distinguish a shoulder around 2852 cm^{-1} and an increased intensity around 2887 cm^{-1} (inset of **Figure 3-13**). These differences are attributed to the presence of N45-7 inside the coacervates.

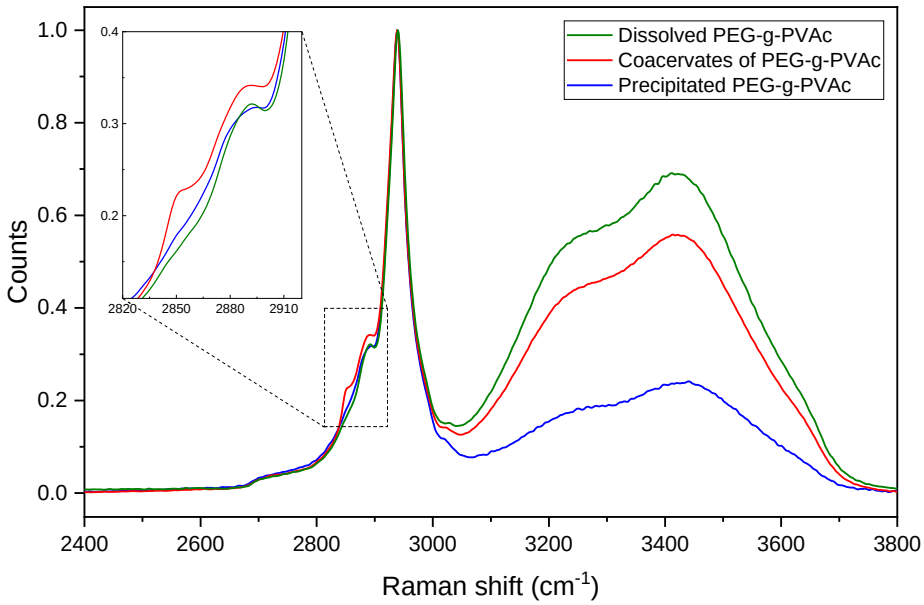

***Figure 3-13**: Raman profiles of different samples containing PEG-g-PVAc are normalized at 2940 cm^{-1} for comparison. The Raman profile of the precipitated copolymer from a sample of 1% w/w PEG-g-PVAc and 6% w/w NaCit appears in blue, the averaged profile of several coacervates is in red, while the one of 25% w/w PEG-g-PVAc in water is in green.*

To better highlight the partition of N45-7 in the coacervates, a two-dimensional Raman intensity map was performed on the sample containing 1% w/w PEG-g-PVAc, 5% w/w NaCit, and 10% w/w N45-7 (**Figure 3-14A**). The collection of Raman spectra was processed to obtain three different intensity distributions: one from the most intense Raman peak of PEG-g-PVAc (2940 cm^{-1}), one from the ester peak of PEG-g-PVAc (1730 cm^{-1}), and one from the N45-7 peak (2852 cm^{-1})

– which appear in red, blue, and green, respectively, in **Figure 3-14A**. The intensity measured for PEG-g-PVAc at 2940 cm^{-1} can include a contribution from N45-7, which also shows Raman scattering in this region, while the intensity at 1730 cm^{-1} is selective for PEG-g-PVAc (see **Figure 6-6** for PEG-g-PVAc and N45-7 spectra comparison). These intensity maps show clearly that the coacervates are rich in PEG-g-PVAc, in line with the fluorescence confocal microscopy images. On the other side, the intensity map at 2852 cm^{-1} (**Figure 3-14A**, green profile) indicates a higher concentration of N45-7 in the medium than in the coacervates, which agrees with the spectral profiles of **Figure 3-12**. It must also be noted that both PEG-g-PVAc and N45-7 have Raman scattering at 2852 cm^{-1}. Therefore, the intensity map of this emission wavelength (in green) originates both from the copolymer and the non-ionic surfactant. However, as seen from the distributions at 2940 and 1730 cm^{-1}, (in red and blue, respectively), PEG-g-PVAc is mainly concentrated inside the coacervates. Therefore, we can assume that the intensity contribution at 2852 cm^{-1} in the medium is mainly from N45-7.

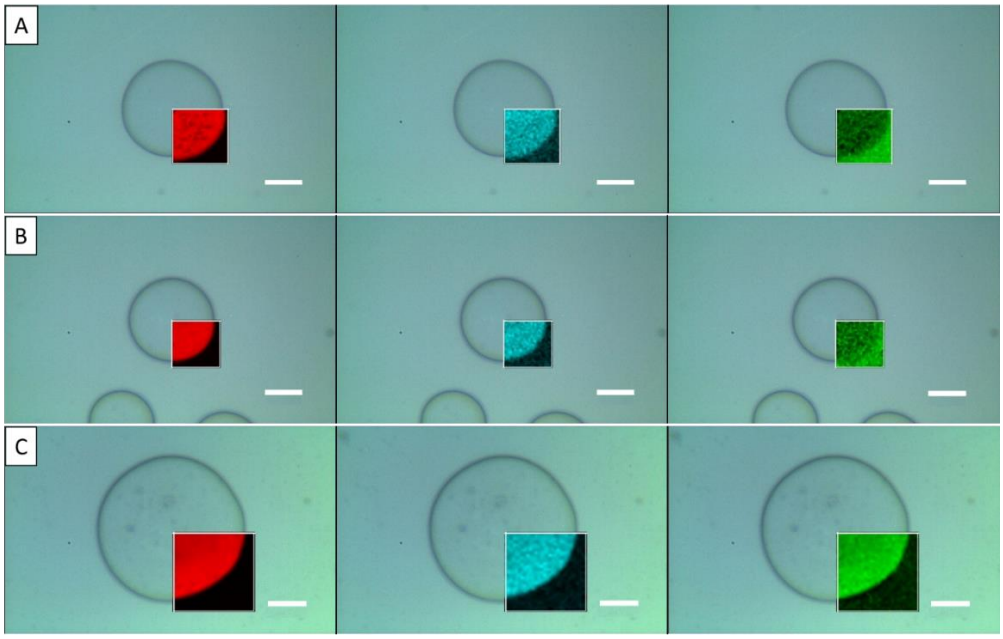

***Figure 3-14**: Two-dimensional intensity maps obtained from the Raman intensity of 1% w/w PEG-g-PVAc, 5% w/w NaCit, and 10% (A), 7% (B), or 4% (C) w/w N45-7. The red distribution represents the Raman intensity measured at 2940 cm^{-1}, the blue represents the intensity at 1730 cm^{-1}, and the green represents the intensity at 2852 cm^{-1}. The scale bar is equivalent to 20 μm in all pictures.*

To better understand the effect of N45-7, we assessed two additional samples with 7% w/w and 4% w/w N45-7 (**Figure 3-14B** and **Figure 3-14C**, respectively), keeping unvaried the concentrations of PEG-g-PVAc (1% w/w) and NaCit (5% w/w). These intensity maps confirm again the localization of PEG-g-PVAc in the coacervates. Interestingly, the main difference between this series of samples is the intensity map at 2852 cm^{-1} (green), presenting either a higher, similar, or lower intensity in the coacervates with respect to the medium for the samples with 4%, 7% and 10% w/w of N45-7, respectively. Clearly, the more N45-7 in the formulation, the higher its presence in the medium rather than in the coacervates. This trend suggests that the N45-7/PEG-g-PVAc mass ratio might not vary much between coacervates, regardless of the bulk N45-7 concentration.

To address this point, the averages of at least fifty Raman spectra from the coacervates of the 7% and 4% w/w N45-7 samples, normalized with respect to the main peak of PEG-g-PVAc (2940 cm^{-1}), were compared with: (i) the averaged spectrum of the coacervates in the 10% w/w N45-7 sample (already used in **Figure 3-13**), and (ii) a reference spectrum of 25% w/w PEG-g-PVAc in water (**Figure 3-15**). This comparison highlights once more the presence of the shoulder around 2852 cm^{-1} in the coacervates, not present for 25% w/w PEG-g-PVAc in water (inset of **Figure 3-15**). However, the intensity increase provided by N45-7 is small for all three concentrations, hence the amount of N45-7 in the coacervates must be low. Bearing this in mind, it can be assumed that the Raman intensity obtained from the inside of the coacervates in the intensity maps measured at 2852 cm^{-1} is mainly coming from PEG-g-PVAc, not from the N45-7 (shown with a green color in **Figure 3-14**). Furthermore, considering the closeness between the Raman profiles of these three samples in the alkane region (between 2800 and 3100 cm^{-1}), we can conclude that the N45-7/PEG-g-PVAc mass ratio inside the coacervates is very similar for the three different N45-7 concentrations. Therefore, an increased N45-7 concentration does not result in its noticeable enrichment inside the coacervates. The same behavior was described for coacervates made of C_{12} E_{10} non-ionic surfactant, where its concentration in the coacervate phase changed very little with increasing its initial concentration [244].

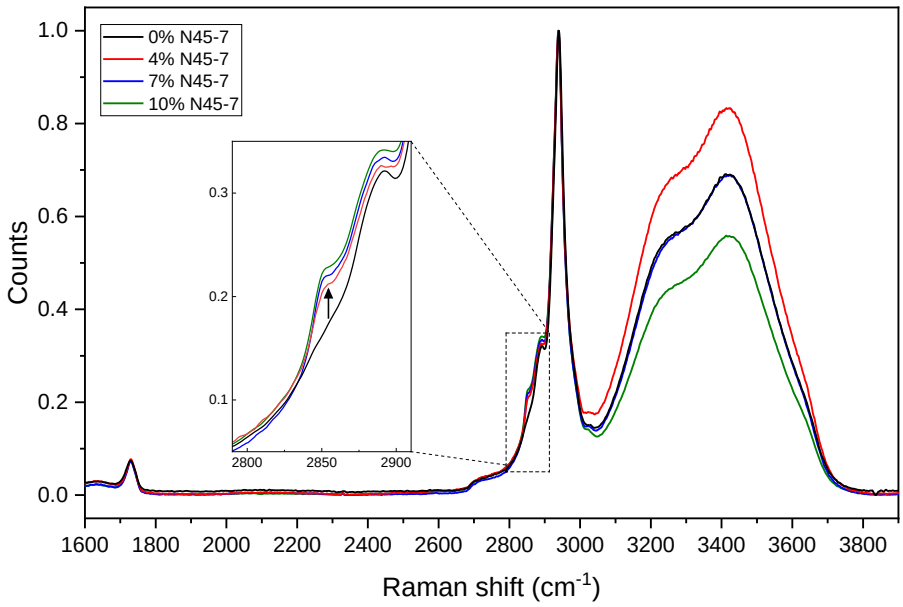

***Figure 3-15**: Averaged Raman profiles of the coacervates from three different samples consisting of 1% w/w PEG-g-PVAc, 5% w/w NaCit, and 4 (red), 7 (blue), or 10% (green) w/w N45-7. The reference Raman profile of 25% w/w PEG-g-PVAc in water (black) is added to notice the effect of N45-7, which is marked with a vertical black arrow in the inset.*

To approximately determine the N45-7/PEG-g-PVAc mass ratio inside the coacervates, two different methods were employed. First, the software of the confocal Raman microscope was used to perform peak deconvolution. The calculated N45-7/PEG-g-PVAc mass ratio varied between 15/85 (0.18) and 10/90 (0.11) among different coacervates obtained from samples with different bulk N45-7 concentrations. Second, a set of reference samples with a constant concentration of PEG-g-PVAc (10% w/w) and a varying concentration of N45-7 (0, 0.5, 1, 1.5, 2, 4, 6, 8, 10% w/w) in water was analyzed under confocal Raman microscopy. The obtained Raman spectra were normalized both at the peak of water (3420 cm^{-1}) and at the main peak of PEG-g-PVAc (2940 cm^{-1}), as shown in **Figure 3-16**. The effect of increasing the N45-7 concentration can be clearly observed in this figure as the intensities of its three main diagnostic Raman peaks (at 2852, 2887, and 2922 cm^{-1}) grow. The most noticeable difference is observed for the N45-7 peak at 2852 cm^{-1}, which is not initially present in the sample containing just PEG-g-PVAc. If the shape of the Raman profiles of these references is visually compared to the shape of those obtained from the

coacervates (**Figure 3-15**), it can be estimated that the N45-7/PEG-g-PVAc mass ratio in the coacervates should be close to 0.2. Considering this approximation and the N45-7/PEG-g-PVAc mass ratio values obtained from the peak deconvolution of the confocal Raman software, the N45-7/PEG-g-PVAc ratio in the coacervates is likely between 0.1 and 0.2.

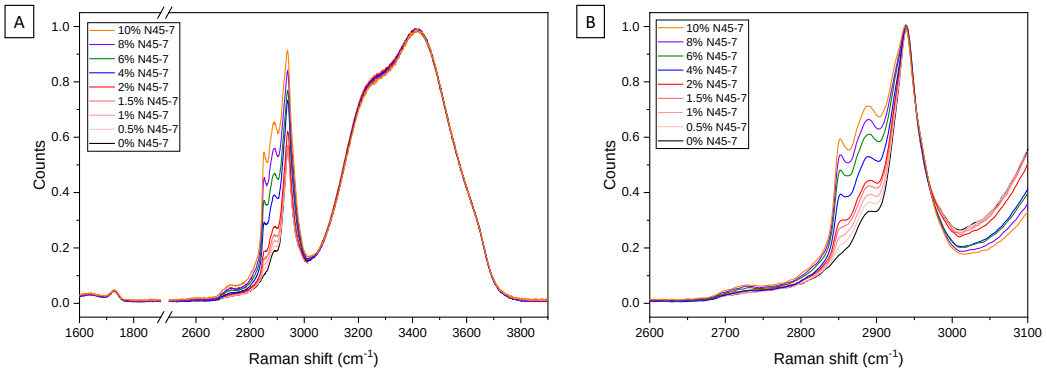

***Figure 3-16**: Raman spectra used to approximately determine the N45-7/PEG-g-PVAc mass ratio inside the coacervates. The spectra of 10% w/w PEG-g-PVAc and 0, 0.5, 1, 1.5, 2, 4, 6, 8, or 10% w/w N45-7 appear normalized at the peak of water (3420 cm^{-1}) in (A) and at the main peak of PEG-g-PVAc (2940 cm^{-1}) in (B). There is a cut in the scale of the X axis of graph A for ease of comparison.*

Interestingly, the most noticeable difference between the three samples of **Figure 3-15** is the water/PEG-g-PVAc content of the coacervates, which decreases as the total concentration of N45-7 increases. This indicates that the non-ionic surfactant causes a decrease of the hydration within the coacervates. A similar effect was reported for NaCl on the water content of simple coacervates [242]. This relates to the cloud point trend since, as previously shown in **Figure 3-4**, the CPT decreases as the concentration of non-ionic surfactant increases. The lower the copolymer's CPT, the lower its affinity for water, which correlates with these Raman profiles showing a lower amount of water inside the PEG-g-PVAc coacervates as more N45-7 is present in solution. This suggests that by controlling the amount of non-ionic surfactant in solution we can modulate the hydrophilicity of the coacervates and, thus, their affinity for actives with different hydrophobicity.

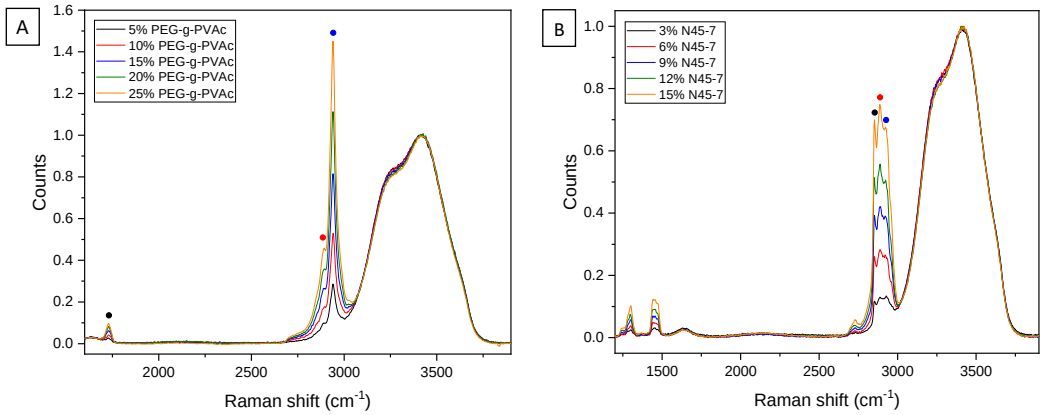

***Figure 3-17**: Raman spectra obtained from water solutions of (A) PEG-g-PVAc at concentrations of 5%, 10%, 15%, 20%, and 25% w/w, and (B) N45-7 at concentrations of 3%, 6%, 9%, 12%, and 15% w/w. The colored dots mark the peaks selected to draw the calibration curves of (**Figure 6-7**).*

Finally, aiming to roughly quantify the relative amounts of PEG-g-PVAc and N45-7 in the coacervates and the medium, a set of reference samples of PEG-g-PVAc in water and another of N45-7 in water (**Figure 3-17**) were used to obtain calibration curves for the PEG-g-PVAc/water and N45-7/water mass ratios (**Figure 6-7**), respectively. Taking advantage of their linear trend, the PEG-g-PVAc/water and N45-7/water mass ratios from the references were extrapolated to the three studied samples with different N45-7 concentrations (**Table 3-4**). The extrapolation is described in detail in section 2.2.5 Confocal Raman Microscopy. Even though these calibration curves cannot be used to obtain absolute concentration values, they allow to determine that all studied coacervates have a PEG-g-PVAc/water mass ratio of at least 0.25, which is equivalent to a sample made of 20% w/w PEG-g-PVAc in water. This outcome agrees with the results shown in **Figure 3-15**, in which the sample containing 7% w/w N45-7 has an identical Raman profile with respect to the reference sample of 25% w/w PEG-g-PVAc in water, suggesting that the PEG-g-PVAc/water ratio of these two samples is very similar. Considering that all samples were prepared with an initial PEG-g-PVAc bulk concentration of 1% w/w, the concentration of copolymer in the coacervates is at least twenty times higher. The increase of the PEG-g-PVAc/water mass ratio in the coacervates at higher N45-7 bulk concentrations is attributed to the decreased hydration, as previously commented with the results of **Figure 3-15**. The results of **Figure 3-12** and **Figure 3-14** let us assume that the

amount of PEG-g-PVAc dissolved in the medium is negligible. Consequently, the extrapolation from these calibration curves also allows to conclude that the N45-7/water mass ratio in the medium is practically the N45-7 initial bulk ratio in each of the three different samples (**Table 3-4**). The outcomes of the extrapolation are in line with previous observations: (i) the PEG-g-PVAc is highly concentrated in the coacervates, with a relative concentration over water much larger than the one set during sample preparation, and (ii) a higher N45-7 bulk concentration results in its higher presence in the medium rather than in the coacervates, as suggested by the intensity maps at 2852 cm^{-1} (**Figure 3-14**).

	Initial ratios (%)		*Measured ratios (%)*	
N45-7 (w/w %)	**PEG-g-PVAc /water**	**N45-7 /water**	**PEG-g-PVAc/water (*in LLPS*)**	**N45-7/water (*in medium*)**
4	1.1	4.4	27 ± 1	4.5 ± 0.2
7	1.1	8.0	35 ± 2	7.7 ± 0.3
10	1.2	11.9	43 ± 2	12.2 ± 0.4

***Table 3-4**: PEG-g-PVAc/water and N45-7/water mass ratios of 1% w/w PEG-g-PVAc, 5% w/w NaCit, and 4, 7, or 10% w/w N45-7. The initial ratios refer to the ones set during sample preparation for both PEG-g-PVAc and N45-7 over water. The measured ratios, which have been obtained from extrapolation of the calibration curves from **Figure 6-7**, consist of both N45-7 over water in the medium and PEG-g-PVAc over water in the coacervates and in the medium.*

3.5 Fragrance inclusion in PEG-g-PVAc coacervates

The results of the previous sections allow shedding some light on the formation of PEG-g-PVAc coacervates, specifying the range of NaCit and N45-7 concentrations necessary to obtain them, and demonstrating their composition. Therefore, the generation of these coacervates at room temperature is properly controlled and defined. However, these coacervates are aimed to be used as perfume encapsulation systems, so that fragrant molecules included in the final product are protected against environmental degradation or early diffusion [8,128,130]. As described in the introduction, coacervates have the property of sequestering molecules from the medium where they exhibit a lower solubility, rendering them as suitable encapsulating tools [8,115]. Indeed, the confocal Raman microscopy results showed that PEG-g-PVAc coacervates have a high density of copolymer and a lower water content, suggesting that they present a more hydrophobic environment that could favorably interact with fragrant molecules.

To explore the potential of PEG-g-PVAc coacervates as perfume microcapsules, we used a premix of RBITC-labelled PEG-g-PVAc (1% w/w) and a perfume (1% w/w) composed of several fragrant molecules with different water affinities (*specifications not given due to intellectual properties*). Coumarin6, an hydrophobic fluorophore, was added to the premix as a tracker of the perfume. Then, the premix (2% w/w) was added to an aqueous solution containing NaCit (5% w/w) and N45-7 (10% w/w), which induced the coacervation of PEG-g-PVAc. After one day, optical and fluorescence microscopy showed the formation of coacervates together with other smaller structures (**Figure 3-18**). While no fluorescence was detected from the medium, coacervates did show co-localization of the red fluorescence coming from the RBITC-labelled copolymer and the green one from Coumarin6. This demonstrates that PEG-g-PVAc coacervates are able to include other compounds from the medium inside their structure, such as Coumarin6. The signal of this tracker appears homogeneously distributed along the coacervate, not following a core-shell structure nor a multiple compartmentalization.

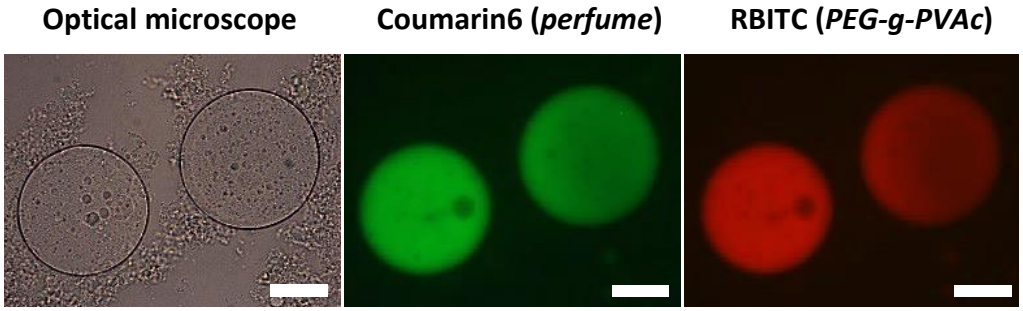

***Figure 3-18**: Optical (left) and fluorescence (middle and right) microscopy pictures from RBITC-labelled PEG-g-PVAc coacervates including Coumarin6* in their internal structure. The fluorescence pictures were taken some seconds later than the optical one. The scale bar corresponds to 50 μm.

We continued by assessing the effect of the copolymer/perfume mass ratio over coacervation. For that, we prepared five samples containing the same concentrations of premix (2% w/w), N45-7 (10% w/w), and NaCit (5%), but different polymer/perfume mass ratios of the premix (1:9, 3:7, 5:5, 7:3, and 9:1). Fluorescence confocal microscopy revealed differences among the coacervates of these five samples (**Figure 3-19)**. When the polymer/perfume mass ratio was low, only a few coacervates were formed, with different shapes, and surrounded by a greenish matrix likely made of surfactant and perfume. This suggests that the perfume was not properly internalized into coacervates. Therefore, it is recommended to do not mix high amounts of perfume with low amounts of copolymer. On the other side, when the ratio was high, there were more and larger coacervates and no greenish matrix was observed. In this case, the solution had a reddish color, indicating that some copolymer was remaining in the medium, probably as single-chain nanoparticles [164], rather than forming part of the coacervate phase. There might be a bit of perfume out of the coacervates, but no Coumarin6 signal is detected in the medium. These results do not provide definitive evidence of the "perfect" ratio where all of the perfume is properly internalized in the coacervates and no extra copolymer remains in solution. However, they demonstrate that the copolymer/perfume mass ratio is an important parameter to consider for an optimized formation of PEG-g-PVAc coacervates and a proper perfume encapsulation, and they suggest that a polymer/perfume mass ratio between 5:5 and 7:3 is optimal.

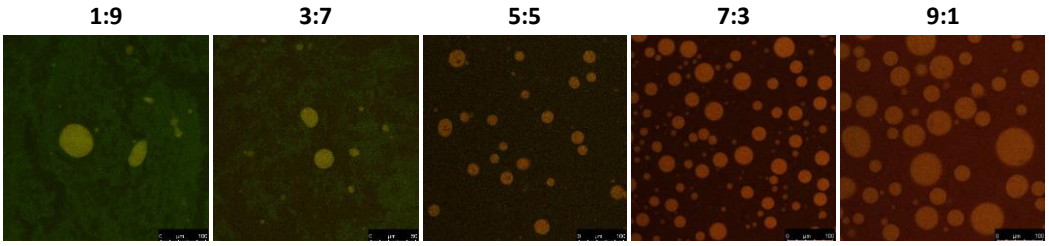

***Figure 3-19**: Fluorescence confocal microscope pictures showing the PEG-g-PVAc coacervates obtained at different copolymer/perfume mass ratios (from left to right: 1:9, 3:7, 5:5, 7:3, and 9:1). The pictures combine both the green fluorescence of Coumarin6 and the red fluorescence of RBITC, showing an orange color for the spaces where both signals are detected.*

To further evaluate the potential of PEG-g-PVAc coacervates as microcapsules, we assessed their stability at dry conditions. For that, we let a droplet of a water solution made of premix (2% w/w, 1:1 copolymer/perfume mass ratio), N45-7 (10% w/w), and NaCit (5% w/w) dry on a microscope glass for a day. Once dry, fluorescence confocal microscopy was used to check the presence of PEG-g-PVAc coacervates (**Figure 3-20**). Due to dehydration, the fluorescence intensity was much lower. However, after increasing the gain of the microscope, we observed the presence of globular domains with both red (RBITC) and green (Coumarin6) fluorescence. These structures are likely the PEG-g-PVAc coacervates containing Coumarin6 that, while drying, deposited on the microscope glass. Remarkably, the coacervates held stable during water evaporation, which can be ascribed to the depression of the cloud point temperature (CPT). As previously demonstrated, N45-7 and NaCit decrease the CPT of PEG-g-PVAc, allowing its coacervation. With water evaporation, the concentration of these two additives increases, and thus the copolymer's CPT lowers. Consequently, PEG-g-PVAc becomes even less soluble in water, keeping the coacervate stable and the Coumarin6 in it. These results suggest that fragrant molecules could be retained in PEG-g-PVAc coacervates even while drying. However, once dry, the fragrances would likely start evaporating. The fluorescence confocal microscope pictures of **Figure 3-20** also show RBITC and Coumarin6 outside the coacervates. Although this could be ascribed to the increased gain of the microscope, it is possible that some Coumarin6 diffused out of the coacervates during the drying process. The dark domains without fluorescence should be coming from bubbles or liquid-

liquid phase separated surfactant due to the increase in NaCit concentration with water evaporation.

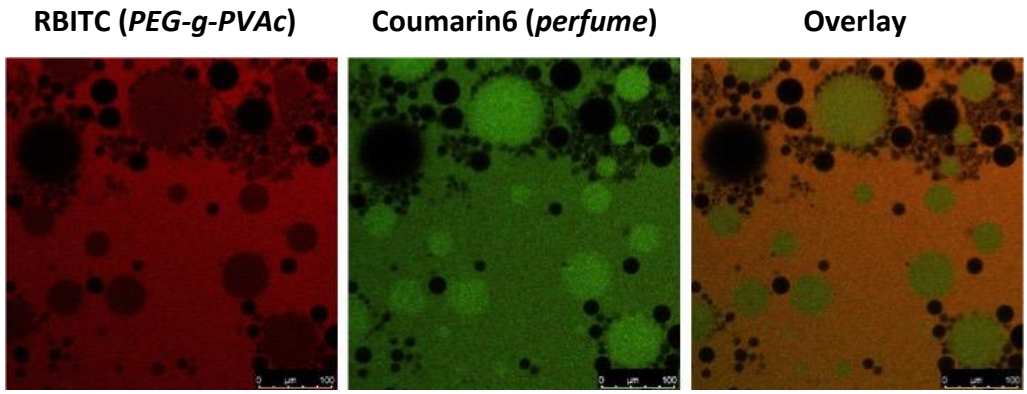

***Figure 3-20**: Fluorescence confocal microscopy pictures of a dried aqueous sample containing premix (2% w/w), N45-7 (10% w/w), and NaCit (5% w/w). They show that PEG-g-PVAc coacervates resisted water evaporation and kept Coumarin6 concentrated in them.*

As observed through fluorescence confocal microscopy, PEG-g-PVAc coacervates do not follow a core-shell structure. Instead, the internal structure of these coacervates resembles a bicontinuous phase [165,166], such as the one of other polymer-nonionic surfactant systems [121]. There is no hard shell around these microstructures, contrary to the commonly used melamine formaldehyde microcapsules [13,14]. Therefore, perfume or, in this case, Coumarin6 is not physically trapped in the coacervates, rather concentrated in them due to a preferred interaction with the LLPS copolymer than with water. To better understand the perfume retention potential of PEG-g-PVAc coacervates, we decided to add the perfume (with Coumarin6) after PEG-g-PVAc coacervation. Therefore, first a sample with PEG-g-PVAc (1% w/w), N45-7 (10% w/w), and NaCit (5% w/w) was prepared to get coacervates and, after checking their formation, perfume (1% w/w) with Coumarin6 was added. Interestingly, the fluorescence signal of the Coumarin6 was detected inside the coacervates, proving the permeation of this fluorophore inside the coacervates even after their formation (**Figure 3-21)**. This result does not only prove the permeability of PEG-g-PVAc coacervates, but it also suggests that perfume added to the medium after coacervation could be spontaneously absorbed by them (later demonstrated in

Figure 3-31). This also eliminates the need of preparing a premix of copolymer and perfume first.

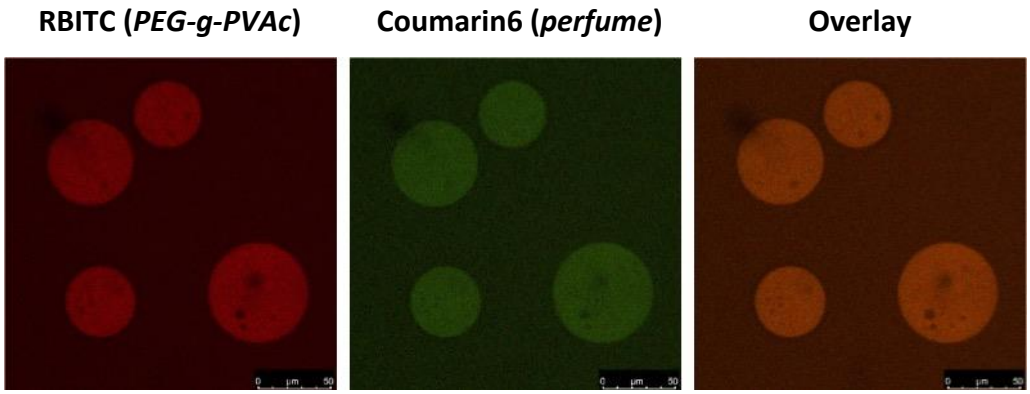

***Figure 3-21**: Fluorescence confocal microscopy pictures of RBITC-labelled PEG-g-PVAc coacervates that absorbed Coumarin6 even though this latter was added at a later stage, after coacervation.*

Considering the aim of PEG-g-PVAc coacervates is to be used as perfume encapsulating agents in beauty and home care formulations, we assessed their formation and perfume retention capability in detergents. These formulations are composed of dozens of additives, but their main ingredients are salts, and both non-ionic and anionic surfactants. As previously demonstrated, kosmotropic salts and non-ionic surfactants decrease the CPT (**Figure 3-4**), favoring PEG-g-PVAc coacervation, while anionic surfactants increase it (**Figure 3-6**), hampering coacervation. Therefore, coacervation is more likely to take place in a detergent where the concentration of kosmotropes and non-ionic surfactant is high while the concentration of anionic surfactant is low. To this regard, PEG-g-PVAc coacervation was assessed in three detergent formulations containing different concentrations of salts and surfactants. Two samples were prepared for each detergent, one with only PEG-g-PVAc (1% w/w), and the other with both PEG-g-PVAc (1% w/w) and the same perfume (1% w/w) containing Coumarin6. No extra salts nor surfactants were added. Coacervation was achieved only in one of the three detergents (**Figure 3-22**), precisely the one with (i) the highest concentration of kosmotropic salts, (ii) the highest concentration of non-ionic surfactant, and (iii) the lowest ionic to non-ionic surfactant mass ratio. Therefore, the composition of the detergent is crucial to use PEG-g-PVAc

coacervates as perfume microcapsules. The sample with PEG-g-PVAc but no perfume proved that PEG-g-PVAc coacervation takes place in this detergent regardless of the perfume presence. However, due to the presence of ionic surfactant, some copolymer remains soluble in the medium giving it this reddish color (**Figure 3-22**). The sample with both PEG-g-PVAc and perfume showed the presence of coacervates with Coumarin6, demonstrating the successful formation of these microstructures in a detergent and suggesting perfume inclusion. The nature of the other microstructures with a lower content of PEG-g-PVAc that can be observed in the fluorescence confocal microscope pictures (**Figure 3-22**) was not studied due to the complexity of these formulations.

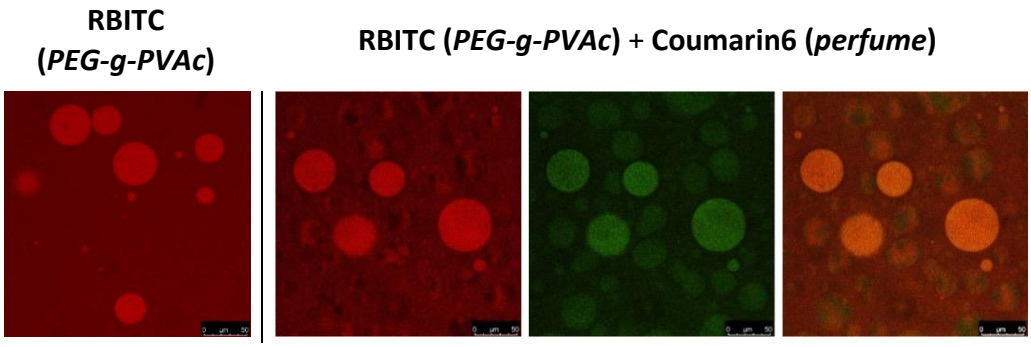

***Figure 3-22**: Fluorescence confocal microscopy pictures of RBITC-labelled PEG-g-PVAc coacervates without (left) and with (right) perfume containing Coumarin6 in a detergent formulation.*

Unfortunately, the internalization of Coumarin6 in PEG-g-PVAc coacervates does not demonstrate the internalization of the perfume itself. It does suggest that other hydrophobic compounds could possibly be internalized and contained in these coacervates, but it does not prove it. Moreover, perfumes are made of several fragrant molecules characterized by different functional groups and water affinities. Therefore, each fragrance could have a different interaction with the coacervated PEG-g-PVAc, leading to different encapsulation efficiencies. To explore the importance of this individual interactions, seven fragrant molecules were chosen: phenyl ethanol, carvone, linalool, florhydral, citronellol, pinene, and limonene (see section 2.1 Materials for further details). Their water affinities, expressed by the octanol/water partition coefficient (log K_{ow}, commonly referred to as log P [245]) are 1.36, 2.74, 2.97, 3.02, 3.30, 4.44, and 4.57, respectively. The higher the value of this coefficient, the more hydrophobic the fragrance is. Then,

aqueous solutions of PEG-g-PVAc (1% w/w) and fragrance (1% w/w) were assessed through fluorescence confocal microscopy. No Coumarin6 was added, so the only fluorescence detected was that of the RBITC-labelled copolymer. The pictures of **Figure 3-23** show the different assemblies obtained for each fragrance, ascribed to the amphiphilicity of PEG-g-PVAc and its specific interactions with the fragrance. Four different scenarios were identified: (i) with phenyl ethanol, the copolymer and the perfume remain dispersed in the medium, (ii) with carvone, florhydral, and citronellol, the copolymer forms globular micron-sized assemblies, (iii) with linalool, precipitate-like assemblies of copolymer appear, showing different non-globular shapes, and (iv) with pinene, and limonene, the copolymer remains dispersed in the medium while the perfume phase separates as droplets. Regarding the partition coefficient, the most hydrophilic fragrance remained dissolved in the aqueous medium, the ones at the middle range showed some favorable interaction with PEG-g-PVAc and generated different assemblies, while the most hydrophobic ones phase separated as droplets. This suggests that fragrances with a logP between 2.74 and 3.30 could interact better with PEG-g-PVAc and thus be easier to encapsulate. However, the different structures obtained for linalool (logP = 2.97) and florhydral (logP = 3.03) demonstrate that the octanol/water partition coefficient is not enough as to predict copolymer-perfume assemblies.

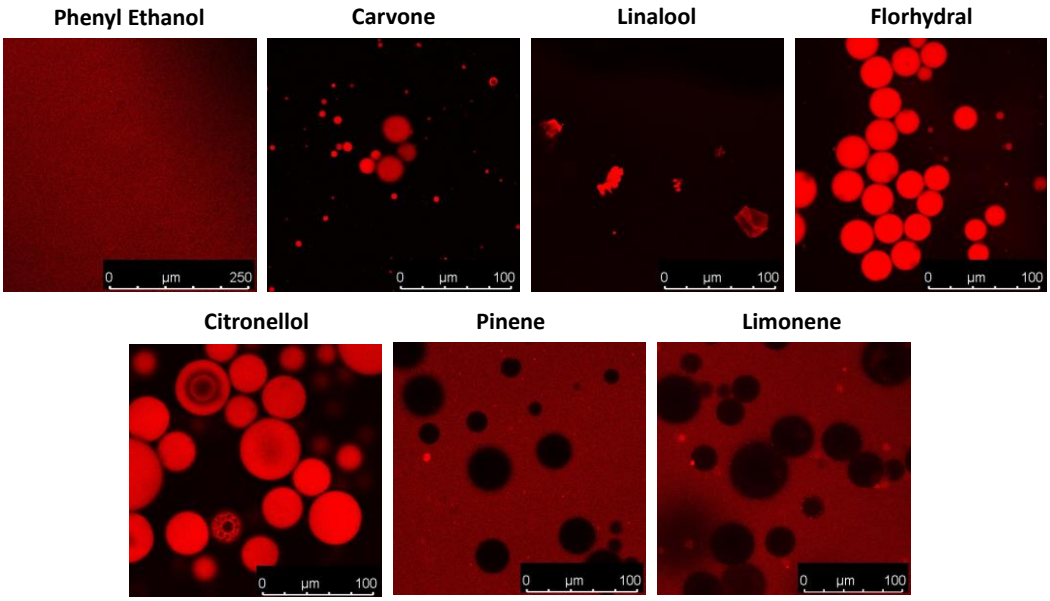

***Figure 3-23**: Fluorescence confocal microscopy pictures of PEG-g-PVAc (1% w/w) with different fragrances (1% w/w) in water. Different PEG-g-PVAc assemblies take place depending on its interaction with the fragrance.*

Overall, these results prove that depending on the fragrance different interactions with the copolymer take place, giving rise to different assemblies and affecting the encapsulation efficiency. Similar studies can be found in the literature remarking the relevance of these specific interactions with different fragrances [170,246,247]. Therefore, although Coumarin6 was internalized in PEG-g-PVAc coacervates, an individual study for each fragrance should be performed to assure it is properly retained in the coacervate, possibly through confocal Raman microscopy [248]. Another option would be to use the Hansen solubility parameters and compare the ones of the copolymer with the ones of the fragrances [249]. These parameters consider the chemical features of the molecule and give it a combination of three values – δD for Dispersion (van der Waals), δP for Polarity (related to dipole moment) and δH for Hydrogen bonding. Depending on how close the values of two different molecules are, one can approximately predict how miscible or interacting they will be.

The globular microstructures distinguished in the samples containing carvone, florhydral, or citronellol have some similarities with PEG-g-PVAc coacervates, but they are not the same system. On the one hand, these fragrance-induced microstructures showed the RBITC-labelled PEG-g-PVAc homogenously distributed within them, except for few cases of the citronellol sample in which inner copolymer-depleted domains were observed. This resembles PEG-g-PVAc coacervates and denies a possible core-shell structure. On the other hand, these fragrance-induced microstructures share some properties with emulsions, since no coalescence was observed, even after being close to each other for long (**Figure 3-24**, left). Moreover, they do not hold stable after water evaporation nor the addition of non-ionic surfactant (N45-7). In the case of water evaporation, they explode once not enough water is around them, like if the pressure inside is too high to keep the structure together. Instead, after N45-7 (1% w/w) addition, they immediately start dismantling into smaller microstructures, like an effervescent pill in water (**Figure 3-24**, right). This kind of behavior has previously been ascribed to the different surface activity of the surfactant and the copolymer [250]. Therefore, these structures are unlikely to hold stable in a surfactant-rich formulation such as liquid detergents. All these differences showcase that PEG-g-PVAc coacervates and fragrance-induced PEG-g-PVAc microstructures are not the same.

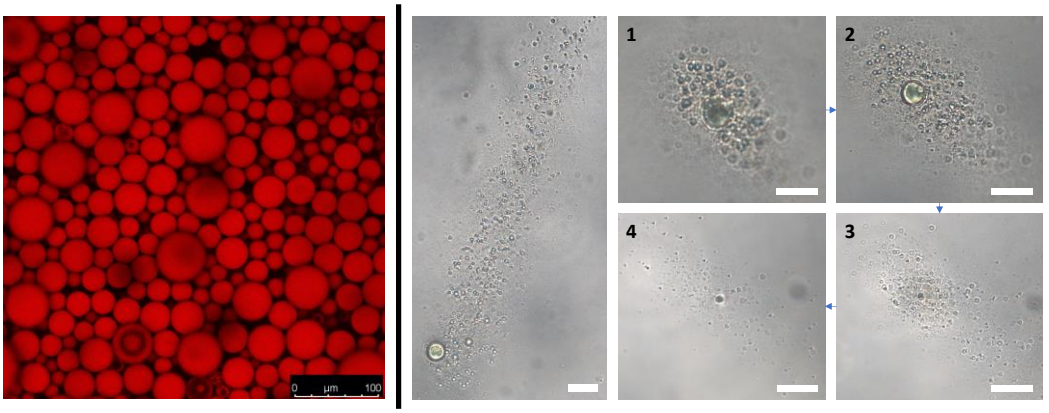

***Figure 3-24**: Florhydral-induced PEG-g-PVAc microstructures (1% w/w florhydral and 1% w/w PEG-g-PVAc in water) showing their lack of coalescence under the fluorescence confocal microscope (left), and their destabilization after N45-7 addition under the optical microscope (right). The scale bars on the optical microscope pictures correspond to 20 µm.*

3.6 Destabilization of PEG-g-PVAc coacervates

PEG-g-PVAc coacervates have shown their ability to spontaneously absorb Coumarin6 from a complex surfactant-rich aqueous medium, suggesting their potential as microcapsules of compounds with a lower water solubility. However, these compounds also need to be released at a certain point. Considering the LCST thermoresponsive nature of PEG-g-PVAc, this copolymer becomes hydrophilic enough to dissolve once the CPT is above room temperature. This increased solubility leads to coacervate disassembly and release of any compound retained in it. Therefore, the destabilization of PEG-g-PVAc coacervates can be achieved by increasing the CPT to values above room temperature (**Figure 3-25**). In regard, the addition of any additive that increases the CPT, such as chaotropic molecules, or a mere decrease of the room temperature, can induce the destabilization of these coacervates and consequently trigger the release of their contained compounds.

To study the destabilization and release of PEG-g-PVAc coacervates, two different techniques were employed. First, fluorescence confocal microscopy together with microfluidics provided a qualitative study of their destabilization profile. Then, UV-Vis spectrophotometry determined in a more quantitative way the encapsulation and release of Coumarin6.

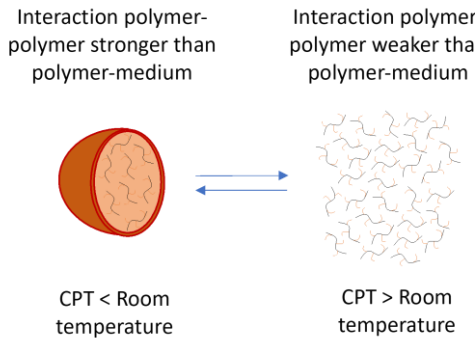

***Figure 3-25**: Schematic representation of the formation and destabilization of PEG-g-PVAc coacervates.*

Coacervates were generated by mixing an aqueous solution of RBITC-labelled PEG-g-PVAc (1% w/w), N45-7 (5% w/w), and NaCit (5% w/w). After formation, Coumarin 6 (≈ 10 mg/L) was added to be able to track the release of an encapsulated compound. Fluorescence confocal microscopy was used to check the presence of PEG-g-PVAc coacervates containing Coumarin6 (**Figure 3-26**).

Once more, the fluorescence of Coumarin6 is homogeneously detected from within the coacervate, together with the fluorescence of the labelled copolymer.

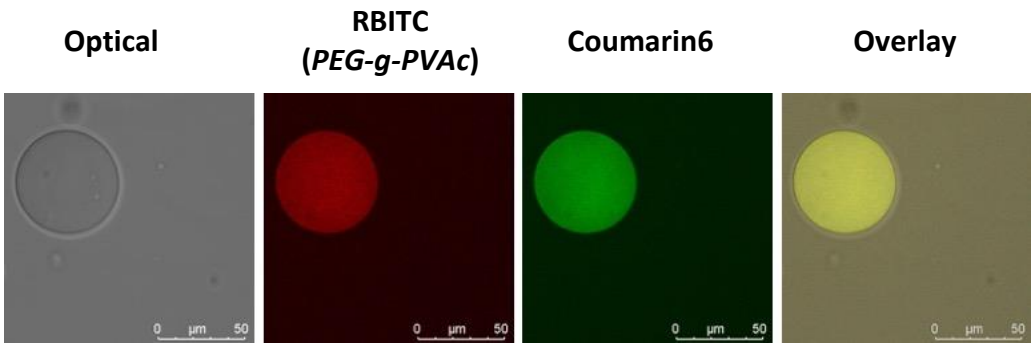

***Figure 3-26**: Optical and fluorescence confocal microscopy pictures of RBITC-labelled PEG-g-PVAc coacervates with Coumarin6 before triggering their destabilization.*

Then, around 50 mg of urea were added on top of the sample (around 4 droplets, so 0.2 mL) deposited over the microscope glass. With the dissolution of this urea, the PEG-g-PVAc becomes more soluble, and thus the CPT of the sample on the microscope glass raises. The consequent destabilization of the coacervates was observed through fluorescence confocal microscopy, identifying seven different stages:

1. Stable coacervate, with fluorescence homogenously distributed within it.
2. Some polymer and perfume depleted domains start appearing around the coacervate, indicating the beginning of the destabilization process.
3. The polymer and perfume depleted domains appear all over the coacervate.
4. These inner domains enlarge, changing the globular shape of the coacervate. Surprisingly, this stage lasts for long in some destabilization assays (**Figure 6-8**). A similar phase was reported for pH sensitive coacervates [163].
5. The large internal domains diffuse along the coacervate, slightly reducing the fluorescence intensity of the core of the coacervate. At this point, the fluorescence distribution resembles a core-shell structure.
6. The “shell” or surrounding of the coacervates breaks and retracts.

7. Both the core and the broken “shell” of the coacervate dissolve along the medium.

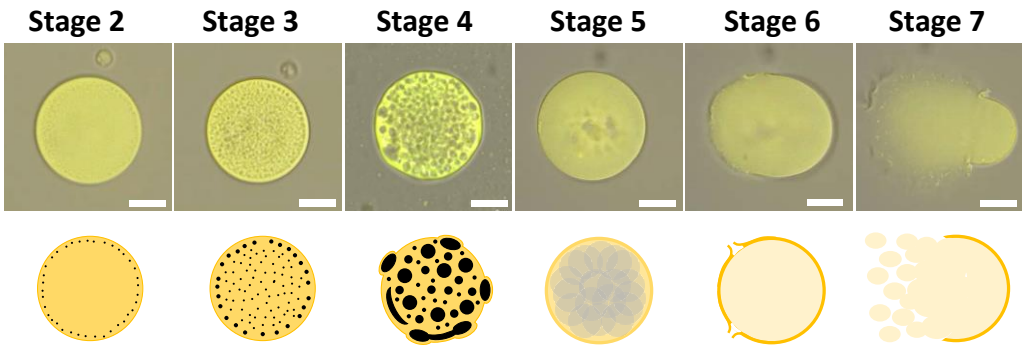

***Figure 3-27**: Fluorescence confocal microscopy pictures and schematic representation of the PEG-g-PVAc coacervates destabilization. The yellow-colored fluorescence comes from the overlay of the red RBITC-labelled PEG-g-PVAc and the green Coumarin6. The stage 1, which is not represented in this figure, corresponds to the stable coacervate. The scale bar is equivalent to 20 μm.*

The different stages of PEG-g-PVAc coacervate destabilization are shown in **Figure 3-27**, demonstrating that both PEG-g-PVAc and Coumarin6 end up being released to the aqueous medium. This suggests that any compound contained in these coacervates would also be released upon destabilization. The same seven stages were observed after adding around 4 water droplets to the sample on the microscope glass (**Figure 6-9**). The addition of water decreases both NaCit and N45-7 concentrations. Once their concentration is low enough as to raise the CPT above room temperature, the copolymer becomes more soluble and the coacervate destabilizes. This suggests that PEG-g-PVAc coacervates could be used in formulations to release all its contained perfume upon water dilution.

The destabilization of PEG-g-PVAc coacervates was also observed using microfluidics. PDMS meander chips, with dimensions close to the average size of PEG-g-PVAc coacervates (see specifics in **Figure 6-10**), were employed to trap and observe their destabilization. Due to the viscosity of these microstructures, it was challenging to keep them for long in the meander traps. Even though the flow rate was very low (0.01 - 0.1 μL/s), it was enough to slowly deform them and, after a short time, push them through the microfluidics trap hole. However, as **Figure 3-28** shows, we were able to capture the destabilization of PEG-g-PVAc

coacervates upon water addition. As expected, once pure water (in green, containing ~0.01% w/w of R110C) reaches the trapped PEG-g-PVAc coacervate (in red, due to the RBITC-labelled copolymer), an immediate destabilization and dissolution takes place. This is ascribed to the abrupt decrease of NaCit and N45-7 concentrations. Another example of this destabilization can be observed in **Figure 6-11**.

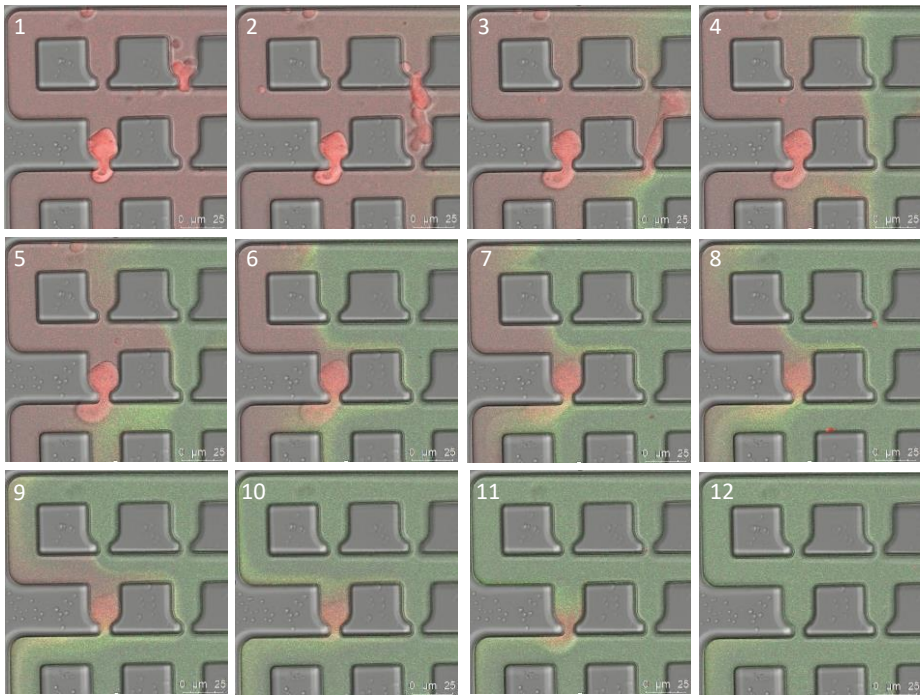

***Figure 3-28**: Destabilization of RBITC-labelled PEG-g-PVAc coacervates (in red) with the addition of water (in green, due to its content of R110C). The pictures of the meander microfluidics chip, taken every 0.5 seconds, were captured using fluorescence confocal microscopy.*

The qualitative study performed with fluorescence confocal microscopy demonstrated how PEG-g-PVAc coacervates destabilize and release the compounds contained in them. To assess the release of Coumarin6 in a more quantitative way, UV-Vis spectrophotometry was used to analyze a sample containing N45-7 (5% w/w), NaCit (5% w/w), and Coumarin6 (≈ 20 mg/L). Coumarin6 does not dissolve in pure water, but it does in presence of surfactants [251]. This fluorescent monophasic sample was used as reference to determine the absorbance of Coumarin6 in the absence of PEG-g-PVAc coacervates, which

resulted to be equal to 1.4 absorbance units (**Figure 3-29**). Then, PEG-g-PVAc (1% w/w) was added to this solution and coacervation took place. Consequently, part of the total Coumarin6 in solution should be spontaneously absorbed into the PEG-g-PVAc coacervates, as suggested by **Figure 3-21**.

After assessing different centrifugation programs (see section 2.2.7 UV-Vis spectrophotometry for further details), we concluded that a centrifugation of 10000 rpm for 10 minutes was enough to obtain a supernatant without LLPS PEG-g-PVAc (**Figure 6-12**). Therefore, part of this sample containing PEG-g-PVAc coacervates was centrifuged at 10000 rpm for 10 minutes, and the supernatant was then assessed through UV-Vis spectrophotometry. This time, the absorbance of Coumarin6 dropped to 0.97 (**Figure 3-29**). This reduction in absorbance proves the spontaneous enrichment of Coumarin6 in the PEG-g-PVAc coacervates. Centrifugation induced the sedimentation of these coacervates, sequestering the Coumarin6 within coacervates from the supernatant. Considering the different absorbances of the sample before (1.4) and after (0.97) PEG-g-PVAc coacervation, we can say that the coacervates absorbed approximately 30% of the Coumarin6 in solution. The rest is likely interacting with the N45-7 dissolved in the medium. This means quite a large amount of the Coumarin6 in the medium was spontaneously internalized in the PEG-g-PVAc coacervates, by using a copolymer concentration as low as 1% w/w. Even though it was not addressed in this thesis, the total internalization of Coumarin6 could probably be enhanced by increasing the number/size of coacervates.

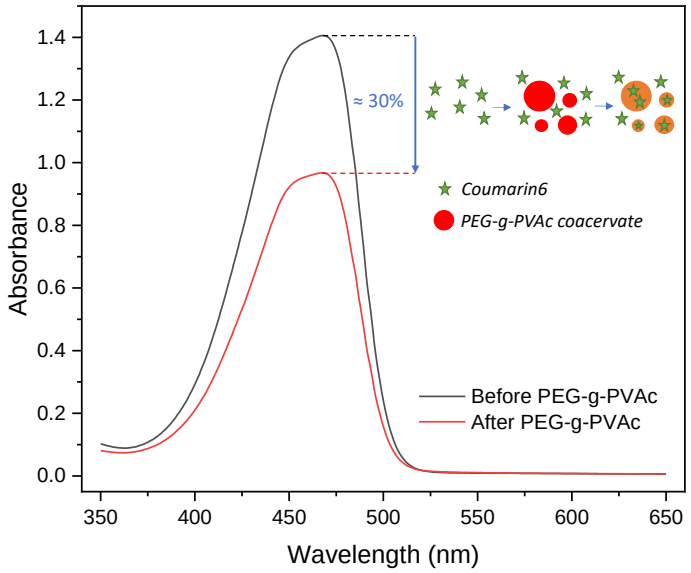

***Figure 3-29**: UV-Vis spectra showing the absorption of Coumarin6 from the supernatants of a centrifuged sample before (black) and after (red) PEG-g-PVAc coacervation.*

Two additional studies were performed using the same sample containing PEG-g-PVAc coacervates. The first one aimed to relate the destabilization of PEG-g-PVAc coacervates and the release of Coumarin6 to the increase of the CPT. Considering the concentrations of N45-7 (5% w/w) and NaCit (5% w/w), this sample should have a CPT around 18 °C (**Figure 3-4**). To study the effect of the CPT over PEG-g-PVAc coacervate stability, 2% w/w urea was stepwise added to increase the CPT around 2 °C. After each addition, the sample was centrifuged at 10000 rpm for 10 minutes and the supernatant assessed through UV-Vis spectrophotometry. The acquired UV-Vis spectra show an increase in the absorbance of Coumarin6 after each urea addition (**Figure 3-30**). This suggests that the addition of urea destabilizes PEG-g-PVAc coacervates, which are then releasing its retained Coumarin6 and consequently increasing the UV-Vis absorbance of the supernatant. As the inset of the graph of **Figure 3-30** shows, the steepest absorbance increase takes place when the CPT is in the room temperature range. This is in line with the PEG-g-PVAc coacervates destabilizing once the CPT is above room temperature. The increase of absorbance does not take place abruptly but progressively due to the acceptable polydispersity of PEG-g-PVAc, which means that the CPT falls on a range of temperatures rather than

on a single one. Moreover, considering that the absorbance of this sample was equal to 1.4 absorbance units in the absence of PEG-g-PVAc (**Figure 3-29**), we know that the release of Coumarin6 from the coacervates must be total after the sixth addition of urea. Additionally, no pellet was found in the sample after the sixth urea addition, suggesting the absence of LLPS PEG-g-PVAc. These results demonstrate in a quantitative way what was previously observed under fluorescence confocal microscopy: (i) urea addition can destabilize PEG-g-PVAc coacervates, and (ii) their destabilization leads to a complete release of the Coumarin6 contained in them.

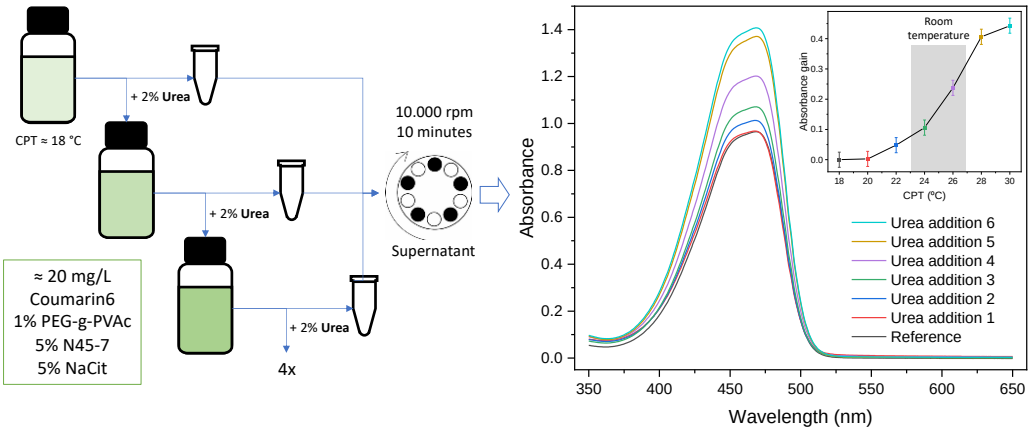

***Figure 3-30**: Schematic representation of the urea addition process (left) and UV-Vis spectra of the same sample after consecutive additions of urea (right). The inset shows how the Coumarin6 absorbance increases as the CPT raises, mainly in the room temperature range.*

The second study focused on the spontaneous absorption and release of Coumarin6 after the formation and destabilization of PEG-g-PVAc coacervates, respectively. This time, 12% w/w of urea and 2.4% w/w of NaCit were alternatively added to the sample. Considering the CPT of this sample (1% w/w PEG-g-PVAc, 5% w/w N45-7, 5% w/w NaCit) is around 18 °C, these amounts of urea and NaCit should be enough to alternatively destabilize and form PEG-g-PVAc coacervates (**Figure 3-4**), respectively. After each addition of either urea or NaCit, the sample was centrifuged at 10000 rpm for 10 minutes and the supernatant assessed through UV-Vis spectrophotometry. Interestingly, the samples after urea addition did not form a pellet after centrifugation, while the samples after NaCit addition did form it, suggesting the absence or presence of

LLPS PEG-g-PVAc after urea or NaCit addition, respectively. The UV-Vis spectra of the supernatants clearly show the effect of PEG-g-PVAc coacervation over the supernatant absorbance (**Figure 3-31**). After each addition of urea, the total Coumarin6 absorbance grows, while after each addition of NaCit, the absorbance decays. Since all the additions of urea and NaCit were performed in the same sample, this demonstrates both the reversible formation of PEG-g-PVAc coacervates and their spontaneous absorption of Coumarin6. The UV-Vis spectra also showed a lower Coumarin6 absorption after each addition cycle. This can be ascribed to the decrease of the Coumarin6 concentration in sample after each urea or NaCit addition. The inset of the graph of **Figure 3-31** shows in a more visual way the abrupt increase and decrease of Coumarin6 absorbance after each addition cycle, as well as the decay in the maximum absorption. A similar trend was reported for pH sensitive coacervates to which the same formation/deformation cycle was applied [163].

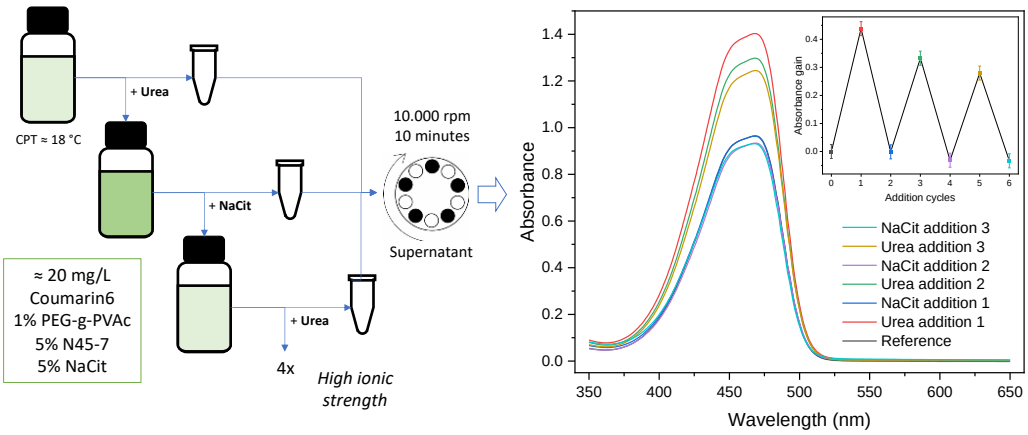

***Figure 3-31**: Schematic representation of the urea/NaCIt addition process (left) and UV-Vis spectra of the same sample after alternative additions of urea and NaCit (right). The inset shows how the Coumarin6 absorbance increases or decreases abruptly after each addition of urea or NaCit, respectively.*

The overall of these results demonstrates the feasibility of PEG-g-PVAc coacervates to spontaneously absorb and then release hydrophobic molecules in a triggered way. The release is total, and it takes place once the CPT is above room temperature. Therefore, it can be triggered by water dilution, addition of chaotropic agents, such as urea, or by merely decreasing room temperature.

4. CONCLUSIONS AND FUTURE PERSPECTIVES

The goal of this thesis was to provide a contribution to the current quest for biodegradable materials and efficient encapsulating agents for home and beauty care products. Several previous studies addressed the self-assembly and perfume encapsulation properties of an amphiphilic LCST-type thermoresponsive graft copolymer (poly(ethylene glycol)-g-poly(vinyl acetate), or PEG-g-PVAc) [164–166,170], suggesting it to be a good candidate for the aims of this project. This thesis expands these previous studies on the LLPS (liquid-liquid phase separation) of PEG-g-PVAc and specifically explores the controlled formation of coacervates to be applied as perfume microcapsules in consumer good products.

First, we addressed the conditions for the LLPS of PEG-g-PVAc in water, to understand and control the formation of coacervates at room temperature. We determined the effect of several additives over the cloud point temperature (CPT) of PEG-g-PVAc, showing that kosmotropes decrease the CPT (NaCit > NaCl > NaBr), while chaotropes increase it (NaCS > urea > MPG). The addition of non-ionic surfactants also reduces the CPT, with the most hydrophobic surfactant showing a higher effectivity (N45-7 > L24-9). Conversely, ionic surfactants markedly increase the CPT, with anionic surfactants being the most effective (HLAS ≈ AE3S > CTAC ≈ CTAB > DTAC > DTAB). These results are in line with the literature reporting the CPT evolution of other LCST (Lower Critical Solution Temperature) copolymers [140,190,224,252].

This set of results suggested that a combination of kosmotropes and non-ionic surfactants is optimal to promote the phase separation of PEG-g-PVAc at room temperature. Therefore, we then investigated the phase behavior of PEG-g-PVAc aqueous solutions in presence of N45-7 and NaCit to monitor the formation of coacervates. We observed that PEG-g-PVAc coacervates can be easily obtained at room temperature, provided that three conditions are met: (i) the CPT of PEG-g-PVAc is decreased below room temperature, (ii) enough N45-7 (at least 4% w/w for a 1% w/w of PEG-g-PVAc) is added to avoid PEG-g-PVAc precipitation, and (iii) the concentration of NaCit is kept below a threshold value to prevent liquid-liquid bulk phase separation. The easy formation of these coacervates at room

temperature in the presence of salts and surfactants confirms PEG-g-PVAc's potential for consumer good products.

Then, we used confocal Raman microscopy to define the composition of these coacervates, finding that their main constituent is PEG-g-PVAc, but they also contain water and N45-7. Interestingly, the amount of non-ionic surfactant in the coacervates did not significantly change when increasing its bulk concentration. This is beneficial for home care products, where it is preferred to maintain surfactants in the dispersion medium to maximize the detergency. We also observed that the hydration of the coacervates decreases as the total concentration of N45-7 increases. This suggests that the amount of non-ionic surfactant can modulate the hydrophilicity of these microdomains, and thus their affinity for fragrant molecules with different water affinities.

We continued by studying the fragrance inclusion in PEG-g-PVAc coacervates. Fluorescence confocal microscopy showed Coumarin6, a hydrophobic fluorophore, to be spontaneously absorbed by previously generated coacervates. This indicates that these coacervates can absorb hydrophobic molecules from the medium even after formation. The self-assembly of these coacervates and the Coumarin6 encapsulation were also demonstrated in a detergent formulation presenting a favorable concentration of salts and surfactants, proving they can be used as encapsulating agents in consumer good products. Additionally, we showed that PEG-g-PVAc self-assembles in different ways depending on the fragrant molecule, suggesting that the fragrance selection is of utmost importance to optimize the perfume encapsulation.

Finally, we demonstrated that the destabilization of PEG-g-PVAc coacervates takes place once the medium conditions are modified to shift the system's CPT above room temperature. This can be achieved by simply lowering the room temperature, but also by dilution in water, which decreases the concentration of NaCit and N45-7, and addition of chaotropes, such as urea. Fluorescence confocal microscopy showed the destabilization follows seven stages, ending up with a full disassembly of the coacervate and the consequent release of any active contained in them. UV-Vis spectrophotometry proved the spontaneous absorption of Coumarin6 from the medium upon coacervate formation as well as its full release after increasing the CPT with urea addition. The capacity of PEG-g-PVAc coacervates to release their absorbed content in a triggered way after

water or urea addition renders them as suitable encapsulating systems for body and beauty care formulations.

Overall, the results here gathered expand the knowledge on self-coacervation of grafted copolymers and define the conditions at which PEG-g-PVAc coacervates can be obtained in a surfactant-rich medium. Additionally, the encapsulation and release properties of these micron-sized domains demonstrate their feasibility as encapsulating agents for some consumer good products applications. The stability dependence of these coacervates on the CPT can be used as an advantage to disassemble them and release their content upon water dilution in formulations such as shampoos or detergents. However, it is also a drawback for applications that aim to keep the microcapsules stable during the washing process and release their content at a later stage, such as softeners.

For this latter case, additional fundamental studies are needed. Based on these results, we would recommend exploring the coacervation of other thermoresponsive copolymers presenting either:

- An LCST profile with a very low critical temperature. This could lead to self-coacervation at room temperature without the need of additives to decrease the CPT, providing the resulting coacervates with a higher resistance against water dilution
- A combination of LCST and UCST blocks in the same copolymer [78]. This could give rise to a copolymer which coacervation takes place for a broad range of temperatures and destabilizes only at quite high or low temperatures. However, the coacervate stability would probably depend on the copolymer concentration too.

Smart copolymers with a sensitivity other than thermal can also be considered. For instance, light sensitive copolymers could be employed to form a stable microcapsule that destabilizes upon UV irradiation. In consumer products, this would lead to microcapsules that would only release their content once illuminated with sunshine.

Since the project aimed to develop fragrance microcapsules for an industrial application, the focus of this thesis has been on the practical utilization of these polymeric coacervates. Therefore, some theoretical foundations on the

thermodynamics of the system would add relevant information and ease the comprehension of the system. It would also be useful to relate the nucleation and growth mechanism to the morphology of this polymeric coacervates. At the same time, it would be interesting to measure the size of these coacervates once formed and observe its evolution over time, which could be explained through the coarsening of the droplet size. We did try particle size analysis in P&G, but unfortunately it did not yield reliable results due to difficulties with the viscosity of those samples. As a future development, we believe all these should be a priority.

Additionally, running some more turbidimetry experiments with different heating/cooling rates could be useful to determine whether the CPTs have a thermodynamic or a kinetic origin. Finally, regarding the inclusion of fragrance into these coacervates, it would be convenient to study the effect of the polymer-depleted internal areas appearing in the microstructures that contain Florhydral and Citronellol, since they can possibly affect release kinetics. For further information, I refer to the PhD thesis of Constantina Sofroniou, another PhD student of the SAMCAPS project, who assessed the interaction of different fragrances (including Florhydral and Citronellol) with Soluplus, an amphiphilic copolymer with similar properties to PEG-g-PVAc.

"Sapere aude"

5. BIBLIOGRAPHY

[1] F. Paulo, L. Santos, Design of experiments for microencapsulation applications: A review, Mater. Sci. Eng. C. 77 (2017) 1327–1340. https://doi.org/10.1016/j.msec.2017.03.219.

[2] F. Casanova, L. Santos, Encapsulation of cosmetic active ingredients for topical application – a review, J. Microencapsul. 33 (2016) 1–17. https://doi.org/10.3109/02652048.2015.1115900.

[3] M.R.I. Shishir, L. Xie, C. Sun, X. Zheng, W. Chen, Advances in micro and nano-encapsulation of bioactive compounds using biopolymer and lipid-based transporters, Trends Food Sci. Technol. 78 (2018) 34–60. https://doi.org/10.1016/j.tifs.2018.05.018.

[4] M. Saifullah, M.R.I. Shishir, R. Ferdowsi, M.R. Tanver Rahman, Q. Van Vuong, Micro and nano encapsulation, retention and controlled release of flavor and aroma compounds: A critical review, Trends Food Sci. Technol. 86 (2019) 230–251. https://doi.org/10.1016/j.tifs.2019.02.030.

[5] C.S.A. de Lima, T.S. Balogh, J.P.R.O. Varca, G.H.C. Varca, A.B. Lugão, L. A. Camacho-Cruz, E. Bucio, S.S. Kadlubowski, An Updated Review of Macro, Micro, and Nanostructured Hydrogels for Biomedical and Pharmaceutical Applications, Pharmaceutics. 12 (2020) 970. https://doi.org/10.3390/pharmaceutics12100970.

[6] C. Avonto, M. Wang, A.G. Chittiboyina, S. Vukmanovic, I.A. Khan, Chemical stability and in chemico reactivity of 24 fragrance ingredients of concern for skin sensitization risk assessment, Toxicol. Vitr. 46 (2018) 237–245. https://doi.org/10.1016/j.tiv.2017.09.007.

[7] C.S. Cortez-Pereira, A.R. Baby, M.V.R. Velasco, Review Article: Fragrance technology for the dermatologist - a review and practical application, J. Cosmet. Dermatol. 9 (2010) 230–241. https://doi.org/10.1111/j.1473-2165.2010.00514.x.

[8] D.R. Perinelli, G.F. Palmieri, M. Cespi, G. Bonacucina, Encapsulation of Flavours and Fragrances into Polymeric Capsules and Cyclodextrins Inclusion Complexes: An Update, Molecules. 25 (2020). https://doi.org/10.3390/molecules25245878.

[9] R. Kaur, D. Kukkar, S.K. Bhardwaj, K.H. Kim, A. Deep, Potential use of polymers and their complexes as media for storage and delivery of fragrances, J. Control. Release. 285 (2018) 81–95. https://doi.org/10.1016/j.jconrel.2018.07.008.

[10] H. Lee, C.-H. Choi, A. Abbaspourrad, C. Wesner, M. Caggioni, T. Zhu, D.A. Weitz, Encapsulation and Enhanced Retention of Fragrance in Polymer Microcapsules, ACS Appl. Mater. Interfaces. 8 (2016) 4007–4013. https://doi.org/10.1021/acsami.5b11351.

[11] L. He, J. Hu, W. Deng, Preparation and application of flavor and fragrance capsules, Polym. Chem. 9 (2018) 4926–4946. https://doi.org/10.1039/c8py00863a.

[12] I.M. Martins, M.F. Barreiro, M. Coelho, A.E. Rodrigues, Microencapsulation of essential oils with biodegradable polymeric carriers for cosmetic applications, Chem. Eng. J. 245 (2014) 191–200. https://doi.org/10.1016/j.cej.2014.02.024.

[13] X. Fei, H. Zhao, B. Zhang, L. Cao, M. Yu, J. Zhou, L. Yu, Microencapsulation mechanism and size control of fragrance microcapsules with melamine resin shell, Colloids Surfaces A Physicochem. Eng. Asp. 469 (2015) 300–306. https://doi.org/10.1016/j.colsurfa.2015.01.033.

[14] C. Sui, J.A. Preece, Z. Zhang, S.H. Yu, Efficient encapsulation of water soluble inorganic

and organic actives in melamine formaldehyde based microcapsules for control release into an aqueous environment, Chem. Eng. Sci. 229 (2021) 116103. https://doi.org/10.1016/j.ces.2020.116103.

[15] D.J. Merline, S. Vukusic, A.A. Abdala, Melamine formaldehyde: Curing studies and reaction mechanism, Polym. J. 45 (2013) 413–419. https://doi.org/10.1038/pj.2012.162.

[16] F. Salvador Cesa, A. Turra, J. Baruque-Ramos, Synthetic fibers as microplastics in the marine environment: A review from textile perspective with a focus on domestic washings, Sci. Total Environ. 598 (2017) 1116–1129. https://doi.org/10.1016/j.scitotenv.2017.04.172.

[17] K. Bruyninckx, M. Dusselier, Sustainable Chemistry Considerations for the Encapsulation of Volatile Compounds in Laundry-Type Applications, ACS Sustain. Chem. Eng. 7 (2019) 8041–8054. https://doi.org/10.1021/acssuschemeng.9b00677.

[18] G. León, N. Paret, P. Fankhauser, D. Grenno, P. Erni, L. Ouali, D.L. Berthier, Formaldehyde-free melamine microcapsules as core/shell delivery systems for encapsulation of volatile active ingredients, RSC Adv. 7 (2017) 18962–18975. https://doi.org/10.1039/c7ra01413a.

[19] J. Hu, X. Zhang, J. Qu, Y. Wen, W. Sun, Synthesis, Characterizations and Mechanical Properties of Microcapsules with Dual Shell of Polyurethane (PU)/Melamine Formaldehyde (MF): Effect of Different Chain Extenders, Ind. Eng. Chem. Res. 57 (2018) 3591–3601. https://doi.org/10.1021/acs.iecr.7b04973.

[20] A.P. Esser-Kahn, S.A. Odom, N.R. Sottos, S.R. White, J.S. Moore, Triggered Release from Polymer Capsules, Macromolecules. 44 (2011) 5539–5553. https://doi.org/10.1021/ma201014n.

[21] I. Insua, A. Wilkinson, F. Fernandez-Trillo, Polyion complex (PIC) particles: Preparation and biomedical applications, Eur. Polym. J. 81 (2016) 198–215. https://doi.org/10.1016/j.eurpolymj.2016.06.003.

[22] U. Kragh-Hansen, M. le Maire, J. V. Møller, The Mechanism of Detergent Solubilization of Liposomes and Protein-Containing Membranes, Biophys. J. 75 (1998) 2932–2946. https://doi.org/10.1016/S0006-3495(98)77735-5.

[23] P.C. Painter, M.M. Coleman, Fundamentals of Polymer Science, Routledge, 2019. https://doi.org/10.1201/9780203755211.

[24] P. Alexandridis, Amphiphilic copolymers and their applications, Curr. Opin. Colloid Interface Sci. 1 (1996) 490–501. https://doi.org/10.1016/S1359-0294(96)80118-X.

[25] K. Holmberg, B. Jönsson, B. Kronberg, B. Lindman, Surfactants and Polymers in Aqueous Solution, 2002. https://doi.org/10.1002/0470856424.

[26] H. Wennerström, B. Lindman, Micelles. Physical chemistry of surfactant association, Phys. Rep. 52 (1979) 1–86. https://doi.org/10.1016/0370-1573(79)90087-5.

[27] R. Nagarajan, E. Ruckenstein, Theory of surfactant self-assembly: a predictive molecular thermodynamic approach, Langmuir. 7 (1991) 2934–2969. https://doi.org/10.1021/la00060a012.

[28] S. Ghosh, A. Ray, N. Pramanik, Self-assembly of surfactants: An overview on general aspects of amphiphiles, Biophys. Chem. 265 (2020) 106429. https://doi.org/10.1016/j.bpc.2020.106429.

[29] H.-U. Kim, K.-H. Lim, A model on the temperature dependence of critical micelle concentration, Colloids Surfaces A Physicochem. Eng. Asp. 235 (2004) 121–128. https://doi.org/10.1016/j.colsurfa.2003.12.019.

[30] D. Bongiorno, L. Ceraulo, S. Indelicato, V. Turco Liveri, S. Indelicato, Charged supramolecular assemblies of surfactant molecules in gas phase, Mass Spectrom. Rev. 35 (2016) 170–187. https://doi.org/10.1002/mas.21476.

[31] H.-A. Klok, S. Lecommandoux, Supramolecular Materials via Block Copolymer Self-Assembly, Adv. Mater. 13 (2001) 1217. https://doi.org/10.1002/1521-4095(200108)13:16<1217::AID-ADMA1217>3.0.CO;2-D.

[32] N.A. Lynd, A.J. Meuler, M.A. Hillmyer, Polydispersity and block copolymer self-assembly, Prog. Polym. Sci. 33 (2008) 875–893. https://doi.org/10.1016/j.progpolymsci.2008.07.003.

[33] Y. Mai, A. Eisenberg, Self-assembly of block copolymers, Chem. Soc. Rev. 41 (2012) 5969. https://doi.org/10.1039/c2cs35115c.

[34] Y. Li, Y. Zhang, D. Yang, Y. Li, J. Hu, C. Feng, S. Zhai, G. Lu, X. Huang, PAA- g -PPO Amphiphilic Graft Copolymer: Synthesis and Diverse Micellar Morphologies, Macromolecules. 43 (2010) 262–270. https://doi.org/10.1021/ma901526j.

[35] C. Cai, J. Lin, T. Chen, X. Tian, Aggregation Behavior of Graft Copolymer with Rigid Backbone, Langmuir. 26 (2010) 2791–2797. https://doi.org/10.1021/la902834m.

[36] L. Atanase, G. Riess, Self-Assembly of Block and Graft Copolymers in Organic Solvents: An Overview of Recent Advances, Polymers (Basel). 10 (2018) 62. https://doi.org/10.3390/polym10010062.

[37] M. Karayianni, S. Pispas, Self-Assembly of Amphiphilic Block Copolymers in Selective Solvents, Springer International Publishing, Cham, 2016. https://doi.org/10.1007/978-3-319-26788-3.

[38] A.K. Teotia, H. Sami, A. Kumar, Thermo-responsive polymers, in: Switch. Responsive Surfaces Mater. Biomed. Appl., Elsevier, 2015: pp. 3–43. https://doi.org/10.1016/B978-0-85709-713-2.00001-8.

[39] T. Manouras, M. Vamvakaki, Field responsive materials: photo-, electro-, magnetic- and ultrasound-sensitive polymers, Polym. Chem. 8 (2017) 74–96. https://doi.org/10.1039/C6PY01455K.

[40] O. Bertrand, J.-F. Gohy, Photo-responsive polymers: synthesis and applications, Polym. Chem. 8 (2017) 52–73. https://doi.org/10.1039/C6PY01082B.

[41] G. Kocak, C. Tuncer, V. Bütün, PH-Responsive polymers, Polym. Chem. 8 (2017) 144–176. https://doi.org/10.1039/c6py01872f.

[42] M.C. García, Ionic-strength-responsive polymers for drug delivery applications, in: Stimuli Responsive Polym. Nanocarriers Drug Deliv. Appl., Elsevier, 2019: pp. 393–409. https://doi.org/10.1016/B978-0-08-101995-5.00014-3.

[43] M. Wei, Y. Gao, X. Li, M.J. Serpe, Stimuli-responsive polymers and their applications, Polym. Chem. 8 (2017) 127–143. https://doi.org/10.1039/C6PY01585A.

[44] P. Bawa, V. Pillay, Y.E. Choonara, L.C. du Toit, Stimuli-responsive polymers and their applications in drug delivery, Biomed. Mater. 4 (2009) 022001. https://doi.org/10.1088/1748-6041/4/2/022001.

[45] X. Zhang, L. Chen, K.H. Lim, S. Gonuguntla, K.W. Lim, D. Pranantyo, W.P. Yong, W.J.T. Yam, Z. Low, W.J. Teo, H.P. Nien, Q.W. Loh, S. Soh, The Pathway to Intelligence: Using Stimuli-Responsive Materials as Building Blocks for Constructing Smart and Functional Systems, Adv. Mater. 31 (2019) 1804540. https://doi.org/10.1002/adma.201804540.

[46] R.B. Grubbs, Z. Sun, Shape-changing polymer assemblies, Chem. Soc. Rev. 42 (2013) 7436. https://doi.org/10.1039/c3cs60079c.

[47] K.T. Oh, H. Yin, E.S. Lee, Y.H. Bae, Polymeric nanovehicles for anticancer drugs with triggering release mechanisms, J. Mater. Chem. 17 (2007) 3987. https://doi.org/10.1039/b707142f.

[48] S. Dai, P. Ravi, K.C. Tam, pH-Responsive polymers: synthesis, properties and applications, Soft Matter. 4 (2008) 435. https://doi.org/10.1039/b714741d.

[49] T.-W. Wang, C.-W. Yeh, C.-H. Kuan, L.-W. Wang, L.-H. Chen, H.-C. Wu, J.-S. Sun, Tailored design of multifunctional and programmable pH-responsive self-assembling polypeptides as drug delivery nanocarrier for cancer therapy, Acta Biomater. 58 (2017) 54–66. https://doi.org/10.1016/j.actbio.2017.06.008.

[50] Y. Yang, X. Xie, Y. Yang, Z. Li, F. Yu, W. Gong, Y. Li, H. Zhang, Z. Wang, X. Mei, Polymer Nanoparticles Modified with Photo- and pH-Dual-Responsive Polypeptides for Enhanced and Targeted Cancer Therapy, Mol. Pharm. 13 (2016) 1508–1519. https://doi.org/10.1021/acs.molpharmaceut.5b00977.

[51] A. DOBRYNIN, M. RUBINSTEIN, Theory of polyelectrolytes in solutions and at surfaces, Prog. Polym. Sci. 30 (2005) 1049–1118. https://doi.org/10.1016/j.progpolymsci.2005.07.006.

[52] Y. Zhang, E. Yildirim, H.S. Antila, L.D. Valenzuela, M. Sammalkorpi, J.L. Lutkenhaus, The influence of ionic strength and mixing ratio on the colloidal stability of PDAC/PSS polyelectrolyte complexes, Soft Matter. 11 (2015) 7392–7401. https://doi.org/10.1039/C5SM01184A.

[53] Y. Anraku, A. Kishimura, M. Oba, Y. Yamasaki, K. Kataoka, Spontaneous Formation of Nanosized Unilamellar Polyion Complex Vesicles with Tunable Size and Properties, J. Am. Chem. Soc. 132 (2010) 1631–1636. https://doi.org/10.1021/ja908350e.

[54] B. BOLTO, J. GREGORY, Organic polyelectrolytes in water treatment, Water Res. 41 (2007) 2301–2324. https://doi.org/10.1016/j.watres.2007.03.012.

[55] K. Köhler, P.M. Biesheuvel, R. Weinkamer, H. Möhwald, G.B. Sukhorukov, Salt-Induced Swelling-to-Shrinking Transition in Polyelectrolyte Multilayer Capsules, Phys. Rev. Lett. 97 (2006) 188301. https://doi.org/10.1103/PhysRevLett.97.188301.

[56] C. Gao, S. Leporatti, S. Moya, E. Donath, H. Möhwald, Swelling and Shrinking of Polyelectrolyte Microcapsules in Response to Changes in Temperature and Ionic Strength, Chem. - A Eur. J. 9 (2003) 915–920. https://doi.org/10.1002/chem.200390113.

[57] O. Azzaroni, S. Moya, T. Farhan, A.A. Brown, W.T.S. Huck, Switching the Properties of Polyelectrolyte Brushes via “Hydrophobic Collapse,” Macromolecules. 38 (2005) 10192–10199. https://doi.org/10.1021/ma051549r.

[58] V.F. Korolovych, P.A. Ledin, A. Stryutsky, V. V. Shevchenko, O. Sobko, W. Xu, L.A. Bulavin, V. V. Tsukruk, Assembly of Amphiphilic Hyperbranched Polymeric Ionic Liquids in Aqueous Media at Different pH and Ionic Strength, Macromolecules. 49 (2016) 8697–8710. https://doi.org/10.1021/acs.macromol.6b01562.

[59] Y.P. Timilsena, T.O. Akanbi, N. Khalid, B. Adhikari, C.J. Barrow, Complex coacervation: Principles, mechanisms and applications in microencapsulation, Int. J. Biol. Macromol. 121 (2019) 1276–1286. https://doi.org/10.1016/j.ijbiomac.2018.10.144.

[60] G.-Y. Li, Q.-H. Chen, C.-R. Su, H. Wang, S. He, J. Liu, A. Nag, Y. Yuan, Soy protein-polysaccharide complex coacervate under physical treatment: Effects of pH, ionic strength and polysaccharide type, Innov. Food Sci. Emerg. Technol. 68 (2021) 102612. https://doi.org/10.1016/j.ifset.2021.102612.

[61] A.B. Kayitmazer, A.F. Koksal, E. Kilic Iyilik, Complex coacervation of hyaluronic acid and

chitosan: effects of pH, ionic strength, charge density, chain length and the charge ratio, Soft Matter. 11 (2015) 8605–8612. https://doi.org/10.1039/C5SM01829C.

[62] V. Kozlovskaya, E. Kharlampieva, M.L. Mansfield, S.A. Sukhishvili, Poly(methacrylic acid) Hydrogel Films and Capsules: Response to pH and Ionic Strength, and Encapsulation of Macromolecules, Chem. Mater. 18 (2006) 328–336. https://doi.org/10.1021/cm0517364.

[63] H.I. Okur, J. Hladílková, K.B. Rembert, Y. Cho, J. Heyda, J. Dzubiella, P.S. Cremer, P. Jungwirth, Beyond the Hofmeister Series: Ion-Specific Effects on Proteins and Their Biological Functions, J. Phys. Chem. B. 121 (2017) 1997–2014. https://doi.org/10.1021/acs.jpcb.6b10797.

[64] S. Chatani, C.J. Kloxin, C.N. Bowman, The power of light in polymer science: photochemical processes to manipulate polymer formation, structure, and properties, Polym. Chem. 5 (2014) 2187–2201. https://doi.org/10.1039/C3PY01334K.

[65] J.-F. Gohy, Y. Zhao, Photo-responsive block copolymer micelles: design and behavior, Chem. Soc. Rev. 42 (2013) 7117. https://doi.org/10.1039/c3cs35469e.

[66] J. Jiang, X. Tong, Y. Zhao, A New Design for Light-Breakable Polymer Micelles, J. Am. Chem. Soc. 127 (2005) 8290–8291. https://doi.org/10.1021/ja0521019.

[67] O. Bertrand, J.-M. Schumers, C. Kuppan, J. Marchand-Brynaert, C.-A. Fustin, J.-F. Gohy, Photo-induced micellization of block copolymers bearing 4,5-dimethoxy-2-nitrobenzyl side groups, Soft Matter. 7 (2011) 6891. https://doi.org/10.1039/c1sm05631j.

[68] D. Han, X. Tong, Y. Zhao, Fast Photodegradable Block Copolymer Micelles for Burst Release, Macromolecules. 44 (2011) 437–439. https://doi.org/10.1021/ma102778d.

[69] D. Wang, X. Wang, Amphiphilic azo polymers: Molecular engineering, self-assembly and photoresponsive properties, Prog. Polym. Sci. 38 (2013) 271–301. https://doi.org/10.1016/j.progpolymsci.2012.07.003.

[70] G. Wang, X. Tong, Y. Zhao, Preparation of Azobenzene-Containing Amphiphilic Diblock Copolymers for Light-Responsive Micellar Aggregates, Macromolecules. 37 (2004) 8911–8917. https://doi.org/10.1021/ma048416a.

[71] X. Tong, G. Wang, A. Soldera, Y. Zhao, How Can Azobenzene Block Copolymer Vesicles Be Dissociated and Reformed by Light?, J. Phys. Chem. B. 109 (2005) 20281–20287. https://doi.org/10.1021/jp0524274.

[72] N. Fomina, J. Sankaranarayanan, A. Almutairi, Photochemical mechanisms of light-triggered release from nanocarriers, Adv. Drug Deliv. Rev. 64 (2012) 1005–1020. https://doi.org/10.1016/j.addr.2012.02.006.

[73] Y. Zhao, Light-Responsive Block Copolymer Micelles, Macromolecules. 45 (2012) 3647–3657. https://doi.org/10.1021/ma300094t.

[74] D. Roy, W.L.A. Brooks, B.S. Sumerlin, New directions in thermoresponsive polymers, Chem. Soc. Rev. 42 (2013) 7214. https://doi.org/10.1039/c3cs35499g.

[75] F. Fernández-Trillo, A. Duréault, J.P.M. Bayley, J.C.M. van Hest, J.C. Thies, T. Michon, R. Weberskirch, N.R. Cameron, Elastin-Based Side-Chain Polymers: Improved Synthesis via RAFT and Stimulus Responsive Behavior, Macromolecules. 40 (2007) 6094–6099. https://doi.org/10.1021/ma070527x.

[76] P.J. Roth, F.D. Jochum, F.R. Forst, R. Zentel, P. Theato, Influence of End Groups on the Stimulus-Responsive Behavior of Poly[oligo(ethylene glycol) methacrylate] in Water, Macromolecules. 43 (2010) 4638–4645. https://doi.org/10.1021/ma1005759.

[77] H. Kim, S. Lee, M. Noh, S.H. Lee, Y. Mok, G. Jin, J.-H. Seo, Y. Lee, Thermosensitivity

control of polyethlyenimine by simple acylation, Polymer (Guildf). 52 (2011) 1367–1374. https://doi.org/10.1016/j.polymer.2011.01.045.

[78] C. Zhao, Z. Ma, X.X. Zhu, Rational design of thermoresponsive polymers in aqueous solutions: A thermodynamics map, Prog. Polym. Sci. 90 (2019) 269–291. https://doi.org/10.1016/j.progpolymsci.2019.01.001.

[79] G. Pasparakis, C. Tsitsilianis, LCST polymers: Thermoresponsive nanostructured assemblies towards bioapplications, Polymer (Guildf). 211 (2020) 123146. https://doi.org/10.1016/j.polymer.2020.123146.

[80] Q. Zhang, C. Weber, U.S. Schubert, R. Hoogenboom, Thermoresponsive polymers with lower critical solution temperature: from fundamental aspects and measuring techniques to recommended turbidimetry conditions, Mater. Horizons. 4 (2017) 109–116. https://doi.org/10.1039/C7MH00016B.

[81] J. Seuring, S. Agarwal, Polymers with Upper Critical Solution Temperature in Aqueous Solution: Unexpected Properties from Known Building Blocks, ACS Macro Lett. 2 (2013) 597–600. https://doi.org/10.1021/mz400227y.

[82] K.K. Bansal, P.K. Upadhyay, G.K. Saraogi, A. Rosling, J.M. Rosenholm, Advances in thermo-responsive polymers exhibiting upper critical solution temperature (UCST), Express Polym. Lett. 13 (2019) 974–992. https://doi.org/10.3144/expresspolymlett.2019.85.

[83] R. Liu, M. Fraylich, B.R. Saunders, Thermoresponsive copolymers: from fundamental studies to applications, Colloid Polym. Sci. 287 (2009) 627–643. https://doi.org/10.1007/s00396-009-2028-x.

[84] C.R. Becer, S. Hahn, M.W.M. Fijten, H.M.L. Thijs, R. Hoogenboom, U.S. Schubert, Libraries of methacrylic acid and oligo(ethylene glycol) methacrylate copolymers with LCST behavior, J. Polym. Sci. Part A Polym. Chem. 46 (2008) 7138–7147. https://doi.org/10.1002/pola.23018.

[85] B.S. Murray, A.W. Jackson, C.S. Mahon, D.A. Fulton, Reactive thermoresponsive copolymer scaffolds, Chem. Commun. 46 (2010) 8651. https://doi.org/10.1039/c0cc03856c.

[86] J.-F. Lutz, A. Hoth, Preparation of Ideal PEG Analogues with a Tunable Thermosensitivity by Controlled Radical Copolymerization of 2-(2-Methoxyethoxy)ethyl Methacrylate and Oligo(ethylene glycol) Methacrylate, Macromolecules. 39 (2006) 893–896. https://doi.org/10.1021/ma0517042.

[87] M.A. Ward, T.K. Georgiou, Thermoresponsive Polymers for Biomedical Applications, Polymers (Basel). 3 (2011) 1215–1242. https://doi.org/10.3390/polym3031215.

[88] A. Bordat, T. Boissenot, J. Nicolas, N. Tsapis, Thermoresponsive polymer nanocarriers for biomedical applications, Adv. Drug Deliv. Rev. 138 (2019) 167–192. https://doi.org/10.1016/j.addr.2018.10.005.

[89] S.R. Abulateefeh, S.G. Spain, J.W. Aylott, W.C. Chan, M.C. Garnett, C. Alexander, Thermoresponsive Polymer Colloids for Drug Delivery and Cancer Therapy, Macromol. Biosci. 11 (2011) 1722–1734. https://doi.org/10.1002/mabi.201100252.

[90] Y. Deng, F. Käfer, T. Chen, Q. Jin, J. Ji, S. Agarwal, Let There be Light: Polymeric Micelles with Upper Critical Solution Temperature as Light-Triggered Heat Nanogenerators for Combating Drug-Resistant Cancer, Small. 14 (2018) 1802420. https://doi.org/10.1002/smll.201802420.

[91] Z.-X. Zhang, K.L. Liu, J. Li, Self-Assembly and Micellization of a Dual Thermoresponsive

Supramolecular Pseudo-Block Copolymer, Macromolecules. 44 (2011) 1182–1193. https://doi.org/10.1021/ma102196q.

[92] Y. Wei, H. Huo, C. Huang, Q. Zhang, R. Hoogenboom, F. Liu, Supramolecular control over self-assembly and double thermoresponsive behavior of an amphiphilic block copolymer, Eur. Polym. J. 125 (2020) 109537. https://doi.org/10.1016/j.eurpolymj.2020.109537.

[93] Q. Li, L. Li, Q. Tian, J. Xu, J. Liu, Doubly Thermo-Responsive Polymers and Their Two-Step Phase Transition Behavior: A Review, Nanosci. Nanotechnol. Lett. 9 (2017) 89–99. https://doi.org/10.1166/nnl.2017.2266.

[94] E.A. Clark, J.E.G. Lipson, LCST and UCST behavior in polymer solutions and blends, Polymer (Guildf). 53 (2012) 536–545. https://doi.org/10.1016/j.polymer.2011.11.045.

[95] F. Dai, P. Wang, Y. Wang, L. Tang, J. Yang, W. Liu, H. Li, G. Wang, Double thermoresponsive polybetaine-based ABA triblock copolymers with capability to condense DNA, Polymer (Guildf). 49 (2008) 5322–5328. https://doi.org/10.1016/j.polymer.2008.09.060.

[96] F. Käfer, F. Liu, U. Stahlschmidt, V. Jérôme, R. Freitag, M. Karg, S. Agarwal, LCST and UCST in One: Double Thermoresponsive Behavior of Block Copolymers of Poly(ethylene glycol) and Poly(acrylamide-co-acrylonitrile), Langmuir. 31 (2015) 8940–8946. https://doi.org/10.1021/acs.langmuir.5b02006.

[97] Y. Shin, C.P. Brangwynne, Liquid phase condensation in cell physiology and disease, Science (80-.). 357 (2017). https://doi.org/10.1126/science.aaf4382.

[98] A.A. Hyman, C.A. Weber, F. Jülicher, Liquid-Liquid Phase Separation in Biology, Annu. Rev. Cell Dev. Biol. 30 (2014) 39–58. https://doi.org/10.1146/annurev-cellbio-100913-013325.

[99] S. Brocca, R. Grandori, S. Longhi, V. Uversky, Liquid–Liquid Phase Separation by Intrinsically Disordered Protein Regions of Viruses: Roles in Viral Life Cycle and Control of Virus–Host Interactions, Int. J. Mol. Sci. 21 (2020) 9045. https://doi.org/10.3390/ijms21239045.

[100] E. Dolgin, What lava lamps and vinaigrette can teach us about cell biology, Nature. 555 (2018) 300–302. https://doi.org/10.1038/d41586-018-03070-2.

[101] S. Alberti, A. Gladfelter, T. Mittag, Considerations and Challenges in Studying Liquid-Liquid Phase Separation and Biomolecular Condensates, Cell. 176 (2019) 419–434. https://doi.org/10.1016/j.cell.2018.12.035.

[102] J. Kim, H. Lee, H.G. Lee, P.J. Seo, Get closer and make hotspots: liquid–liquid phase separation in plants, EMBO Rep. 22 (2021) 1–15. https://doi.org/10.15252/embr.202051656.

[103] Q. Su, S. Mehta, J. Zhang, Liquid-liquid phase separation: Orchestrating cell signaling through time and space, Mol. Cell. 81 (2021) 4137–4146. https://doi.org/10.1016/j.molcel.2021.09.010.

[104] B. Wang, L. Zhang, T. Dai, Z. Qin, H. Lu, L. Zhang, F. Zhou, Liquid–liquid phase separation in human health and diseases, Signal Transduct. Target. Ther. 6 (2021) 290. https://doi.org/10.1038/s41392-021-00678-1.

[105] C.D. Crowe, C.D. Keating, Liquid–liquid phase separation in artificial cells, Interface Focus. 8 (2018). https://doi.org/10.1098/rsfs.2018.0032.

[106] N. Martin, Dynamic Synthetic Cells Based on Liquid–Liquid Phase Separation, ChemBioChem. 20 (2019) 2553–2568. https://doi.org/10.1002/cbic.201900183.

[107] F.W.Z. Tiebackx, Gleichzeitige Ausflockung zweier Kolloide, Chem. Ind. Kolloide. 8 (1911) 198–201. https://ia600708.us.archive.org/view_archive.php?archive=/28/items/crossref-pre-1923-scholarly-works/10.1007%252Fbf01498362.zip&file=10.1007%252Fbf01503532.pdf.

[108] H.G. Bungenberg de Jong, H.R. Kruyt, Coacervation (partial miscibility in colloid systems), in: Proc. K. Ned. Akad. Wet, 1929: pp. 849–856.

[109] E. Astoricchio, C. Alfano, L. Rajendran, P.A. Temussi, A. Pastore, The Wide World of Coacervates: From the Sea to Neurodegeneration, Trends Biochem. Sci. 45 (2020) 706–717. https://doi.org/10.1016/j.tibs.2020.04.006.

[110] T.Z. Jia, K. Chandru, Y. Hongo, R. Afrin, T. Usui, K. Myojo, H.J. Cleaves, Membraneless polyester microdroplets as primordial compartments at the origins of life, Proc. Natl. Acad. Sci. 116 (2019) 15830–15835. https://doi.org/10.1073/pnas.1902336116.

[111] N.A. Yewdall, A.A.M. André, T. Lu, E. Spruijt, Coacervates as models of membraneless organelles, Curr. Opin. Colloid Interface Sci. 52 (2021) 101416. https://doi.org/10.1016/j.cocis.2020.101416.

[112] S. Park, R. Barnes, Y. Lin, B. Jeon, S. Najafi, K.T. Delaney, G.H. Fredrickson, J.-E. Shea, D.S. Hwang, S. Han, Dehydration entropy drives liquid-liquid phase separation by molecular crowding, Commun. Chem. 3 (2020) 83. https://doi.org/10.1038/s42004-020-0328-8.

[113] X. Wang, P. Zhang, L. Tian, Spatiotemporal organization of coacervate microdroplets, Curr. Opin. Colloid Interface Sci. 52 (2021) 101420. https://doi.org/10.1016/j.cocis.2021.101420.

[114] M. Wang, Y. Wang, Development of surfactant coacervation in aqueous solution, Soft Matter. 10 (2014) 7909–7919. https://doi.org/10.1039/c4sm01386g.

[115] J.G. Nairm, 3 Coacervation-phase separation technology, in: Adv. Pharm. Sci., 1995: pp. 93–219. https://doi.org/10.1016/S0065-3136(06)80005-1.

[116] A. Melnyk, J. Namieśnik, L. Wolska, Theory and recent applications of coacervate-based extraction techniques, TrAC Trends Anal. Chem. 71 (2015) 282–292. https://doi.org/10.1016/j.trac.2015.03.013.

[117] F.H. Quina, W.L. Hinze, Surfactant-Mediated Cloud Point Extractions: An Environmentally Benign Alternative Separation Approach, Ind. Eng. Chem. Res. 38 (1999) 4150–4168. https://doi.org/10.1021/ie980389n.

[118] A. Veis, A review of the early development of the thermodynamics of the complex coacervation phase separation, Adv. Colloid Interface Sci. 167 (2011) 2–11. https://doi.org/10.1016/j.cis.2011.01.007.

[119] H.B. Bohidar, Coacervates : A novel state of soft matter - An overview, J. Surf. Sci. Technol. 24 (2008) 105–124. https://doi.org/10.18311/jsst/2008/1893.

[120] E. Kizilay, A.B. Kayitmazer, P.L. Dubin, Complexation and coacervation of polyelectrolytes with oppositely charged colloids, Adv. Colloid Interface Sci. 167 (2011) 24–37. https://doi.org/10.1016/j.cis.2011.06.006.

[121] W. Zhao, Y. Wang, Coacervation with surfactants: From single-chain surfactants to gemini surfactants, Adv. Colloid Interface Sci. 239 (2017) 199–212. https://doi.org/10.1016/j.cis.2016.04.005.

[122] A.Z. Naqvi, Kabir-ud-Din, Clouding phenomenon in amphiphilic systems: A review of five decades, Colloids Surfaces B Biointerfaces. 165 (2018) 325–344. https://doi.org/10.1016/j.colsurfb.2018.01.060.

[123] B. Lindman, G. Karlström, Nonionic polymers and surfactants: Temperature anomalies revisited, Comptes Rendus Chim. 12 (2009) 121–128. https://doi.org/10.1016/j.crci.2008.06.017.

[124] A. Gupta, H.B. Bohidar, Kinetics of phase separation in systems exhibiting simple coacervation, Phys. Rev. E. 72 (2005) 011507. https://doi.org/10.1103/PhysRevE.72.011507.

[125] N.V.N. Jyothi, P.M. Prasanna, S.N. Sakarkar, K.S. Prabha, P.S. Ramaiah, G.Y. Srawan, Microencapsulation techniques, factors influencing encapsulation efficiency, J. Microencapsul. 27 (2010) 187–197. https://doi.org/10.3109/02652040903131301.

[126] A. Madene, M. Jacquot, J. Scher, S. Desobry, Flavour encapsulation and controlled release - a review, Int. J. Food Sci. Technol. 41 (2006) 1–21. https://doi.org/10.1111/j.1365-2621.2005.00980.x.

[127] R. Arshady, Microcapsules for food, J. Microencapsul. 10 (1993) 413–435. https://doi.org/10.3109/02652049309015320.

[128] M. Mamusa, C. Resta, C. Sofroniou, P. Baglioni, Encapsulation of volatile compounds in liquid media: Fragrances, flavors, and essential oils in commercial formulations, Adv. Colloid Interface Sci. 298 (2021) 102544. https://doi.org/10.1016/j.cis.2021.102544.

[129] N.R. Johnson, Y. Wang, Coacervate delivery systems for proteins and small molecule drugs, Expert Opin. Drug Deliv. 11 (2014) 1829–1832. https://doi.org/10.1517/17425247.2014.941355.

[130] A.M. Bakry, S. Abbas, B. Ali, H. Majeed, M.Y. Abouelwafa, A. Mousa, L. Liang, Microencapsulation of Oils: A Comprehensive Review of Benefits, Techniques, and Applications, Compr. Rev. Food Sci. Food Saf. 15 (2016) 143–182. https://doi.org/10.1111/1541-4337.12179.

[131] B.S. Beşen, Production of Disposable Antibacterial Textiles Via Application of Tea Tree Oil Encapsulated into Different Wall Materials, Fibers Polym. 20 (2019) 2587–2593. https://doi.org/10.1007/s12221-019-9350-9.

[132] M.A. Teixeira, O. Rodríguez, S. Rodrigues, I. Martins, A.E. Rodrigues, A case study of product engineering: Performance of microencapsulated perfumes on textile applications, AIChE J. 58 (2012) 1939–1950. https://doi.org/10.1002/aic.12715.

[133] C.S.N. Rodrigues Teixeira, I.M.D. Martins, V.L.G. Mata, M.F.F. Barreiro, A.E. Rodrigues, Characterization and evaluation of commercial fragrance microcapsules for textile application, J. Text. Inst. 103 (2011) 1–13. https://doi.org/10.1080/00405000.2011.566312.

[134] K. Knop, R. Hoogenboom, D. Fischer, U.S. Schubert, Poly(ethylene glycol) in Drug Delivery: Pros and Cons as Well as Potential Alternatives, Angew. Chemie Int. Ed. 49 (2010) 6288–6308. https://doi.org/10.1002/anie.200902672.

[135] J.M. Harris, Poly(Ethylene Glycol) Chemistry: Biotechnical and Biomedical Applications, Springer US, 1992. https://books.google.it/books?id=UheNFtAB7cAC.

[136] Q. Li, A.P. Constantinou, T.K. Georgiou, A library of thermoresponsive PEG-based methacrylate homopolymers: How do the molar mass and number of ethylene glycol groups affect the cloud point?, J. Polym. Sci. 59 (2021) 230–239. https://doi.org/10.1002/pol.20200720.

[137] R.D.C. Cruz, R.J. Martins, M.J.E. de M. Cardoso, O.E. Barcia, Volumetric Study of Aqueous Solutions of Polyethylene Glycol as a Function of the Polymer Molar Mass in the Temperature Range 283.15 to 313.15 K and 0.1 MPa, J. Solution Chem. 38 (2009)

957–981. https://doi.org/10.1007/s10953-009-9388-1.
[138] A. Saraiva, O. Persson, A. Fredenslund, An experimental investigation of cloud-point curves for the poly(ethylene glycol)/water system at varying molecular weight distributions, Fluid Phase Equilib. 91 (1993) 291–311. https://doi.org/10.1016/0378-3812(93)85105-U.
[139] S.K. Han, B.H. Jhun, Effect of additives on the cloud point of polyethylene glycols, Arch. Pharm. Res. 7 (1984) 1–9. https://doi.org/10.1007/BF02856915.
[140] P. Patidar, A. Bahadur, Modulating effect of different biomolecules and other additives on cloud point and aggregation of amphiphilic linear and starblock copolymer, J. Mol. Liq. 249 (2018) 219–226. https://doi.org/10.1016/j.molliq.2017.11.019.
[141] A.H. Conner, M.S.H. Bhuiyan, Wood: Adhesives, in: Ref. Modul. Mater. Sci. Mater. Eng., Elsevier, 2017: pp. 1–18. https://doi.org/10.1016/B978-0-12-803581-8.01932-9.
[142] A. Kaboorani, B. Riedl, Mechanical performance of polyvinyl acetate (PVA)-based biocomposites, in: Biocomposites, Fourteenth, Elsevier, 2015: pp. 347–364. https://doi.org/10.1016/B978-1-78242-373-7.00009-3.
[143] J.A. Brydson, Poly(vinyl acetate) and its Derivatives, in: Plast. Mater., Elsevier, 1995: pp. 371–382. https://doi.org/10.1016/B978-0-7506-1864-9.50020-X.
[144] Drugs.com, PVAc as pharmacologically inactive substance, (n.d.). https://www.drugs.com/inactive/polyvinyl-acetate-507.html (accessed November 29, 2021).
[145] M. Amann, O. Minge, Biodegradability of poly(vinyl acetate) and related polymers, in: Adv. Polym. Sci., Springer, Berlin, Heidelberg, 2012: pp. 137–172. https://doi.org/10.1007/12-2011-153.
[146] R. Sharma, P. Bahadur, Effect of different additives on the cloud point of a polyethylene oxide-polypropylene oxide-polyethylene oxide block copolymer in aqueous solution, J. Surfactants Deterg. 5 (2002) 263–268. https://doi.org/10.1007/s11743-002-0226-9.
[147] P. Patidar, S.A. Pillai, P. Bahadur, A. Bahadur, Tuning the self-assembly of EO-PO block copolymers and quercetin solubilization in the presence of some common pharmacuetical excipients: A comparative study on a linear triblock and a starblock copolymer, J. Mol. Liq. 241 (2017) 511–519. https://doi.org/10.1016/j.molliq.2017.06.035.
[148] P. Alexandridis, T. Alan Hatton, Poly(ethylene oxide)□poly(propylene oxide)□poly(ethylene oxide) block copolymer surfactants in aqueous solutions and at interfaces: thermodynamics, structure, dynamics, and modeling, Colloids Surfaces A Physicochem. Eng. Asp. 96 (1995) 1–46. https://doi.org/10.1016/0927-7757(94)03028-X.
[149] S.K. Filippov, A. Bogomolova, L. Kaberov, N. Velychkivska, L. Starovoytova, Z. Cernochova, S.E. Rogers, W.M. Lau, V. V. Khutoryanskiy, M.T. Cook, Internal Nanoparticle Structure of Temperature-Responsive Self-Assembled PNIPAM- b -PEG- b -PNIPAM Triblock Copolymers in Aqueous Solutions: NMR, SANS, and Light Scattering Studies, Langmuir. 32 (2016) 5314–5323. https://doi.org/10.1021/acs.langmuir.6b00284.
[150] F. Seidi, P. Heshmati, Synthesis of a PEG-PNIPAm thermosensitive dendritic copolymer and investigation of its self-association, Chinese J. Polym. Sci. 33 (2015) 192–202. https://doi.org/10.1007/s10118-015-1561-y.
[151] Y.-L. Luo, W. Yu, F. Xu, L.-L. Zhang, Novel thermo-responsive self-assembly micelles from

a double brush-shaped PNIPAM- g -(PA- b -PEG- b -PA)- g -PNIPAM block copolymer with PNIPAM polymers as side chains, J. Polym. Sci. Part A Polym. Chem. 50 (2012) 2053–2067. https://doi.org/10.1002/pola.25980.

[152] C.Y. Gong, S. Shi, P.W. Dong, B. Kan, M.L. Gou, X.H. Wang, X.Y. Li, F. Luo, X. Zhao, Y.Q. Wei, Z.Y. Qian, Synthesis and characterization of PEG-PCL-PEG thermosensitive hydrogel, Int. J. Pharm. 365 (2009) 89–99. https://doi.org/10.1016/j.ijpharm.2008.08.027.

[153] B. Bogdanov, A. Vidts, A. Van Den Bulcke, R. Verbeeck, E. Schacht, Synthesis and thermal properties of poly(ethylene glycol)-poly(e-caprolactone) copolymers, Polymer (Guildf). 39 (1998) 1631–1636. https://doi.org/10.1016/S0032-3861(97)00444-8.

[154] M. Qindeel, N. Ahmed, K.U. Shah, N. Ullah, Asim.ur.Rehman, New, Environment Friendly Approach for Synthesis of Amphiphilic PCL–PEG–PCL Triblock Copolymer: An Efficient Carrier for Fabrication of Nanomicelles, J. Polym. Environ. 28 (2020) 1237–1251. https://doi.org/10.1007/s10924-020-01683-1.

[155] M. Prabaharan, J.J. Grailer, D.A. Steeber, S. Gong, Thermosensitive micelles based on folate-conjugated poly(N-vinylcaprolactam)-block-poly(ethylene glycol) for tumor-targeted drug delivery, Macromol. Biosci. 9 (2009) 744–753. https://doi.org/10.1002/mabi.200800366.

[156] J. Siirilä, S. Häkkinen, H. Tenhu, The emulsion polymerization induced self-assembly of a thermoresponsive polymer poly(N -vinylcaprolactam), Polym. Chem. 10 (2019) 766–775. https://doi.org/10.1039/C8PY01421C.

[157] M. Qiao, D. Chen, X. Ma, Y. Liu, Injectable biodegradable temperature-responsive PLGA–PEG–PLGA copolymers: Synthesis and effect of copolymer composition on the drug release from the copolymer-based hydrogels, Int. J. Pharm. 294 (2005) 103–112. https://doi.org/10.1016/j.ijpharm.2005.01.017.

[158] N.Y. Steinman, M. Haim-Zada, I.A. Goldstein, A.H. Goldberg, T. Haber, J.M. Berlin, A.J. Domb, Effect of PLGA block molecular weight on gelling temperature of PLGA-PEG-PLGA thermoresponsive copolymers, J. Polym. Sci. Part A Polym. Chem. 57 (2019) 35–39. https://doi.org/10.1002/pola.29275.

[159] C. Feng, Y. Li, D. Yang, J. Hu, X. Zhang, X. Huang, Well-defined graft copolymers: from controlled synthesis to multipurpose applications, Chem. Soc. Rev. 40 (2011) 1282–1295. https://doi.org/10.1039/B921358A.

[160] A. Ding, J. Xu, G. Gu, G. Lu, X. Huang, PHEA-g-PMMA Well-Defined Graft Copolymer: ATRP Synthesis, Self-Assembly, and Synchronous Encapsulation of Both Hydrophobic and Hydrophilic Guest Molecules, Sci. Rep. 7 (2017) 12601. https://doi.org/10.1038/s41598-017-12710-y.

[161] X. Jiang, G. Lu, C. Feng, Y. Li, X. Huang, Poly(acrylic acid)-graft-poly(N-vinylcaprolactam): a novel pH and thermo dual-stimuli responsive system, Polym. Chem. 4 (2013) 3876. https://doi.org/10.1039/c3py00415e.

[162] B. Xu, G. Gu, C. Feng, X. Jiang, J. Hu, G. Lu, S. Zhang, X. Huang, (PAA-g-PS)-co-PPEGMEMA asymmetric polymer brushes: synthesis, self-assembly, and encapsulating capacity for both hydrophobic and hydrophilic agents, Polym. Chem. 7 (2016) 613–624. https://doi.org/10.1039/C5PY01644D.

[163] A. Perro, L. Giraud, N. Coudon, S. Shanmugathasan, V. Lapeyre, B. Goudeau, J.P. Douliez, V. Ravaine, Self-coacervation of ampholyte polymer chains as an efficient encapsulation strategy, J. Colloid Interface Sci. 548 (2019) 275–283.

https://doi.org/10.1016/j.jcis.2019.04.033.
[164] A. Bartolini, P. Tempesti, C. Resta, D. Berti, J. Smets, Y.G. Aouad, P. Baglioni, Poly(ethylene glycol)-graft-poly(vinyl acetate) single-chain nanoparticles for the encapsulation of small molecules, Phys. Chem. Chem. Phys. 19 (2017) 4553–4559. https://doi.org/10.1039/c6cp07967a.
[165] M. Mamusa, P. Tempesti, A. Bartolini, E. Carretti, A.F. Ghobadi, J. Smets, Y.G. Aouad, P. Baglioni, Associative properties of poly(ethylene glycol)–poly(vinyl acetate) comb-like graft copolymers in water, Nanoscale. 11 (2019) 6635–6643. https://doi.org/10.1039/C8NR10453K.
[166] A. Bartolini, P. Tempesti, A.F. Ghobadi, D. Berti, J. Smets, Y.G. Aouad, P. Baglioni, Liquid-liquid phase separation of polymeric microdomains with tunable inner morphology: Mechanistic insights and applications, J. Colloid Interface Sci. 556 (2019) 74–82. https://doi.org/10.1016/j.jcis.2019.08.015.
[167] R. J. Holland, A. V. York, R. M. Ruppert, Pre-treating textiles with dspersions of graft polymers based on polyalkylene oxdesto mpart sol release properties thereto, 4,999,869, 1991.
[168] S. Gopalkrishnan, E. J. Parker, R. J. Holland, S. Patterson, Detergency boosting polymer blends asadditives for laundry formulations, 5,733,856, 1998.
[169] D. Boeck, L. Herrera Taboada, A. Kavarnou-Seiler, G. Konrad, B. Reinhard, A.L. Casado-Dominguez, F. Hulskotter, J. Lee Danziger, Cleaning Compositions with Amphiphilic Graft Polymers Based on Polyalkylene Oxides and Vinyl Esters, US8143209 B2, 2012.
[170] M. Mamusa, C. Sofroniou, C. Resta, S. Murgia, E. Fratini, J. Smets, P. Baglioni, Tuning the Encapsulation of Simple Fragrances with an Amphiphilic Graft Copolymer, ACS Appl. Mater. Interfaces. 12 (2020) 28808–28818. https://doi.org/10.1021/acsami.0c05892.
[171] M. Mamusa, R. Mastrangelo, T. Glen, S. Murgia, G. Palazzo, J. Smets, P. Baglioni, Rational Design of Sustainable Liquid Microcapsules for Spontaneous Fragrance Encapsulation, Angew. Chemie. 133 (2021) 24042–24050. https://doi.org/10.1002/ange.202110446.
[172] W. Kunz, J. Henle, B.W. Ninham, 'Zur Lehre von der Wirkung der Salze' (about the science of the effect of salts): Franz Hofmeister's historical papers, Curr. Opin. Colloid Interface Sci. 9 (2004) 19–37. https://doi.org/10.1016/j.cocis.2004.05.005.
[173] P.K. Grover, R.L. Ryall, Critical Appraisal of Salting-Out and Its Implications for Chemical and Biological Sciences, Chem. Rev. 105 (2005) 1–10. https://doi.org/10.1021/cr030454p.
[174] S.Z. Moghaddam, E. Thormann, The Hofmeister series: Specific ion effects in aqueous polymer solutions, J. Colloid Interface Sci. 555 (2019) 615–635. https://doi.org/10.1016/j.jcis.2019.07.067.
[175] Y. Marcus, Effect of Ions on the Structure of Water: Structure Making and Breaking, Chem. Rev. 109 (2009) 1346–1370. https://doi.org/10.1021/cr8003828.
[176] R.W. Gurney, Ionic processes in solution, 1953.
[177] K.D. Collins, G.W. Neilson, J.E. Enderby, Ions in water: Characterizing the forces that control chemical processes and biological structure, Biophys. Chem. 128 (2007) 95–104. https://doi.org/10.1016/j.bpc.2007.03.009.
[178] A.P. Lyubartsev, K. Laasonen, A. Laaksonen, Hydration of Li+ ion. An ab initio molecular dynamics simulation, J. Chem. Phys. 114 (2001) 3120–3126. https://doi.org/10.1063/1.1342815.

[179] A.W. Omta, M.F. Kropman, S. Woutersen, H.J. Bakker, Negligible Effect of Ions on the Hydrogen-Bond Structure in Liquid Water, Science (80-.). 301 (2003) 347–349. https://doi.org/10.1126/science.1084801.

[180] A.W. Omta, M.F. Kropman, S. Woutersen, H.J. Bakker, Influence of ions on the hydrogen-bond structure in liquid water, J. Chem. Phys. 119 (2003) 12457–12461. https://doi.org/10.1063/1.1623746.

[181] B. Kang, H. Tang, Z. Zhao, S. Song, Hofmeister Series: Insights of Ion Specificity from Amphiphilic Assembly and Interface Property, ACS Omega. 5 (2020) 6229–6239. https://doi.org/10.1021/acsomega.0c00237.

[182] C. Zhang, S. Yue, A.Z. Panagiotopoulos, M.L. Klein, X. Wu, Dissolving salt is not equivalent to applying a pressure on water, Nat. Commun. 13 (2022) 822. https://doi.org/10.1038/s41467-022-28538-8.

[183] V. Mazzini, V.S.J. Craig, Specific-ion effects in non-aqueous systems, Curr. Opin. Colloid Interface Sci. 23 (2016) 82–93. https://doi.org/10.1016/j.cocis.2016.06.009.

[184] C.F. Schwenk, T.S. Hofer, B.M. Rode, "Structure Breaking" Effect of Hydrated Cs +, J. Phys. Chem. A. 108 (2004) 1509–1514. https://doi.org/10.1021/jp037179v.

[185] R. Mancinelli, A. Botti, F. Bruni, M.A. Ricci, A.K. Soper, Perturbation of water structure due to monovalent ions in solution, Phys. Chem. Chem. Phys. 9 (2007) 2959. https://doi.org/10.1039/b701855j.

[186] S. Wang, W. Fang, T. Li, F. Li, C. Sun, Z. Li, Y. Huang, Z. Men, An insight into liquid water networks through hydrogen bonding halide anion: Stimulated Raman scattering, J. Appl. Phys. 119 (2016) 163104. https://doi.org/10.1063/1.4947292.

[187] S. Shimizu, Formulating rationally via statistical thermodynamics, Curr. Opin. Colloid Interface Sci. 48 (2020) 53–64. https://doi.org/10.1016/j.cocis.2020.03.008.

[188] M.W.A. Centre, Renishaw | inVia Qontor | Raman Microscope, (n.d.). https://www.analytical.unsw.edu.au/facilities/speclab/instruments/renishaw-invia-qontor-raman-microscope-325-442-and-514-nm.

[189] A. Piruska, I. Nikcevic, S.H. Lee, C. Ahn, W.R. Heineman, P.A. Limbach, C.J. Seliskar, The autofluorescence of plastic materials and chips measured under laser irradiation, Lab Chip. 5 (2005) 1348. https://doi.org/10.1039/b508288a.

[190] S.Z. Moghaddam, E. Thormann, The Hofmeister series: Specific ion effects in aqueous polymer solutions, J. Colloid Interface Sci. 555 (2019) 615–635. https://doi.org/10.1016/j.jcis.2019.07.067.

[191] L. Xiuli, X. Jian, H. Wanguo, S. Dejun, Effect of additives on the cloud points of two tri-block copolymers in aqueous solution, Colloids Surfaces A Physicochem. Eng. Asp. 237 (2004) 1–6. https://doi.org/10.1016/j.colsurfa.2004.02.008.

[192] Y. Zhang, S. Furyk, D.E. Bergbreiter, P.S. Cremer, Specific ion effects on the water solubility of macromolecules: PNIPAM and the Hofmeister series, J. Am. Chem. Soc. 127 (2005) 14505–14510. https://doi.org/10.1021/ja0546424.

[193] K.P. Gregory, G.B. Webber, E.J. Wanless, A.J. Page, Lewis Strength Determines Specific-Ion Effects in Aqueous and Nonaqueous Solvents, J. Phys. Chem. A. 123 (2019) 6420–6429. https://doi.org/10.1021/acs.jpca.9b04004.

[194] V. Mazzini, G. Liu, V.S.J. Craig, Probing the Hofmeister series beyond water: Specific-ion effects in non-aqueous solvents, J. Chem. Phys. 148 (2018) 222805. https://doi.org/10.1063/1.5017278.

[195] R.L. Burns, Hydrotropic properties of a novel alkylnaphthalene sulfonate, J. Surfactants

Deterg. 2 (1999) 483–488. https://doi.org/10.1007/s11743-999-0096-1.
[196] S. Mahbub, The impact of electrolyte and urea on the phase separation of Triton X-100, J. Mol. Liq. 307 (2020) 112912. https://doi.org/10.1016/j.molliq.2020.112912.
[197] R.C. Da Silva, W. Loh, Effect of Additives on the Cloud Points of Aqueous Solutions of Ethylene Oxide–Propylene Oxide–Ethylene Oxide Block Copolymers, J. Colloid Interface Sci. 202 (1998) 385–390. https://doi.org/10.1006/jcis.1998.5456.
[198] R. Zangi, R. Zhou, B.J. Berne, Urea's Action on Hydrophobic Interactions, J. Am. Chem. Soc. 131 (2009) 1535–1541. https://doi.org/10.1021/ja807887g.
[199] J.H. Ma, C. Guo, Y.L. Tang, L. Chen, P. Bahadur, H.Z. Liu, Interaction of urea with pluronic block copolymers by1H NMR spectroscopy, J. Phys. Chem. B. 111 (2007) 5155–5161. https://doi.org/10.1021/jp070887m.
[200] S.A. Pillai, C.-F. Lee, D. Ray, V.K. Aswal, M.-R. Wang, L.-J. Chen, P. Bahadur, Influence of urea on single and mixed micellar systems of Tetronics®, J. Mol. Liq. 252 (2018) 9–17. https://doi.org/10.1016/j.molliq.2017.12.101.
[201] E. V Lage, S.A. Pillai, H. Pal, A. Bahadur, M. Casas, I. Sández-Macho, P. Bahadur, Urea induced changes in self-assembly and aggregate microstructures of amphiphilic star block copolymers with widely different hydrophobicity, Colloids Surfaces A Physicochem. Eng. Asp. 537 (2018) 259–267. https://doi.org/10.1016/j.colsurfa.2017.10.032.
[202] B. Bharatiya, C. Guo, J.H. Ma, P.A. Hassan, P. Bahadur, Aggregation and clouding behavior of aqueous solution of EO-PO block copolymer in presence of n-alkanols, Eur. Polym. J. 43 (2007) 1883–1891. https://doi.org/10.1016/j.eurpolymj.2007.02.010.
[203] J.L. Li, D.S. Bai, B.H. Chen, Effects of additives on the cloud points of selected nonionic linear ethoxylated alcohol surfactants, Colloids Surfaces A Physicochem. Eng. Asp. 346 (2009) 237–243. https://doi.org/10.1016/j.colsurfa.2009.06.020.
[204] C. Honda, Y. Katsumata, R. Yasutome, S. Yamazaki, S. Ishii, K. Matsuoka, K. Endo, Temperature dependence of pyrene fluorescence spectra in aqueous solutions of CnEm (C14E7, C16E7, and C16E6) nonionic surfactant micelles, J. Photochem. Photobiol. A Chem. 182 (2006) 151–157. https://doi.org/10.1016/j.jphotochem.2006.02.003.
[205] J. Venzmer, Determination of CMCs Results from CESIO / TEGEWA Working Groups, SOFW J. 146 (2020). https://www.tegewa.de/en/wp-content/uploads/sites/2/2021/05/Publication-CMCs-SOFW-Journal-March-2020.pdf.
[206] L.A. Sanova, A.N. Lisitsyn, Simulation of foaming ability, multiplicity, and foam stability of shampoo, Russ. J. Appl. Chem. 85 (2012) 898–906. https://doi.org/10.1134/S1070427212050110.
[207] M.. García, E. Campos, M. Dalmau, I. Ribosa, J. Sánchez-Leal, Structure–activity relationships for association of linear alkylbenzene sulfonates with activated sludge, Chemosphere. 49 (2002) 279–286. https://doi.org/10.1016/S0045-6535(02)00182-0.
[208] J. Mata, D. Varade, P. Bahadur, Aggregation behavior of quaternary salt based cationic surfactants, Thermochim. Acta. 428 (2005) 147–155. https://doi.org/10.1016/j.tca.2004.11.009.
[209] Y. Takata, Y. Shimatsu, T. Nagahashi, T. Miyayama, A. Hyono, H. Ohshima, Effect of Ionic Surfactants on Ion Vibration Current and Colloid Vibration Current, J. Oleo Sci. 59 (2010) 401–406. https://doi.org/10.5650/jos.59.401.
[210] J. Appell, G. Porte, M. Rawiso, Interactions between nonionic surfactant micelles introduced by a telechelic polymer. A small angle neutron scattering study, Langmuir.

14 (1998) 4409–4414. https://doi.org/10.1021/la9712395.
[211] K.-W. Zhang, G. Karlström, B. Lindman, Phase behaviour of systems of a non-ionic surfactant and a non-ionic polymer in aqueous solution, Colloids and Surfaces. 67 (1992) 147–155. https://doi.org/10.1016/0166-6622(92)80294-C.
[212] G. Zhao, C.C. Khin, S.B. Chen, B.-H. Chen, Nonionic Surfactant and Temperature Effects on the Viscosity of Hydrophobically Modified Hydroxyethyl Cellulose Solutions, J. Phys. Chem. B. 109 (2005) 14198–14204. https://doi.org/10.1021/jp051955c.
[213] N. Rehman, H. Ullah, S. Alam, A.K. Jan, S.W. Khan, M. Tariq, Surface and thermodynamic study of micellization of non ionic surfactant/diblock copolymer system as revealed by surface tension and conductivity, J. Mater. Environ. Sci. 8 (2017) 1161–1167.
[214] D. Bai, C.C. Khin, S.B. Chen, C.-C. Tsai, B.-H. Chen, Interaction between a Nonionic Surfactant and a Hydrophobically Modified 2-Hydroxyethyl Cellulose, J. Phys. Chem. B. 109 (2005) 4909–4916. https://doi.org/10.1021/jp045538w.
[215] E. Feitosa, W. Brown, P. Hansson, Interactions between the non-ionic surfactant C12E5 and poly(ethylene oxide) studied using dynamic light scattering and fluorescence quenching, Macromolecules. 29 (1996) 2169–2178. https://doi.org/10.1021/ma950516g.
[216] E. Alami, M. Almgren, W. Brown, Interaction of Hydrophobically End-Capped Poly(ethylene oxide) with Nonionic Surfactants in Aqueous Solution. Fluorescence and Light Scattering Studies, Macromolecules. 29 (1996) 5026–5035. https://doi.org/10.1021/ma9518161.
[217] P. Hansson, B. Lindman, Surfactant-polymer interactions, Curr. Opin. Colloid Interface Sci. 1 (1996) 604–613. https://doi.org/10.1016/s1359-0294(96)80098-7.
[218] R. Tanaka, J. Meadows, P.A. Williams, G.O. Phillips, Interaction of hydrophobically modified hydroxyethyl cellulose with various added surfactants, Macromolecules. 25 (1992) 1304–1310. https://doi.org/10.1021/ma00030a016.
[219] A. Slastanova, R.A. Campbell, T. Snow, E. Mould, P. Li, R.J.L. Welbourn, M. Chen, E. Robles, W.H. Briscoe, Synergy, competition, and the “hanging” polymer layer: Interactions between a neutral amphiphilic ‘tardigrade’ comb co-polymer with an anionic surfactant at the air-water interface, J. Colloid Interface Sci. 561 (2020) 181–194. https://doi.org/10.1016/j.jcis.2019.11.017.
[220] Q. Qiu, P. Somasundaran, B.A. Pethica, Hydrophobic complexation of poly(vinyl caprolactam) with sodium dodecyl sulfate and dodecyltrimethylammonium bromide in solution, Langmuir. 18 (2002) 3482–3486. https://doi.org/10.1021/la011702k.
[221] T.F. Tadros, The interaction of cetyltrimethylammonium bromide and sodium dodecylbenzene sulfonate with polyvinyl alcohol. adsorption of the polymer-surfactant complexes on silica, J. Colloid Interface Sci. 46 (1974) 528–540. https://doi.org/10.1016/0021-9797(74)90064-2.
[222] S. Aktar, M. Saha, S. Mahbub, M.A. Halim, M.A. Rub, M.A. Hoque, D.M.S. Islam, D. Kumar, Y.G. Alghamdi, A.M. Asiri, Influence of polyethylene glycol on the aggregation/clouding phenomena of cationic and non-ionic surfactants in attendance of electrolytes (NaCl & Na2SO4): An experimental and theoretical analysis, J. Mol. Liq. 306 (2020). https://doi.org/10.1016/j.molliq.2020.112880.
[223] J.P. Mata, P.R. Majhi, M. Yamashita, A. Khanal, K. Nakashima, P. Bahadur, Aggregation behavior of pluronic-L64 in presence of sodium dodecyl sulphate in water, J. Dispers. Sci. Technol. 29 (2008) 1248–1256. https://doi.org/10.1080/01932690701857152.

[224] T. Patel, P. Bahadur, J. Mata, The clouding behaviour of PEO-PPO based triblock copolymers in aqueous ionic surfactant solutions: A new approach for cloud point measurements, J. Colloid Interface Sci. 345 (2010) 346–350. https://doi.org/10.1016/j.jcis.2010.01.079.

[225] S. Chatterjee, R. Prajapati, A. Bhattacharya, T.K. Mukherjee, Microscopic evidence of "necklace and bead"-like morphology of polymer-surfactant complexes: A comparative study on poly(vinylpyrrolidone)- sodium dodecyl sulfate and poly(diallyldimethylammonium chloride)-sodium dodecyl sulfate systems, Langmuir. 30 (2014) 9859–9865. https://doi.org/10.1021/la5022615.

[226] A. Bonincontro, P. Michiotti, C. La Mesa, Structure and Dynamics of Polymer-Surfactant Complexes: Dielectric Relaxation Studies, J. Phys. Chem. B. 107 (2003) 14164–14170. https://doi.org/10.1021/jp035326j.

[227] D.J. Cooke, J.A.K. Blondel, J. Lu, R.K. Thomas, Y. Wang, B. Han, H. Yan, J. Penfold, Interaction between Poly(ethylene oxide) and Monovalent Dodecyl Sulfates Studied by Neutron Reflection, Langmuir. 14 (1998) 1990–1995. https://doi.org/10.1021/la971129y.

[228] M. Cao, M. Hai, Investigation on the Interaction between Sodium Dodecyl Sulfate and Polyethylene Glycol by Electron Spin Resonance, Ultraviolet Spectrum, and Viscosity, J. Chem. Eng. Data. 51 (2006) 1576–1581. https://doi.org/10.1021/je060067n.

[229] K. Pandya, K. Lad, P. Bahadur, Effect of Additives on the Clouding Behavior of an Ethylene Oxide-Propylene Oxide Block Copolymer in Aqueous Solution, J. Macromol. Sci. Part A. 30 (1993) 1–18. https://doi.org/10.1080/10601329308009387.

[230] N. Sardar, M.S. Ali, M. Kamil, Kabir-ud-Din, Phase Behavior of Nonionic Polymer Hydroxypropylmethyl Cellulose: Effect of Gemini and Single-Chain Surfactants on the Energetics at the Cloud Point, J. Chem. Eng. Data. 55 (2010) 4990–4994. https://doi.org/10.1021/je100572d.

[231] E.J. Kim, D.O. Shah, Effect of surfactants on the cloud point of amphiphilic drug solutions, Colloids Surfaces A Physicochem. Eng. Asp. 227 (2003) 105–111. https://doi.org/10.1016/S0927-7757(03)00415-1.

[232] M.S. Bakshi, S. Sachar, K. Singh, A. Shaheen, Mixed micelle behavior of Pluronic L64 and Triton X-100 with conventional and dimeric cationic surfactants, J. Colloid Interface Sci. 286 (2005) 369–377. https://doi.org/10.1016/j.jcis.2004.12.044.

[233] B. Vyas, S.A. Pillai, S. Tiwari, P. Bahadur, Effects of head group and counter-ion variation in cationic surfactants on the microstructures of EO-PO block copolymer micelles, Colloid Interface Sci. Commun. 33 (2019) 100216. https://doi.org/10.1016/j.colcom.2019.100216.

[234] S. Manet, Y. Karpichev, D. Bassani, R. Kiagus-Ahmad, R. Oda, Counteranion Effect on Micellization of Cationic Gemini Surfactants 14-2-14: Hofmeister and Other Counterions, Langmuir. 26 (2010) 10645–10656. https://doi.org/10.1021/la1008768.

[235] T. Nakashima, T. Fujiwara, Effects of Surfactant Counter-Ions and Added Salts on Reverse Micelle Formation of Cetyltrimethylammonium Surfactant Studied by Using (5 , 10 , 15 , 20-Tetraphenylporphyrinato) zinc (II) as a Probe, Anal. Sci. 17 (2001) 1241–1244.

[236] S. Berr, R.R.M. Jones, J.S. Johnson, Effect of counterion on the size and charge of alkyltrimethylammonium halide micelles as a function of chain length and concentration as determined by small-angle neutron scattering, J. Phys. Chem. 96

(1992) 5611–5614. https://doi.org/10.1021/j100192a075.
[237] J. Mata, Hydrodynamic and Clouding Behavior of Triton X-100+SDS Mixed Micellar Systems in the Presence of Sodium Chloride, J. Dispers. Sci. Technol. 27 (2006) 49–54. https://doi.org/10.1081/DIS-200066708.
[238] A. Carlsson, G. Karlstroem, B. Lindman, Synergistic surfactant-electrolyte effect in polymer solutions, Langmuir. 2 (1986) 536–537. https://doi.org/10.1021/la00070a027.
[239] F. Comert, A.J. Malanowski, F. Azarikia, P.L. Dubin, Coacervation and precipitation in polysaccharide–protein systems, Soft Matter. 12 (2016) 4154–4161. https://doi.org/10.1039/C6SM00044D.
[240] F. Comert, D. Nguyen, M. Rushanan, P. Milas, A.Y. Xu, P.L. Dubin, Precipitate–Coacervate Transformation in Polyelectrolyte–Mixed Micelle Systems, J. Phys. Chem. B. 121 (2017) 4466–4473. https://doi.org/10.1021/acs.jpcb.6b12895.
[241] F. Comert, P.L. Dubin, Liquid-liquid and liquid-solid phase separation in protein-polyelectrolyte systems, Adv. Colloid Interface Sci. 239 (2017) 213–217. https://doi.org/10.1016/j.cis.2016.08.005.
[242] F.M. Menger, B.M. Sykes, Anatomy of a Coacervate, Langmuir. 14 (1998) 4131–4137. https://doi.org/10.1021/la980208m.
[243] E. Spruijt, A.H. Westphal, J.W. Borst, M.A. Cohen Stuart, J. Van Der Gucht, Binodal compositions of polyelectrolyte complexes, Macromolecules. 43 (2010) 6476–6484. https://doi.org/10.1021/ma101031t.
[244] Y. Huang, W. Qin, X. Huo, Y. Dai, Surfactant distribution in the clouding of C12E10, Colloids Surfaces A Physicochem. Eng. Asp. 276 (2006) 228–231. https://doi.org/10.1016/j.colsurfa.2005.11.053.
[245] J. Sangster, Octanol-Water Partition Coefficients of Simple Organic Compounds, J. Phys. Chem. Ref. Data. 18 (1989) 1111–1229. https://doi.org/10.1063/1.555833.
[246] E. Fischer, W. Fieber, C. Navarro, H. Sommer, D. Benczédi, M.I. Velazco, M. Schönhoff, Partitioning and Localization of Fragrances in Surfactant Mixed Micelles, J. Surfactants Deterg. 12 (2009) 73–84. https://doi.org/10.1007/s11743-008-1104-4.
[247] R. Nagarajan, M. Barry, E. Ruckenstein, Unusual selectivity in solubilization by block copolymer micelles, Langmuir. 2 (1986) 210–215. https://doi.org/10.1021/la00068a017.
[248] R.B. Godinho, M.C. Santos, R.J. Poppi, Determination of fragrance content in perfume by Raman spectroscopy and multivariate calibration, Spectrochim. Acta - Part A Mol. Biomol. Spectrosc. 157 (2016) 158–163. https://doi.org/10.1016/j.saa.2015.12.025.
[249] C.M. Hansen, On application of the three dimensional solubility parameter to the prediction of mutual solubility and compatibility, F ä Rb Och Lack. 13 (1967) 132–138.
[250] L.B. Petrovic, V.J. Sovilj, J.M. Katona, J.L. Milanovic, Influence of polymer–surfactant interactions on o/w emulsion properties and microcapsule formation, J. Colloid Interface Sci. 342 (2010) 333–339. https://doi.org/10.1016/j.jcis.2009.10.077.
[251] R. Banerjee, P. Purkayastha, Revival of the nearly extinct fluorescence of coumarin 6 in water and complete transfer of energy to rhodamine 123, Soft Matter. 13 (2017) 5506–5508. https://doi.org/10.1039/C7SM01198A.
[252] L. Pérez-Fuentes, D. Bastos-González, J. Faraudo, C. Drummond, Effect of organic and inorganic ions on the lower critical solution transition and aggregation of PNIPAM, Soft Matter. 14 (2018) 7818–7828. https://doi.org/10.1039/c8sm01679h.

6. APPENDIX

First, we are proud to add that part of the results presented in chapter 3 have recently been published in the Journal of Colloid and Interface Science (JCIS), a premier journal in the field of colloid science. The details of the research article are the following:

Xavier Castellvi Corrons, Jeremie Gummel, Johan Smets, Debora Berti
Liquid-liquid phase separated microdomains of an amphiphilic graft copolymer in a surfactant-rich medium
Journal of Colloid and Interface Science; Volume 615, 2022; Pages 807-820
ISSN 0021-9797
https://doi.org/10.1016/j.jcis.2022.02.020.

In this final section of the thesis, the reader can find additional figures that provide extra information to ease the comprehension of the results described above.

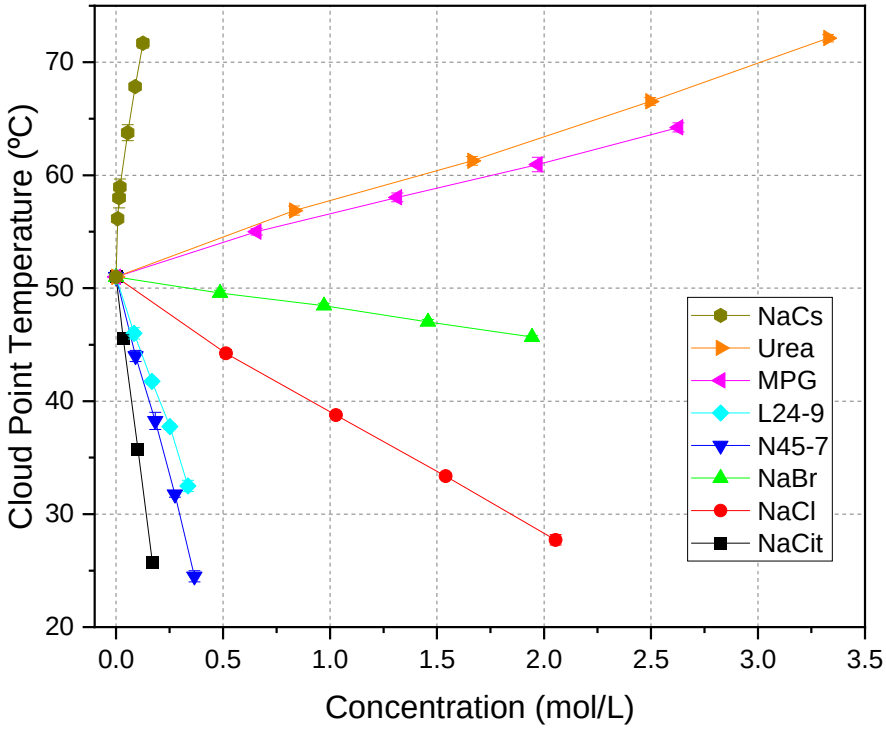

***Figure 6-1**: Effect of kosmotropes, chaotropes, and non-ionic surfactants on the CPT of 1% w/w PEG-g-PVAc in water measured through turbidimetry and expressed in mol/L. Each point corresponds to the average of at least three measurements. Some of the error bars are not visible because they fall within the data points drawn.*

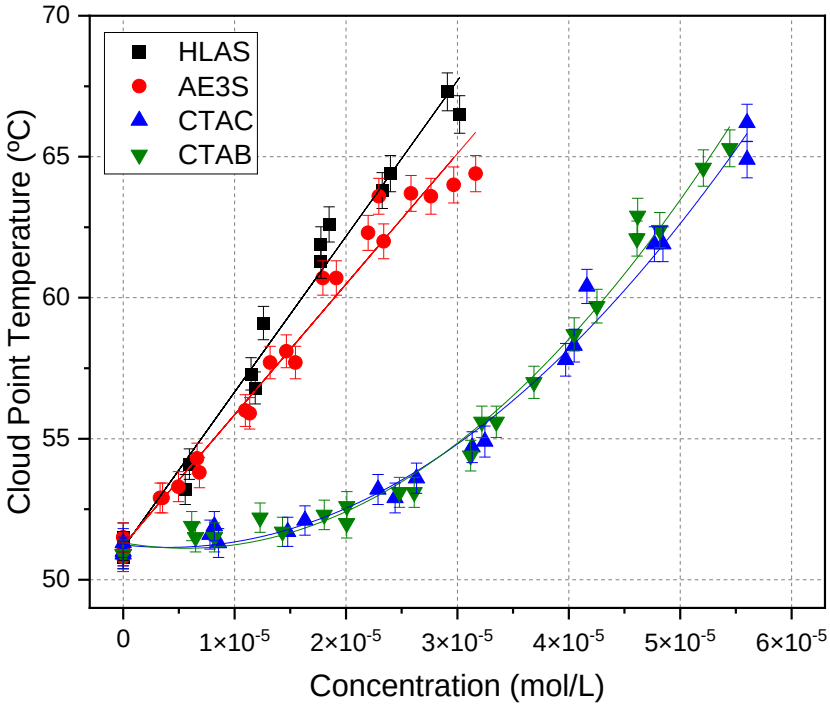

***Figure 6-2**: Effect of anionic (HLAS, AE3S) and cationic (CTAC, CTAB) surfactants on the cloud point temperature of PEG-g-PVAc (1% w/w in water), expressed in mol/L and measured through turbidimetry. Each point corresponds to a single measurement due to the difficulty in obtaining the same low concentrations.*

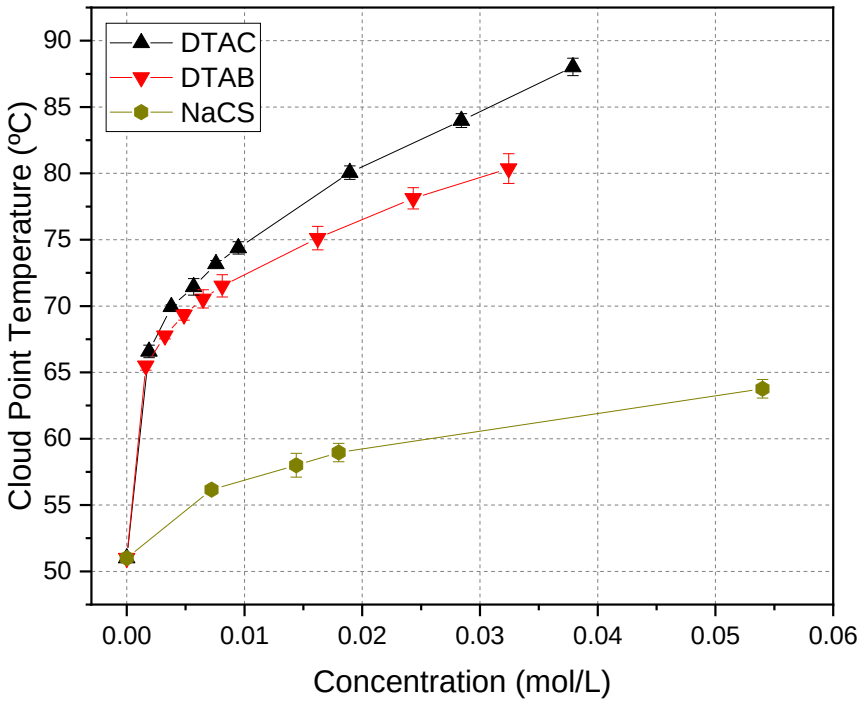

***Figure 6-3**: Effect of cationic surfactants (DTAC, DTAB) and the chaotrope NaCS on the cloud point temperature of PEG-g-PVAc (1% w/w in water), expressed in mol/L and measured through turbidimetry. Each point corresponds to the average of three measurements. Some of the error bars are not visible because they fall within the data points drawn.*

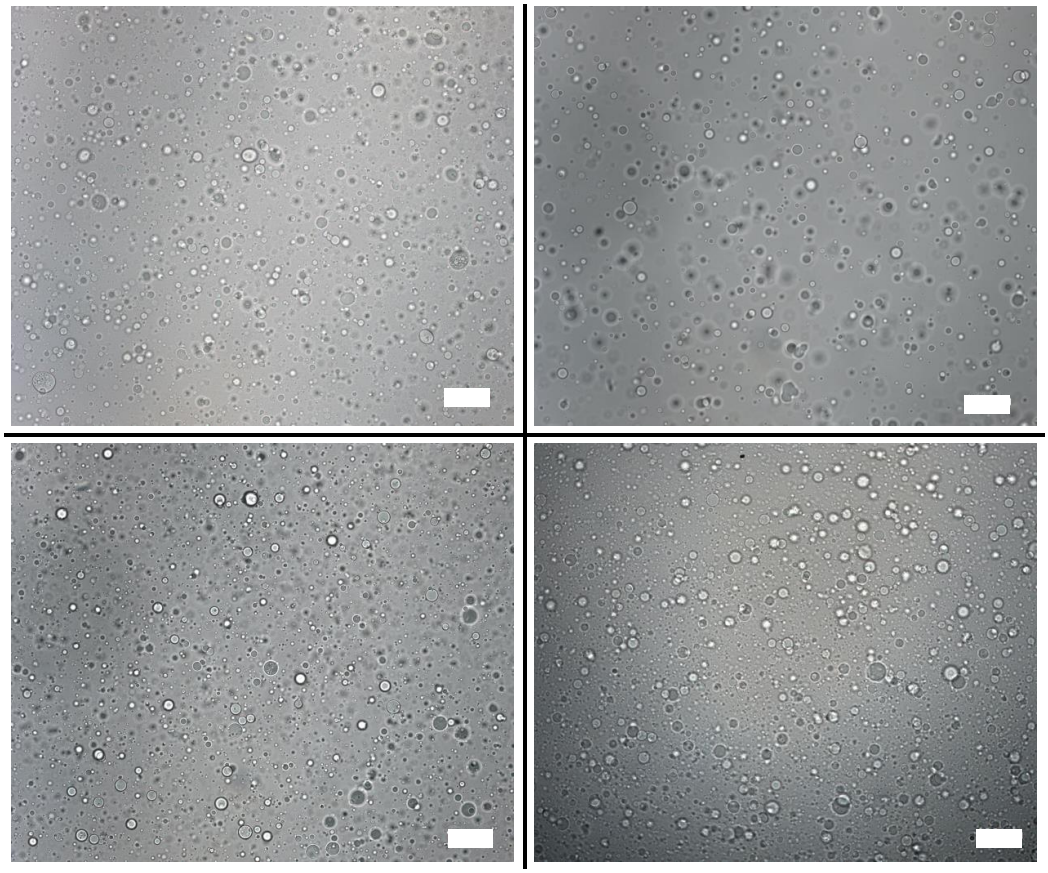

***Figure 6-4**: Optical microscope pictures of PEG-g-PVAc coacervates. Each picture corresponds to a different sample with concentrations of N45-7 and NaCit within the region 2 of **Figure 3-8**. The white bars are equivalent to 100 µm.*

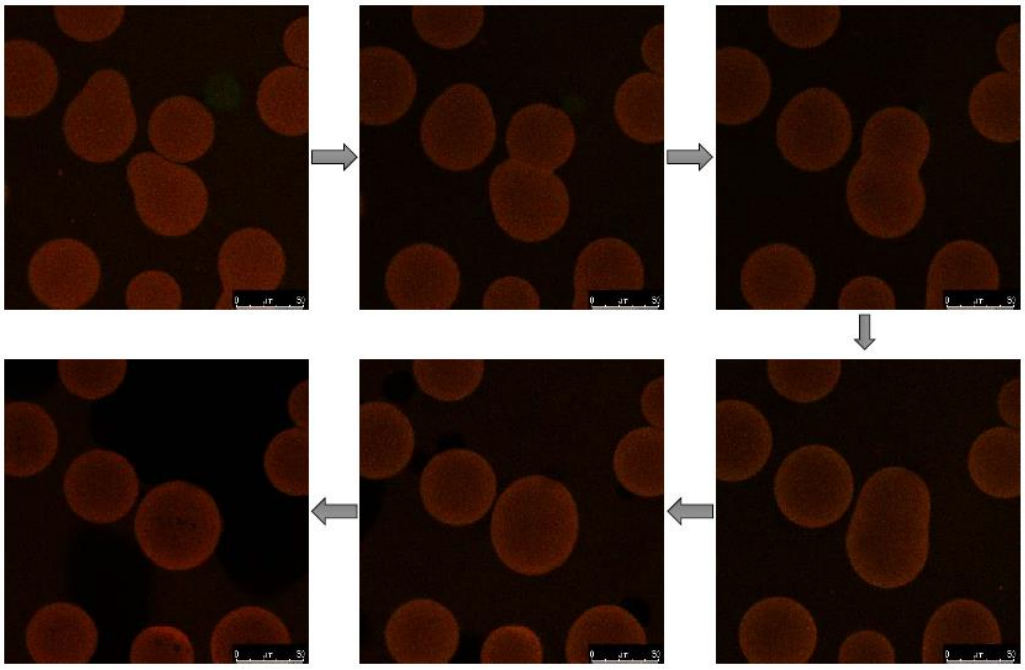

***Figure 6-5**: Fluorescence confocal microscopy pictures of RBITC-labelled PEG-g-PVAc coacervates coalescing. Pictures were captured every ten minutes.*

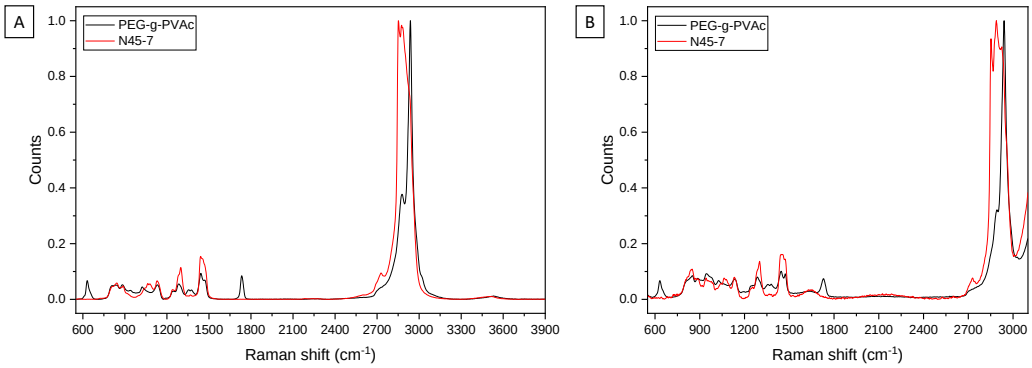

***Figure 6-6**: Reference Raman spectra of PEG-g-PVAc (black) and N45-7 (red) when analyzed as pure solids (A) and dissolved in water (B). Spectra normalized at their highest peak intensity in both figures for ease of comparison.*

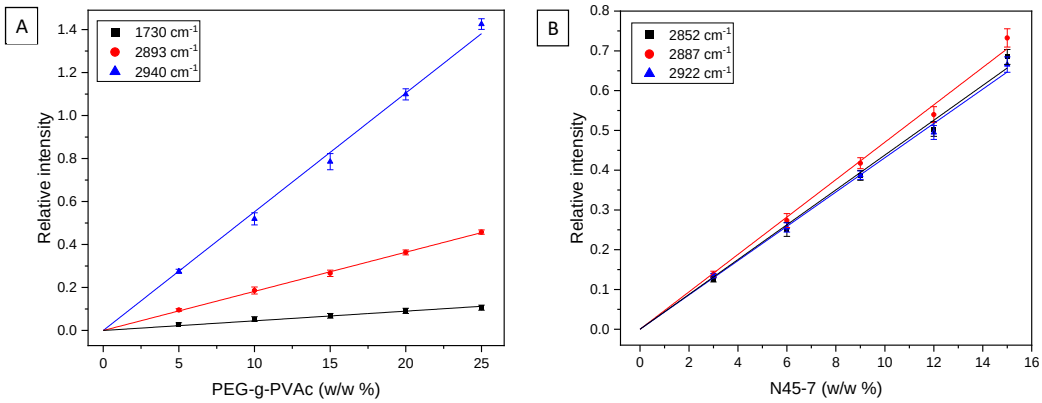

***Figure 6-7**: (A) Calibration curves of the PEG-g-PVAc/water ratio, obtained from the relative intensities of three different Raman peaks of PEG-g-PVAc (1730, 2893, and 2940 cm^{-1}) in comparison to the peak of water (3420cm^{-1}) (see **Figure 3-17A**). The linear equations (y = Ax + B, B=0) are as follows: y = 0.00450x, R^2 = 0.9939 (1730 cm^{-1}); y = 0.0182x, R^2 = 0.9998 (2893 cm^{-1}), and y = 0.0552x, R^2 = 0.9988 (2940 cm^{-1}); where "y" is the relative intensity and "x" the concentration of PEG-g-PVAc in w/w %. (B) Calibration curves of the N45-7/water ratio, obtained from the relative intensities of three different Raman peaks of N45-7 (2852, 2887, and 2922 cm^{-1}) in comparison to the peak of water (3420cm^{-1}) (see **Figure 3-17B**). The linear equations (y = Ax + B, B=0), are as follows: y = 0.0438x, R^2 = 0.9985 (2852 cm^{-1}); y = 0.0470x, R^2 = 0.9987 (2887 cm^{-1}), and y = 0.0431x, R^2 = 0.9990 (2922 cm^{-1}); where "y" is the relative intensity and "x" the concentration of N45-7 in w/w %.*

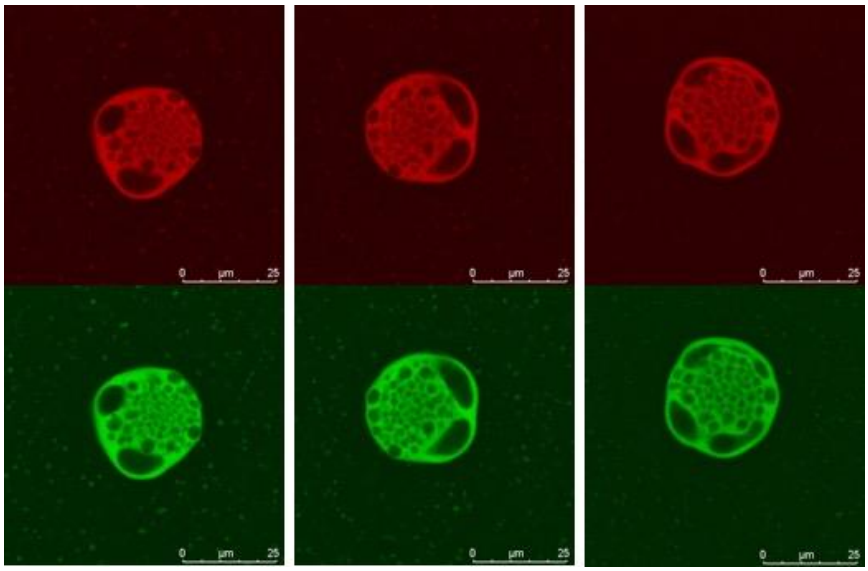

***Figure 6-8**: Fluorescence confocal microscopy pictures of the very same RBITC-labelled PEG-g-PVAc coacervate at the fourth stage of its destabilization (see **Figure 3-27**). The top pictures show the fluorescence of the RBITC-labelled PEG-g-PVAc (in red), while the bottom ones show the fluorescence of Coumarin6 (in green). These pictures demonstrate the mobility of the dark copolymer-depleted inner domains that appear in these coacervates once they are unstable in the medium.*

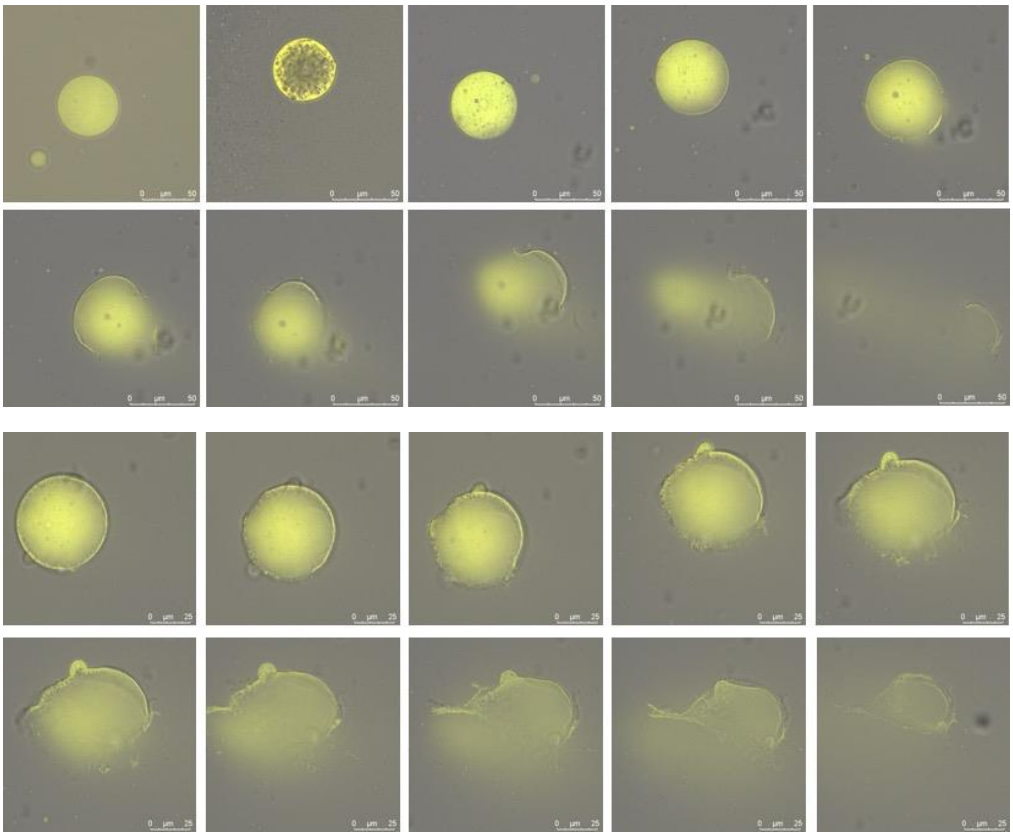

***Figure 6-9**: Fluorescence confocal microscopy pictures showing the destabilization of RBITC-labelled PEG-g-PVAc coacervates containing Coumarin6 after water addition. The yellow color is attributed to the fluorescence overlay of the RBITC-labelled PEG-g-PVAc (red) and Coumarin6 (green).*

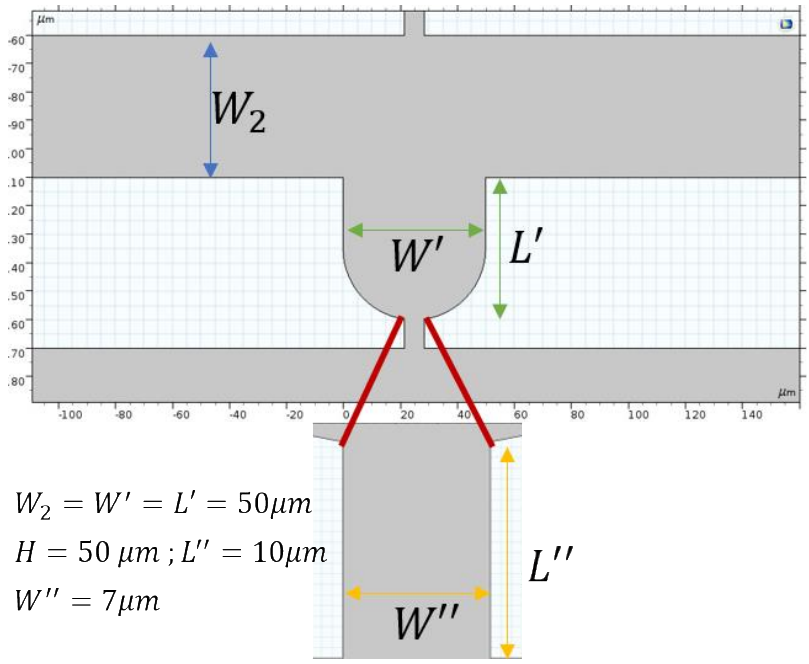

***Figure 6-10**: Schematic representation showing the shape and dimensions of the meander microfluidic chip used to trap PEG-g-PVAc coacervates and observe their destabilization after water addition.*

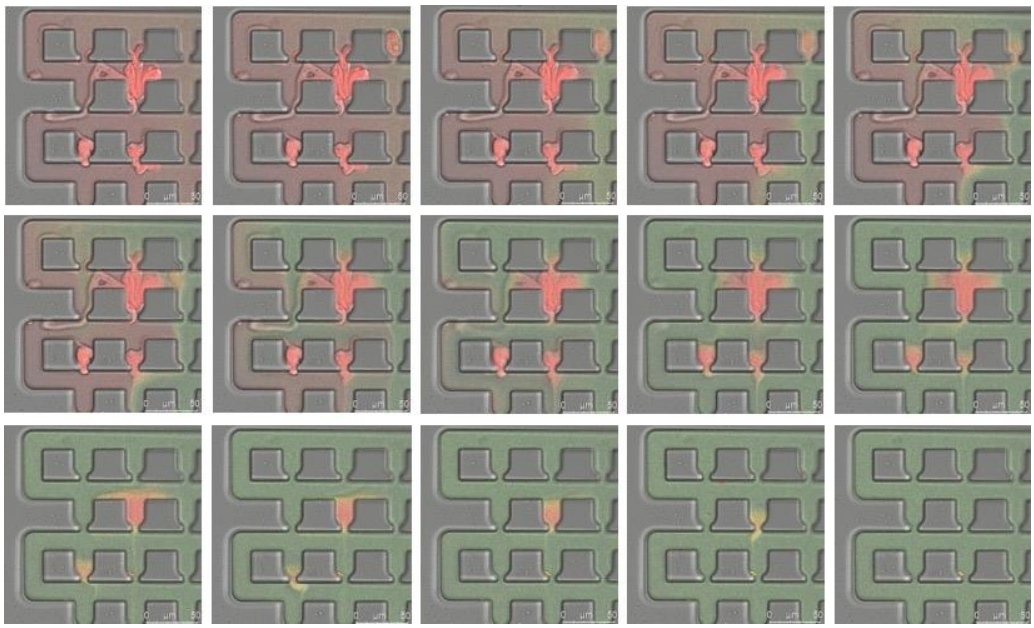

***Figure 6-11**: Fluorescence confocal microscopy pictures showing the destabilization of trapped liquid-liquid phase separated RBITC-labelled PEG-g-PVAc (in red) after water reaches them (in green, due to its content of rhodamine 110 chloride). The pictures were obtained from a meander microfluidic chip every 0.5 seconds.*

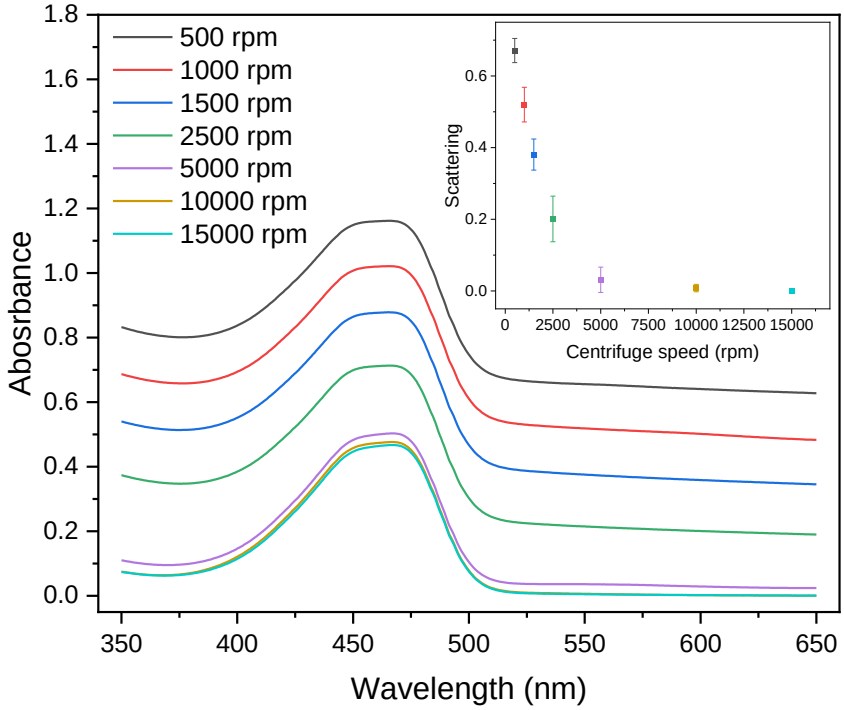

***Figure 6-12**: UV-Vis spectra of the supernatants obtained after centrifuging at 500, 1000, 1500, 2500, 5000, 10000, or 15000 rpm for 10 minutes from a sample containing PEG-g-PVAc coacervates (1% w/w PEG-g-PVAc, 5% w/w N45-7, and 5% w/w NaCit), and Coumarin6 (≈10 mg/mL). As the inset shows, the scattering coming from PEG-g-PVAc coacervates diminishes by increasing the centrifuging speed, suggesting that from 10000 rpm there are no coacervates in the supernatant.*